INFORMATION TO USERS

The most advanced technology has been used to photograph and reproduce this manuscript from the microfilm master. UMI films the text directly from the original or copy submitted. Thus, some thesis and dissertation copies are in typewriter face, while others may be from any type of computer printer.

The quality of this reproduction is dependent upon the quality of the copy submitted. Broken or indistinct print, colored or poor quality illustrations and photographs, print bleedthrough, substandard margins, and improper alignment can adversely affect reproduction.

In the unlikely event that the author did not send UMI a complete manuscript and there are missing pages, these will be noted. Also, if unauthorized copyright material had to be removed, a note will indicate the deletion.

Oversize materials (e.g., maps, drawings, charts) are reproduced by sectioning the original, beginning at the upper left-hand corner and continuing from left to right in equal sections with small overlaps. Each original is also photographed in one exposure and is included in reduced form at the back of the book. These are also available as one exposure on a standard 35mm slide or as a 17" x 23" black and white photographic print for an additional charge.

Photographs included in the original manuscript have been reproduced xerographically in this copy. Higher quality 6" x 9" black and white photographic prints are available for any photographs or illustrations appearing in this copy for an additional charge. Contact UMI directly to order.

U·M·I

University Microfilms International
A Bell & Howell Information Company
300 North Zeeb Road, Ann Arbor, MI 48106-1346 USA
313/761-4700 800/521-0600

Order Number 8907404

Microstructure effects on light propagation in zinc sulfide thin film waveguides

Himel, Marc David, Ph.D.

The University of Arizona, 1988

U·M·I
300 N. Zeeb Rd.
Ann Arbor, MI 48106

MICROSTRUCTURE EFFECTS ON LIGHT PROPAGATION IN ZINC SULFIDE THIN FILM WAVEGUIDES

by

Marc David Himel

A Dissertation Submitted to the Faculty of the

COMMITTEE ON OPTICAL SCIENCES (GRADUATE)

In Partial Fulfillment of the Requirements
For the Degree of

DOCTOR OF PHILOSOPHY

In the Graduate College

THE UNIVERSITY OF ARIZONA

1 9 8 8

THE UNIVERSITY OF ARIZONA
GRADUATE COLLEGE

As members of the Final Examination Committee, we certify that we have read the dissertation prepared by Marc David Himel

entitled MICROSTRUCTURE EFFECTS ON LIGHT PROPAGATION IN ZINC SULFIDE THIN FILM WAVEGUIDES

and recommend that it be accepted as fulfilling the dissertation requirement for the Degree of Doctor of Philosophy.

Ursula J. Gibson	10/19/88 Date
James J. Burke	10/19/88 Date
Laura A. Weller-Brophy	10/19/88 Date
	Date
	Date

Final approval and acceptance of this dissertation is contingent upon the candidate's submission of the final copy of the dissertation to the Graduate College.

I hereby certify that I have read this dissertation prepared under my direction and recommend that it be accepted as fulfilling the dissertation requirement.

Dissertation Director Ursula J. Gibson — 10/19/88 Date

STATEMENT BY AUTHOR

This dissertation has been submitted in partial fulfillment of requirements for an advanced degree at the University of Arizona and is deposited in the University Library to be made available to borrowers under rules of the Library.

Brief quotations from this dissertation are allowable without special permission, provided that accurate acknowledgment of source is made. Requests for permission for extended quotation from or reproduction of this manuscript in whole or in part may be granted by the head of the major department or the Dean of the Graduate College when in his or her judgment the proposed use of the material is in the interests of scholarship. In all other instances, however, permission must be obtained from the author.

SIGNED: 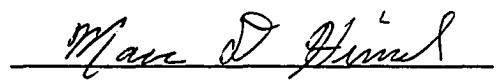

ACKNOWLEDGEMENTS

The work described in this dissertation would not have been possible without the help and support of many people. I would like to take this opportunity to extend my appreciation to them all.

I would like to extend my gratitude to Ursula Gibson, my dissertation advisor, for all the help she has given me over the last four years. She allowed me to set the direction of my research and work at my own pace. Although Ursi gave me the freedom to follow my own ideas (no matter what she thought of them), she was always there with excellent suggestions when I needed them.

Getting started on this project would have been extremely difficult if not for the people who taught me the basics. To Rance Fortenberry, Robert Moshrefzadeh, and Jesus Valera for their patience and instruction in prism coupling. To Fred Hickernell for helping with waveguide loss measurements and supplying a seemingly endless supply of silicon substrates. To Dilip Kuchibhatla, Carolyn Hickey, and Charles Kennemore III for teaching me the ins and outs of thin film deposition and vacuum system maintenence.

Working in the Optical Materials Group has been a wonderful experience in large part because of the group members. I am extremely grateful to Heidi Ruffner. Her efforts on this project entitle her to a co-authorship. After all, she was the one who deposited the low-loss waveguides and made all of the XRD measurements. To Ken Cornett for all the two a.m. conversations and for putting up with me as a housemate for a year. I must also thank Heidi and Ken for their help in editing this manuscript. To Frank Suits for always keeping me on my toes. To the rest of the group: Joy, Murray, Andy, and Tony for making my stay so enjoyable.

Outside of the lab, I would like to thank Laura Weller-Brophy and Jim Burke for their help in preparing this manuscript. I also thank H. Angus Macleod, Bertrand Bovard, Mike Jacobson, George Stegemen, and Colin Seaton for their many useful discussions and suggestions. To J. A. Leavitt, L. C. McIntyre, M. D. Ashbaugh, and J. G. Oder of the Physics department for the RBS measurements. I would also like to acknowledge the Optical Circuitry Cooperative for funding this research.

On a more personal note, I thank all my friends at the Optical Sciences Center, especially those who RISKed their all to make my stay in Tucson a pleasant one. To my family and friends outside Arizona for putting up with me throughout the years. Finally, I am deeply indebted to Bruce Alley, for without his constant support, I never would have made it this far.

TABLE OF CONTENTS

TABLE OF CONTENTS - Continued

Page

TABLE OF CONTENTS - Continued

LIST OF ILLUSTRATIONS

LIST OF ILLUSTRATIONS - Continued

LIST OF ILLUSTRATIONS - Continued

LIST OF TABLES

ABSTRACT

The optical propagation losses resulting from the internal microstructure of ZnS thin films were investigated using a waveguide technique. Waveguide losses were determined by measuring the scattered light as a function of propagation distance along the film. Accurate measurements were obtained by using a technique we developed that employes a coherent fiber bundle to transfer the scattered light streak to a remote image plane that was scanned with an apertured photomultiplier tube. Microstructure effects on losses were found to dominate effects caused by substrate surface finish. The magnitude of the loss was found to depend upon two independent parameters: the average grain size of the polycrystalline films and the refractive index difference between ZnS and the interstitial material. Increasing the H_2O partial pressure led to lower losses as a result of reduced crystallite size, and a change in preferential crystallite orientation. A similar change in orientation was observed for films deposited onto heated substrates. Increasing the O_2 partial pressure during deposition also resulted in slightly lower waveguide losses, possibly as a result of void filling with ZnO. The modal dependence of the losses for ZnS films deposited at ambient temperature suggests that volume losses dominate surface losses for the lowest order mode while the ratio of surface to volume losses increases for higher order modes. By depositing ZnS onto substrates cooled with liquid nitrogen, adatom surface mobility was reduced which resulted in amorphous films. Losses were minimized ($\leq$ 0.5

dB/cm at λ = 633 nm) for a substrate temperature of -50°C. These losses are lower than any previously reported for ZnS. However, further reduction of the substrate temperature resulted in an increase in tensile stress which eventually led to higher waveguide losses and crazing. The films deposited onto cooled substrates exhibited a low refractive index which indicates a low packing density and increased porosity. Differential water desorption, which is further evidence of increased porosity, was most noticeable in films with lower refractive indices when nonlinear prism coupling was attempted.

CHAPTER 1

INTRODUCTION

The optics industry has long been interested in thin film coatings because of their ability to modify the optical performance of a component. Coatings may be used to increase or decrease the reflectance of a surface as in the case of beamsplitters and anti-reflection coatings, or to reduce the spectral passband as in narrow-band filters (Macleod, 1986). For high reflectivity applications such as laser ring gyro and high power laser mirrors, coatings with extremely low scatter and absorption are required. Thin film coatings may also play an important role in the future of integrated optics, in which several optical devices will be integrated onto a single substrate (Hunsperger, 1984). Because the optical signal must propagate several centimeters within a layer, these coatings must also have extremely low losses.

When thin film coatings were first developed, researchers assumed that their properties were identical to that of the bulk material. Deviations in optical performance, and the development of high resolution microscopy, however, showed that this is not the case. In fact, the structure of a thin film can differ significantly from that of the bulk material (Pearson,1970; Lissberger and Pearson, 1976; Pulker and Jung, 1971; Guenther and Pulker, 1976). This variation may affect optical and mechanical properties such as refractive index, loss, stability, and durability (Macleod, 1986; Binh, Netterfield, and Martin, 1985; Al-Douri, 1986; Himel, Ruffner, and Gibson, 1987, 1988). The microstructure of a film may usually be described

by either a columnar or dense polycrystalline structure (Macleod, 1986; Chopra, 1979; Maissel and Glang, 1970). That microstructure can introduce scattering losses caused by refractive index fluctuations within the film or enhanced surface roughness at the upper film interface (Marcuse, 1969; Miyanaga, Asakura, and Imai, 1978, 1979, 1980; Hall, 1980, 1981; Ames and Hall, 1983; Arnz and Ponath, 1986). As the demands for improved coating performance increase, it is necessary to accurately characterize coating performance. By comparing the optical properties with the internal microstructure of a coating it may be possible to modify the fabrication technique to improve film performance.

Waveguiding techniques provide an accurate and convienient means to determine the thickness, refractive index, and total attenuation of a thin film coating (Hunsperger, 1984). These techniques tend to be more accurate and useful than the traditional measurement techniques used in the coating industry. For example, one of the most difficult optical properties to measure is the total attenuation of a coating. Transmission measurements are capable of measuring losses greater than 43 dB/cm (Westwood and Wei, 1979) while waveguide methods can measure losses as low as 0.01 dB/cm (Westwood and Wei, 1979). This greater sensitivity is possible because light interacts along the film for several millimeters or centimeters rather than the few micrometers characteristic standard transmission measurements. Although the simpler waveguide techniques have a typical sensitivity of 0.1 dB/cm, (Dutta, *et al.* 1981; Himel and Gibson, 1986; Weber, Dunn, and Leibolt, 1973) this still represents an increase in sensitivity of at least two orders of magnitude.

The goal of this dissertation is to investigate experimentally the effects of internal film microstructure on the optical propagation in ZnS thin film waveguides. This requires accurate characterization of both the optical properties and the

internal microstructure of the thin films. Because of the increased sensitivity over standard transmission techniques, a waveguide method was used to determine each film's thickness, refractive index, and attenuation. By comparing the film microstructure and optical properties, the dominant loss mechanism may be determined and its effects reduced by modifying the deposition process.

ZnS was chosen for several reasons. First, it is an important material in the coating industry because its high refractive index (2.35) makes it suitable for use as high index layers in multiple layer coatings. Furthermore, its wide wavelength passband (0.4 - 13 μm) allows for both visible and infrared applications. ZnS also has a large thermal nonlinearity which may be used to demonstrate nonlinear and bistable integrated optical devices (Svensson, 1988; Sprague, *et al.* 1983). Unlike the majority of thin film materials that exhibit columnar structure, low packing densities, and tensile stress, thermally evaporated ZnS films are polycrystalline, exhibit high packing densities, and compressive stress (Wenz and Hoffman, 1977; Pulker and Mäser, 1979). While ion processes such as ion-assisted-deposition and ion-beam-sputtering can be used to densify and reduce the losses of films with low packing densities (Binh, Netterfield, and Martin, 1985), these processes introduce additional compressive stress (Saxe, 1985) and, therefore, cannot be used to improve the optical properties of ZnS films. Therefore, other techniques must be employed to reduce the losses of ZnS thin films.

Chapter 2 presents a discussion of dielectric waveguide theory and thin-film microstructure. The chapter begins with a discussion of light propagation in lossless dielectric waveguides. Both the ray-optic and electromagnetic field approaches are described. This is followed by a description of coupling methods, where emphasis is placed on the prism coupler. Waveguide loss mechanisms are

then introduced and Marcuse's (1969) theory for scattering from a rough interface is presented. This is followed by a description of thin film microstructure and its effects upon light scattering. Finally, several recent experimental studies that used waveguide techniques to characterize various thin film materials are reviewed.

Chapter 3 describes the fabrication and characterization of the ZnS films. Because accurate measurements of waveguide loss are necessary, a technique was developed that uses a coherent fiber bundle to transfer the scattered light streak to a remote image plane, where it is scanned by a photomultiplier tube. This technique is accurate, easy to align, and can be set up inexpensively. Microstructure characterization techniques are also described.

The experimental results of the losses of ZnS waveguides fabricated under different deposition conditions are described in chapter 4. Once it was determined that the losses of the lowest order mode were dominated by volume scattering from the crystallites, films were deposited onto liquid nitrogen cooled substrates in order to quench the crystallinity. These ZnS waveguides had losses lower than any previously reported.

The final chapter summarizes the results of this research and suggests future studies to improve the performance of the low-loss ZnS waveguides.

CHAPTER 2

PLANAR WAVEGUIDE AND THIN FILM BACKGROUND

An optical waveguide is a device that confines and carries light in one or more dimensions, much as an electrical wire confines and carries electrons. Waveguides come in several geometries: optical fibers are used in communications, as interconnections between circuit boards, and can also be used, at a higher level of integration, as interconnections between chips on a single circuit board. Two other waveguide geometries are the planar and channel structures which are useful for the fabrication of integrated optical devices. Planar and channel waveguides confine light in one and two dimensions, respectively, and can be fabricated on a large substrate, thus benefiting from the technology developed by the integrated electronics industry.

Combining thin film technology with basic techniques for characterizing optical waveguides, high quality coatings can be fabricated and their quality verified. Waveguiding techniques allow the accurate measurement of refractive index, thickness, and total film attenuation. Measurements using a waveguide geometry can yield very accurate values of total attenuation, because of the long interaction lengths allowed by the geometry. Waveguide attenuation can be measured over a distance of a few centimeters while most other thin film measurement techniques are restricted to looking through the film, which is only a few micrometers thick, in transmission. The work in this dissertation shows that waveguide attenuation is greatly affected by small changes in the internal

microstructure of a coating.

This chapter will start with a description of the basic theory behind waveguide propagation. First, a ray-optic picture will be used to develop the waveguide dispersion relation and introduce the concept of discrete modes. Second, because the ray-optic approach does not yield any information on the field distribution within a waveguide, an electromagnetic field picture will be employed to derive the field distributions both inside and outside the waveguide. This will be followed by the description of several different methods for coupling light into a waveguide. Then the scattering and absorptive mechanisms that contribute to waveguide attenuation will be discussed. A brief description of thin film microstructure and how it affects waveguide losses will be presented and finally, several recent experimental studies on loss mechanisms will be reviewed.

Slab Waveguide Guided Modes

Ray-Optics

The simplest waveguide structure is the planar (or slab) waveguide which consists of a thin layer of refractive index n_f on a substrate with refractive index n_s. Light confinement within the film is achieved through total internal reflection at the two film interfaces. Therefore the refractive indices of both the substrate and cover layers must be lower than that of the film. A ray-optic or plane-wave approach, as shown in figure 2.1, may be used to describe a planar, isotropic, and homogeneous waveguide. Here the field is represented by a wavevector that is normal to the wavefront. As the field propagates in the thin film, it will be totally internally reflected at the boundaries and thus confined within the film ("guided") if the angle of incidence, θ, of the ray at each of the two boundaries is greater than the critical angle, defined as:

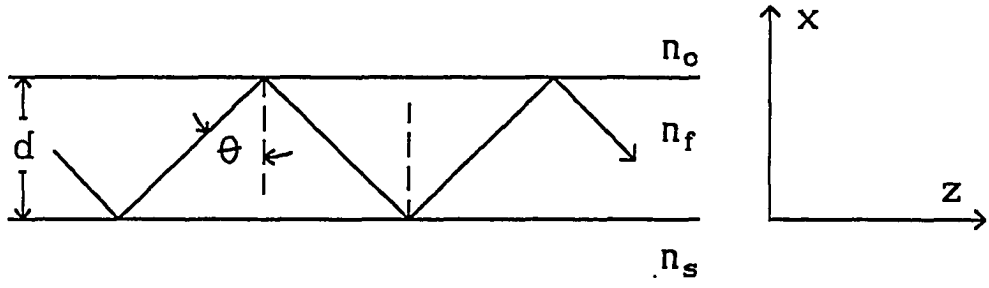

Figure 2.1. The ray-optics picture of the planar waveguide.

$$\theta_c = \sin^{-1}(n_l/n_h), \qquad 2\text{-}1$$

where n_h and n_l are the refractive indices of the high index and low index layers, respectively. The propagation constant is defined as the z-component of the wave vector

$$\beta = kn_f\sin\theta, \qquad 2\text{-}2$$

where $k = 2\pi/\lambda$ is the wave vector in free space.

Total internal reflection is not the only requirement for a guided wave. After the field undergoes a reflection from both surfaces, this new wavefront must be in phase with the unreflected wavefront. That phase matching condition is responsible for the discrete nature of guided modes. By taking into account the total phase shift associated with the optical path difference and phase changes upon reflection from the surfaces, the waveguide dispersion relation is determined. Figure 2.2 shows the phase fronts of both the reflected and unreflected fields. The optical path difference between these fields is $2n_f d\cos\theta$, where d is the film thickness. The phase changes on reflection, which depend on whether the field is polarized parallel or perpendicular to the plane of incidence, can be determined from the Fresnel equations for a linear, isotropic, and lossless medium. If we define:

$$\tan(\phi_{c,TE}) = \frac{\sqrt{n_f^2\sin^2\theta - n_c^2}}{n_f\cos\theta}$$

$$\tan(\phi_{s,TE}) = \frac{\sqrt{n_f^2\sin^2\theta - n_s^2}}{n_f\cos\theta} \qquad 2\text{-}3$$

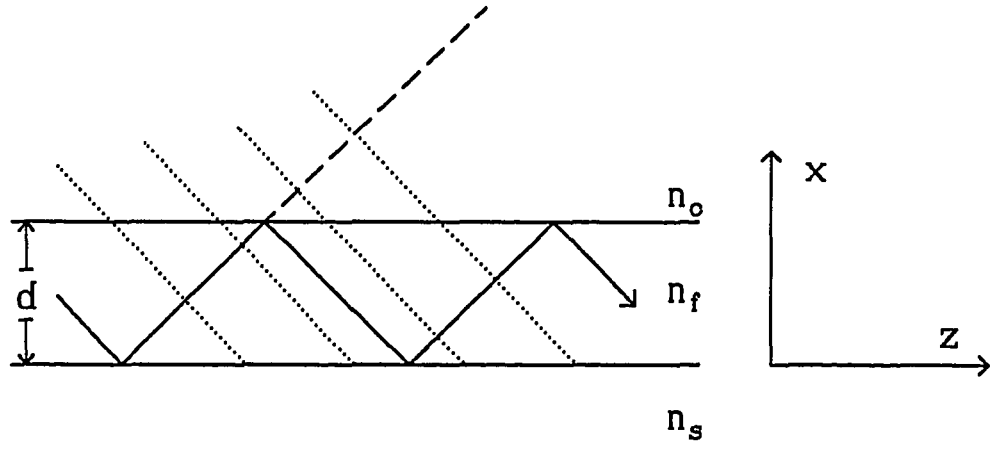

Figure 2.2. Geometry of the "transverse resonance condition" for obtaining a modal solution in a planar waveguide.

$$\tan(\phi_{c,TM}) = \frac{n_f^2}{n_c^2} \frac{\sqrt{n_f^2 \sin^2\theta - n_c^2}}{n_f \cos\theta}$$

$$\tan(\phi_{s,TM}) = \frac{n_f^2}{n_s^2} \frac{\sqrt{n_f^2 \sin^2\theta - n_s^2}}{n_f \cos\theta},$$

where TE and TM refer to light polarized parallel and perpendicular to the plane of the film, respectively, then the total phase change, which must equal an integral multiple of 2π, is

$$2\nu\pi = 2n_f kd\cos\theta + 2\phi_c + 2\phi_s, \qquad 2\text{-}4$$

where the phase changes for the appropriate polarization must be used. This is the waveguide dispersion relation for guided modes, where ν is the mode number.

Electromagnetic Field Picture

Although the ray-optic approach can be used to determine the guided mode dispersion relation, it does not yield any information on the field profiles within the guide. To determine field profiles one must apply Maxwell's equations and the known boundary conditions. Of course, the field approach will also yield the dispersion relation determined above.

Consider the TE modes of the planar waveguide shown in figure 2.1. Maxwell's equations are

$$\nabla \times \mathbf{E} = -\partial \mathbf{B}/\partial t$$

$$\nabla \times \mathbf{H} = \partial \mathbf{D}/\partial t, \qquad 2\text{-}5$$

where the fields have the form

$$E = \mathcal{E} e^{j(k_z z - \omega t)} + \text{c.c.} \quad . \qquad 2\text{-}6$$

where c.c. refers to the complex conjugate. For a lossless dielectric material and monochromatic field, Maxwell's equations reduce to

$$\nabla \times E = j\omega\mu H$$

$$\nabla \times H = -j\omega\epsilon E. \qquad 2\text{-}7$$

These equations have been solved previously by Kogelnik (1979), Kapany and Burke (1972), Tein (1971), Hunsperger (1984), Hall (1987), and Marcuse (1974), to name a few. Their results are quoted here for brevity. For TE-polarized guided modes the solutions are

$$E_y = E_c e^{-\gamma_c (x-d)}, \qquad \text{for } d < x$$

$$E_y = E_f \cos(\kappa_f x - \phi_s), \qquad \text{for } 0 < x < d$$

$$E_y = E_s e^{\gamma_s x}, \qquad \text{for } x < 0, \qquad 2\text{-}8$$

where E_c, E_f, and E_s correspond to the peak intensities for the cover, film, and substrate regions, respectively, and

$$-\gamma^2_{s,c} = n^2_{s,c} k^2 - \beta^2,$$

$$\kappa_f{}^2 = n_f{}^2 k^2 - \beta^2. \qquad 2\text{-}9$$

The following boundary conditions are applied at the interfaces:

$$\hat{e}_n \cdot (B_1 - B_2) = 0 \qquad \hat{e}_n \cdot (D_1 - D_2) = 0$$

$$\hat{e}_n \times (E_1 - E_2) = 0 \qquad \hat{e}_n \times (H_1 - H_2) = 0 \,. \tag{2-10}$$

They yield the Fresnel phase-shifts,

$$\tan\phi_s = \gamma_s/\kappa_f, \qquad \tan\phi_c = \gamma_c/\kappa_f, \tag{2-11}$$

and the waveguide dispersion relation,

$$\nu\pi = \kappa_f d - \phi_s - \phi_c, \tag{2-12}$$

which is in agreement with that obtained from the ray-optic picture. This relation shows that, for a given film refractive index, the number of guided modes the waveguide will support is dependent upon the film thickness. In addition, the larger the refractive index difference between the film of a given thickness and the surrounding media the greater is the number of modes that will be supported.

The above solution is shown graphically for the three lowest order modes in figure 2.3. An interesting feature that can not be determined from the ray-optic picture is the existence of exponentially decaying (or evanescent) fields propagating in the substrate and superstrate. This is a direct result of the boundary condition that requires the electric field to be continuous across the interface. The relation between the peak fields E_s, E_f, and E_c is

$$E^2_f(n^2_f - N^2) = E^2_s(n^2_f - n^2_s) = E^2_c(n^2_f - n^2_c)\,, \tag{2-13}$$

where $N = \beta/k$ is the effective refractive index and

$$E^2_f = \sqrt{\frac{\mu_0}{\epsilon_0}}\,\frac{P}{Nd_{eff}}\,, \tag{2-14}$$

where

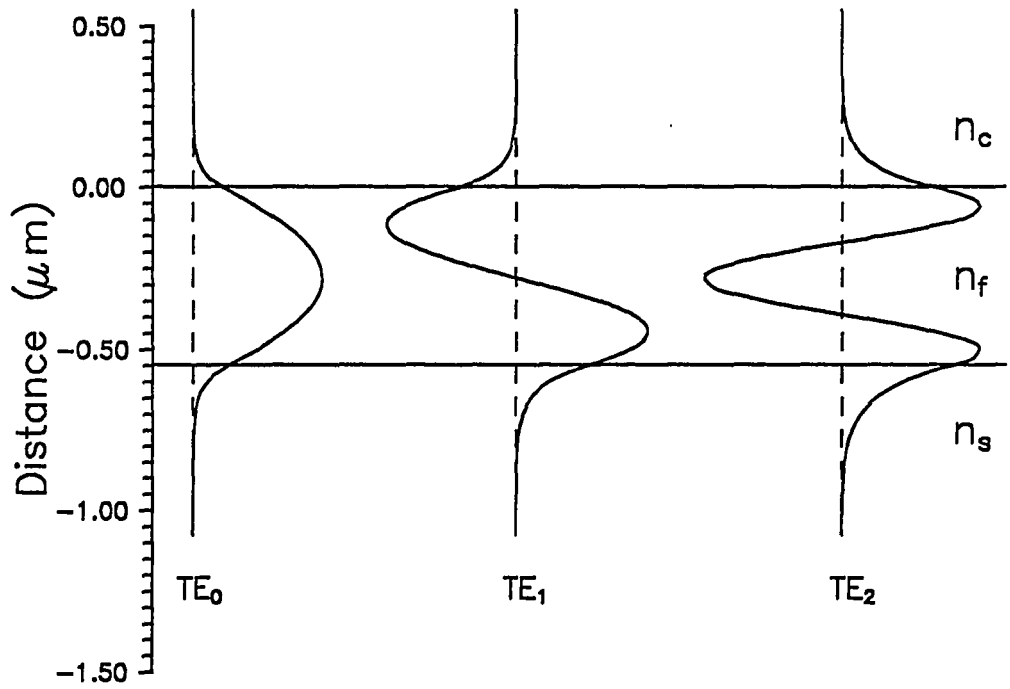

Figure 2.3. Field distributions of the three lowest order TE modes for a 0.55 μm thick ZnS planar waveguide. Profiles are normalized for equal input powers.

$$d_{eff} = d + \frac{1}{\gamma_s} + \frac{1}{\gamma_c}, \qquad 2\text{-}15$$

is the effective thickness of the waveguide and P is the power carried by the mode.

It is often useful to consider what fraction of the energy carried by the waveguide is actually contained within the physical boundaries of the waveguide. The confinement factor, Γ, defined as the ratio of the power contained within the waveguide boundaries to the total power carried by the mode is

$$\Gamma = \frac{2\beta}{\omega\mu} \frac{\int_0^d E^2_y(x)dx}{\sqrt{\epsilon_0/\mu_0} N d_{eff} E^2_f}, \qquad 2\text{-}16$$

which yields

$$\Gamma = \frac{h}{h_{eff}}\left[1 + \frac{\gamma_s}{hk^2(n^2_f - n^2_s)} + \frac{\gamma_c}{hk^2(n^2_f - n^2_c)}\right]. \qquad 2\text{-}17$$

The next section will show that the evanescent field allows for efficient coupling of energy into and out of a waveguide.

Waveguide Couplers

The previous section discussed the propagation of light in a thin film dielectric waveguide, but no mention was made of how to convert the energy of a propagating beam into a guided mode. This section will therefore discuss the methods for coupling light into a waveguide. Waveguide couplers can be separated into two categories: the transverse coupler and the distributed coupler. The transverse coupler works by bringing the energy of an external field to the polished end-face of a waveguide. Several geometries are shown in figure 2.4. The first

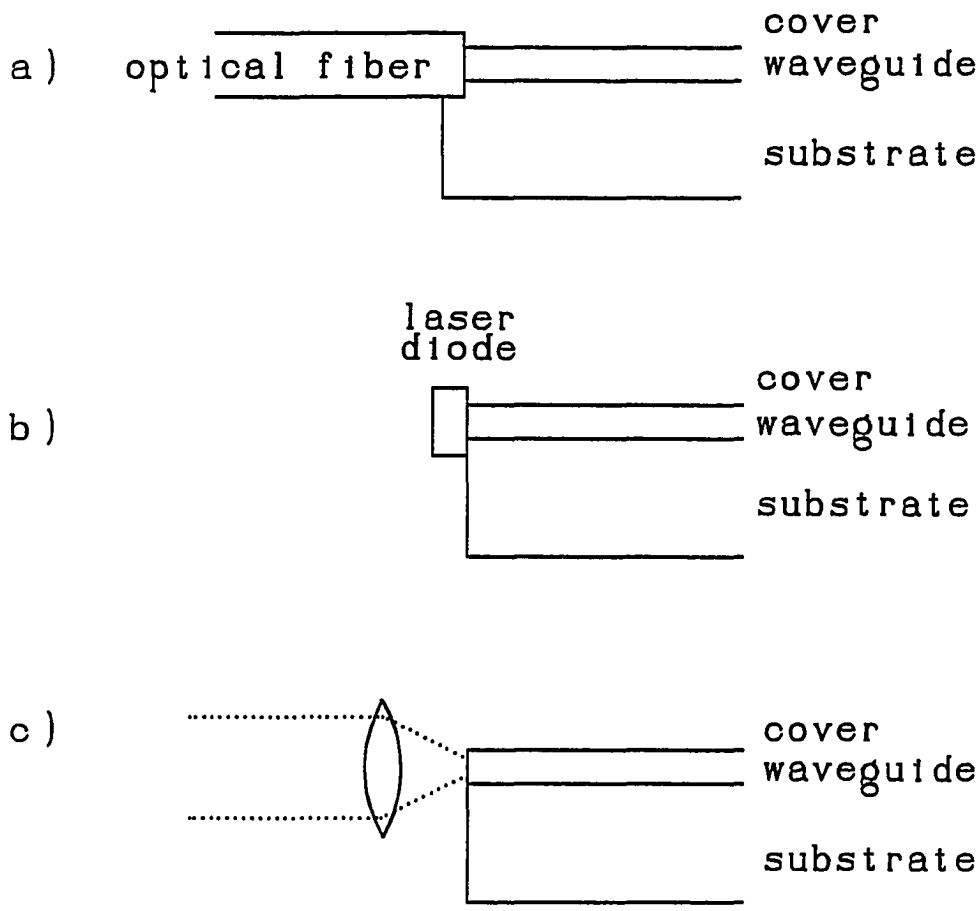

Figure 2.4. Typical end-fire coupling geometries.

two require the direct connection of either an optical fiber or a diode laser to the waveguide (Hall, Rice, and Zino, 1979; Hall, 1979). Although this form of coupler is useful in fiber optic communication, it is unsuitable when the waveguide itself is the primary object of study.

For efficient coupling, a transverse coupler requires matching the incident field profile with the waveguide mode profile being excited. Figure 2.4c shows a typical laboratory transverse coupler that uses a lens to focus the gaussian beam from a laser onto the end of the waveguide. Although efficient coupling to the lowest order mode is possible (> 90%), matching the profile for any other mode is difficult (Tien, 1971; Hunsperger, 1984). Coupling energy to higher order modes, however, is not impossible. In fact, it is highly probable, if there is any misalignment of the coupler or if the surface is not perfectly flat. Because alignment is so critical and the incident beam must be focused to a spot size on the order of one micron, transverse couplers are often impractical in laboratory situations. Distributed (or longitudinal) couplers on the other hand are efficient, easy to use, and do not suffer from the alignment problems of transverse couplers.

In a distributed coupler, coupling takes place over a region along the waveguide. Of course, distributed coupling is a reversible process, so that light will couple both into and out of the waveguide over the entire coupling region. Therefore, to maximize the input coupling efficiency, the coupling region must be terminated so that most of the energy is trapped in the waveguide. The two most useful distributed couplers are the grating and prism couplers. Because prism couplers were used for most of the research, they are emphasized in this section.

A prism coupler works by "frustrated" total internal reflection. As shown in figure 2.5, a laser beam is incident on the base of a prism with a refractive

index greater than that of the waveguide. If the angle of incidence is greater than the critical angle at the prism/air interface, light will be totally internally reflected and an evanescent field that decays exponentially away from the surface will exist beneath the prism interface. If the waveguide and prism are in close proximity, such that the evanescent fields of the guided mode to be excited and the prism overlap, the fields are weakly coupled and energy will be exchanged. This process is known as optical tunneling or frustrated total internal reflection.

Once again, total internal reflection is not the only requirement needed to build up the guided mode. For any given point along the coupling region, the coupled energy must interfere constructively with energy coupled at all other locations within the coupling region. This yields the phase matching condition that the z-component of the incident field must equal the propagation constant of the waveguide mode. This may be written

$$\beta = kn_p \sin\theta_p, \qquad 2\text{-}18$$

where β was defined in equation 2-2, θ_p is indicated in figure 2.5, and n_p is the prism refractive index. This phase match condition indicates that the coupling process is selective. That is, for a given angle of incidence on the prism base, only one guided mode can be excited. In the absence of inhomogeneities that scatter light, the angle must be changed to excite a different guided mode. This is an important advantage of distributed couplers over transverse couplers, allowing analysis of the individual modes. By adjusting parameters such as beam diameter and gap spacing between the prism and waveguide, it is possible to obtain a coupling efficiency of 80% for the case of an incident beam with a Gaussian profile, using a prism coupler with a uniform air gap (Ulrich, 1970). but

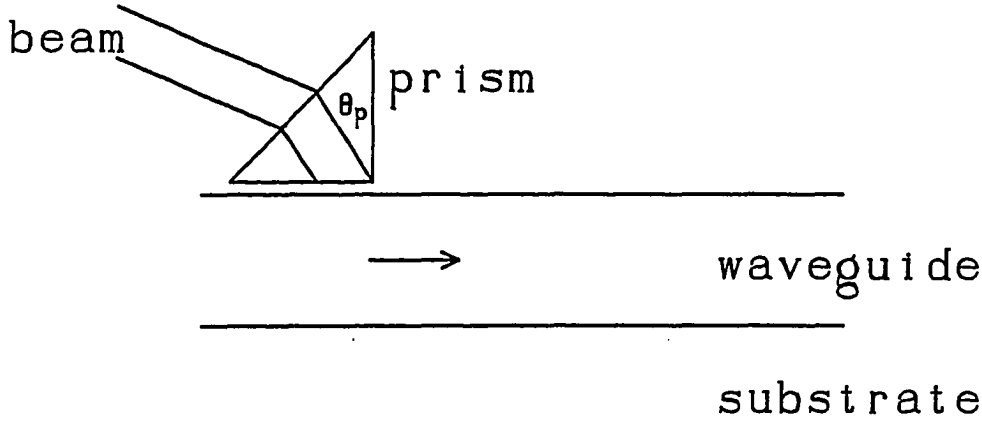

Figure 2.5. The prism coupler.

efficiencies of 20 - 60% are more typical (Tien, 1971).

Another type of distributed coupler, the grating coupler, is shown in figure 2.6. Instead of using total internal reflection, the grating uses diffraction to couple light into one of the guided modes. The grating coupler must obey the same phase matching constraints as the prism coupler. The phase match condition may be written

$$\beta = k\sin\theta + 2\nu\pi/\Lambda, \quad \nu = 0,\pm1,\pm2,\cdots, \qquad 2\text{-}19$$

where Λ is the grating periodicity, θ is the angle in figure 2.6, and ν is the diffracted order.

By appropriate selection of grating periodicity Λ, groove profile, and etch depth the coupling efficiency may be optimized. By selecting a small grating period, only one diffracted order will exist and energy will not be lost to higher diffracted orders. Gratings can be fabricated with many different profiles from sinusoidal to rectangular. The rectangular grating is the most efficient symmetric profile (Tamir and Peng, 1977). For the symmetric grating, however, energy will still be lost to both the specularly reflected and transmitted beams. These losses can be overcome if the grating is given an asymmetric profile so that the reflected and transmitted energy may be reduced (Born and Wolf, 1980). The grating depth has the most impact on the coupling length. The depth should be chosen such that the coupling length is optimized with respect to the diameter of the incident beam.

The grating coupler offers several advantages over prisms. Because a grating is fabricated on or beneath a thin film waveguide, the coupling efficiency will not change with repeated use, as it will if a prism has to be remounted onto the guide. That remounting process can also damage the waveguide. One

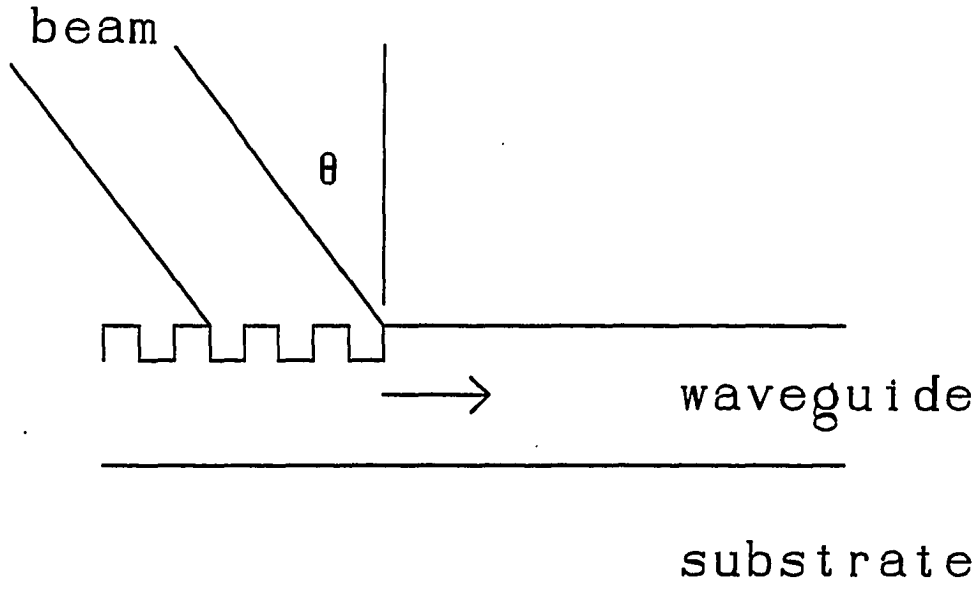

Figure 2.6. The grating coupler.

disadvantage of the grating is that it cannot be relocated to a different position on the waveguide.

Light Propagation in Dielectric Waveguides

The first section of this chapter discussed the basic principles of a lossless slab waveguide that interacted with a monochromatic plane wave. The electromagnetic field solutions (equation 2-8) show that the mode profiles do not change with time and vary only in the transverse direction. Therefore, upon propagation in an ideal, lossless waveguide, the mode remains unchanged in amplitude and field distribution. Unfortunately, all dielectric waveguides exhibit losses (as discussed in the next section). The losses in optical fibers are very low ($\cong$ 1.0 dB/km) and are caused by the intrinsic Rayleigh scattering of the material. Losses in slab waveguides, on the other hand, are significantly higher and are caused by numerous mechanisms including interface scattering; internal defect scattering, and absorption.

Even in the absence of loss, there are other limitations to waveguide performance. The major application for optical waveguides (either fibers or planar) is high speed data transmission. Because no information can be carried on an infinite monochromatic plane wave, short pulses of light must be used. The shorter the pulse, the higher the data rate. Fourier analysis shows that a temporal light pulse is not monochromatic but is a superposition of plane waves with different frequencies (Goodman, 1968; Gaskill, 1978). The actual frequency spectrum of a pulse is dependent on the pulse shape but in general the shorter the pulse, the broader the frequency spectrum. Therefore, in data transmission applications dispersion becomes important. Waveguides exhibit material dispersion, and two forms of modal dispersion.

Material dispersion is introduced because the refractive index changes with wavelength. Therefore, the group velocities for light of different frequencies will be different and a light pulse will broaden as it propagates. Usually, this effect is slight, but it is not negligible for high speed data transmission. For multimode waveguides, a light pulse that is shared by many guided modes will split into several pulses as it propagates because the group velocity is different for each mode. This "multimode dispersion" exists even in the absence of material dispersion. Modal dispersion also exists within a single mode because the transverse resonance condition is wavelength dependent. The different frequency components within a pulse will propagate at slightly different values of β.

Waveguide Loss Mechanisms

Scattering Theories

The previous section describing basic waveguide principles assumes that the waveguides are homogeneous, isotropic, and lossless with plane parallel surfaces. Experimentally, this is not the case because thin films exhibit a very complex microstructure which is described in detail later in this chapter. The microstructure introduces deviations from an ideal homogeneous and isotropic film. These deviations, along with irregularities at the substrate/film interface, introduce scattering and absorptive losses into a waveguide structure. Absorption manifests itself as the conversion of optical energy to phonon energy and the generation of heat. These losses may be caused by impurities, atomic defects and the intrinsic material properties. Scattering, on the other hand, is the coupling of optical energy from one guided mode to radiation modes or other guided modes. There are several contributors to scattering losses including defects, scratches, interface scattering, volume scattering caused by index inhomogeneities, and the intrinsic Rayleigh

scattering of the material. The best waveguide performance will be achieved when the intrinsic material properties are the only loss mechanisms present.

The primary focus of this doctoral research is to observe the effect of changes in film microstructure on the propagation losses in ZnS waveguides. For this to be possible, losses caused by film microstructure must dominate losses introduced by substrate surface roughness. Over the past two decades several theories have been published that relate interface roughness to waveguide attenuation. These include a ray-optic approach by Wlodarczyk (1987), coupled mode approaches by Arnz and Ponath (1986) and Findakly, Garmire, and Moon (1979), and perturbation theory by Ames and Hall (1983), Walter and Houghton (1978), and Marcuse (1969, 1972). In this thesis, the coupled mode theory of Marcuse is used to determine the approximate magnitude of the scatter loss contributed from interface roughness. Although this theory is two-dimensional in nature, Marcuse expects that the results are correct within an order of magnitude. For brevity, the perturbation approach of Marcuse is outlined and the results of calculations for a ZnS film are presented. For more information on the theory the interested reader may refer to the literature.

The theory utilizes a perturbation approach to describe the losses that the lowest order TE mode suffers because of roughness introduced on one of the interfaces of a symmetric waveguide. The theory is modified slightly here for the case of an asymmetric guide with two rough interfaces. The geometry is shown in figure 2.7. The wall imperfections may be described by an index distribution

$$n^2(x,z) = n_0^2(x,z) + \Delta n^2(x,z). \qquad 2\text{-}20$$

The first term on the right describes the ideal waveguide while the second term

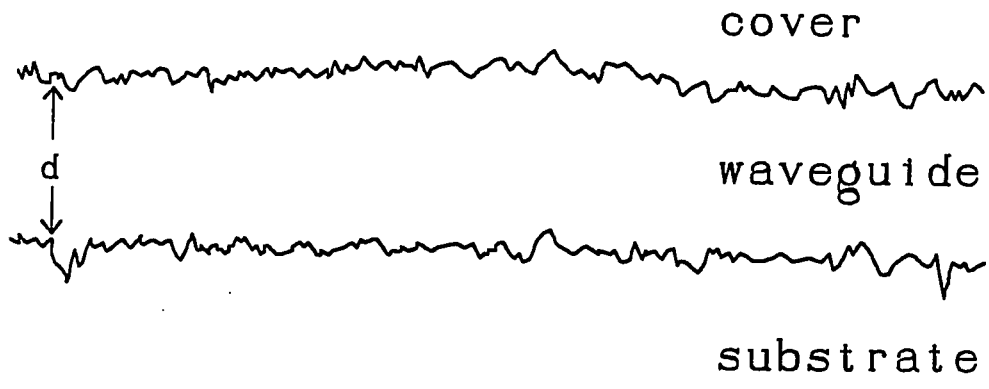

Figure 2.7. Dielectric planar waveguide with surface imperfections.

describes the deviation from perfect flatness. The field distribution in the lossy waveguide must be a solution of the perturbed wave equation

$$\frac{\partial^2 E_y}{\partial x^2} + \frac{\partial^2 E_y}{\partial z^2} = (n_0^2 + \Delta n^2)k^2 E_y. \qquad 2\text{-}21$$

The solution may be expressed as the sum over all the allowed guided modes plus the sum over the continuum of radiation modes

$$E_y = \sum_n C_n(z)\, E_n + \int_0^\infty g(\rho,z)E(\rho)d\rho, \qquad 2\text{-}22$$

where ρ is the transverse propagation constant for the continuum of modes

$$\rho = \sqrt{n^2_{s,c}k^2 - \beta^2} \qquad 2\text{-}23$$

The expansion coefficients $C_n(z)$ and $g(\rho,z)$ may be determined by generating and solving a set of first order coupled wave equations. Once the expansion coefficients are known, the normalized power loss, $\Delta P/P$, may be written

$$\frac{\Delta P}{P} = \sum_{n=1}^{\infty} [|C_n^{(+)}(L)|^2 + |C_n^{(-)}(0)|^2] + \int_0^\infty [|g^{(+)}(\rho,L)|^2 + |g^{(-)}(\rho,0)|^2]\, d\rho, \qquad 2\text{-}24$$

where the (+) and (-) refer to forward and backward scattered energy, respectively. According to Marcuse, the integral equation (2-24) can only be solved approximately and first order perturbation theory should therefore be applied. This is valid not only for $n_f^2 - n^2_{c,s} \ll 1$ but also when $n_f^2 - n^2_{c,s}$ is large and the surface roughness of the interface is sufficiently small.

Equation 2-24 gives the loss of a guided mode for a well defined deviation

in the boundary of a waveguide. Polished surfaces seldom have a well defined surface but are described statistically. It is then possible to take an ensemble average of 2-24 if the statistics of the surface can be described. Marcuse employs an exponential surface correlation function of the form

$$R(u) = \delta^2 e^{-|u|/B}, \qquad 2\text{-}25$$

to describe the surface statistics, where δ is the rms surface roughness and B is the surface correlation length. Performing the average yields

$$\left\langle \frac{\Delta P}{P} \right\rangle_{av} = \frac{\delta^2 k^4 L}{2\pi B} (n_f^2 - n_{c,s}^2)^2 \cdot \int_{-n_{c,s}k}^{n_{c,s}k} \left[\frac{\rho \cos^2(\kappa_0 d/2)}{\left[(\beta_0 - \beta)^2 + \frac{1}{B^2}\right]\left[\beta_0 d + \frac{\beta_0}{\gamma_0}\right]} \cdot f(\rho,\sigma) \right] d\beta \qquad 2\text{-}26$$

$$f(\rho,\sigma) = \frac{\cos^2(\sigma d/2)}{\rho^2 \cos^2(\sigma d/2) + \sigma^2 \sin^2(\sigma d/2)} + \frac{\sin^2(\sigma d/2)}{\rho^2 \sin^2(\sigma d/2) + \sigma^2 \cos^2(\sigma d/2)}, \qquad 2\text{-}27$$

where

$$\begin{aligned} \sigma &= \sqrt{k^2 n_f^2 - \beta^2} \\ \rho &= \sqrt{k^2 n_{c,s}^2 - \beta^2} \\ \kappa_0 &= \sqrt{k^2 n_f^2 - \beta_0^2} \\ \gamma_0 &= \sqrt{k^2 n_f^2 - \beta_0^2}, \end{aligned} \qquad 2\text{-}28$$

and β_0 is the solution to the dispersion relation for the fundamental guided mode of the unperturbed waveguide (Marcuse, 1969). The perturbation theory holds only for small values of $\Delta P/P$. However, it is reasonable to expect that no appreciable amount of power conversion from the radiation field to the guided mode occurs. The incremental power loss, $\Delta P/P = -\alpha L$, is therefore the same for any section of the guide so that the total scattering loss into the continuum of radiation modes is

$$P(z) = P_0 e^{-\alpha L} \quad . \qquad 2\text{-}29$$

By convention waveguide attenuation is usually measured in dB

$$\text{Loss (dB)} = 10 \log_{10}(P_0/P). \qquad 2\text{-}30$$

Therefore

$$\text{Loss (dB/cm)} = 10 \left\langle \frac{\Delta P}{P} \right\rangle_{av} \log_{10} e. \qquad 2\text{-}31$$

Figures 2.8 through 2.12 show numerical integrations of equation 2-26. Figures 2.8 and 2.9 are for a film of refractive index 1.01 with $\delta = 0.9$ nm surrounded by vacuum. To determine if our software was producing the correct results, the parameters chosen were the same as those used by Marcuse. Figure 2.8 agrees with Marcuse's results. Figure 2.9 shows the wavelength dependence of waveguide loss. Because of the Rayleigh-like scattering a $1/\lambda^4$ dependence is expected. However a $1/\lambda^{2.2}$ dependence is observed as a result of the two-dimensional nature of the theory and the modal properties of the field.

To determine the effects of surface roughness on the losses of a ZnS film, the theory was applied to a film of refractive index 2.35 on a substrate with refractive index 1.46. The results are shown in figures 2.10 through 2.12 for scattering from the film/substrate interface assuming an rms roughness of 0.4nm, which is representative of the surface roughness for the Si wafers used in this research. Figure 2.10 shows that for a wavelength of 600nm the losses peak at approximately 0.1 dB/cm. This is two orders of magnitude lower than the losses observed experimentally in conventionally evaporated ZnS films ($\cong$ 10.0 dB/cm). The plot also shows that loss does not decrease monotonically with increasing

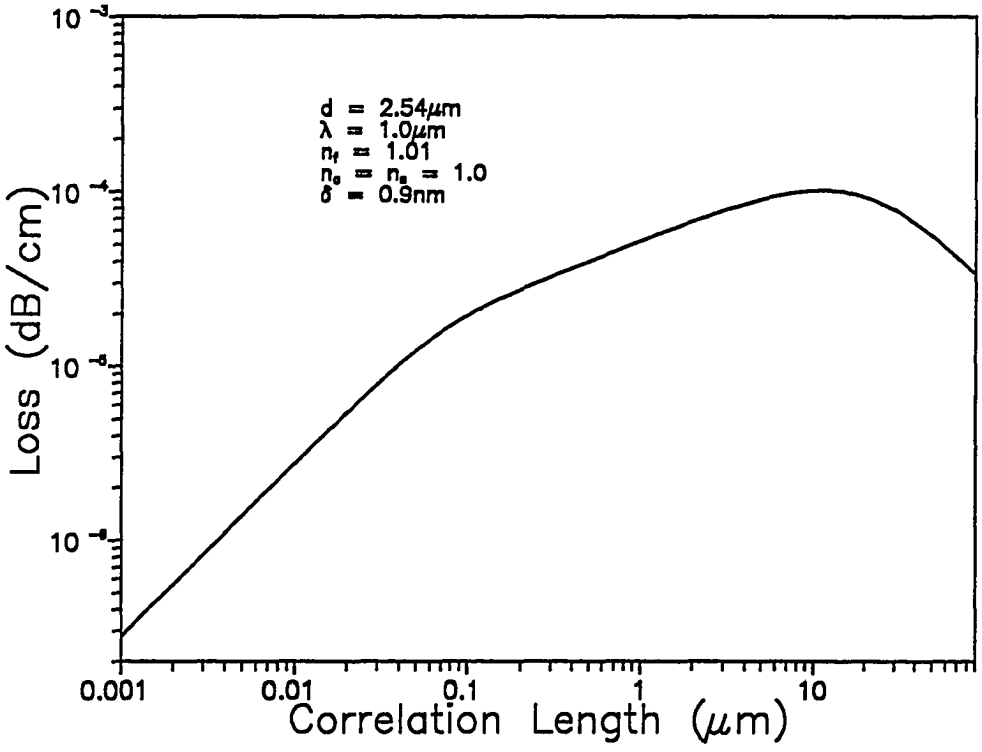

Figure 2.8. Losses caused by surface scatter from a waveguide with $n_f = 1.01$ as a function of surface correlation length. Scattering occurs at one surface.

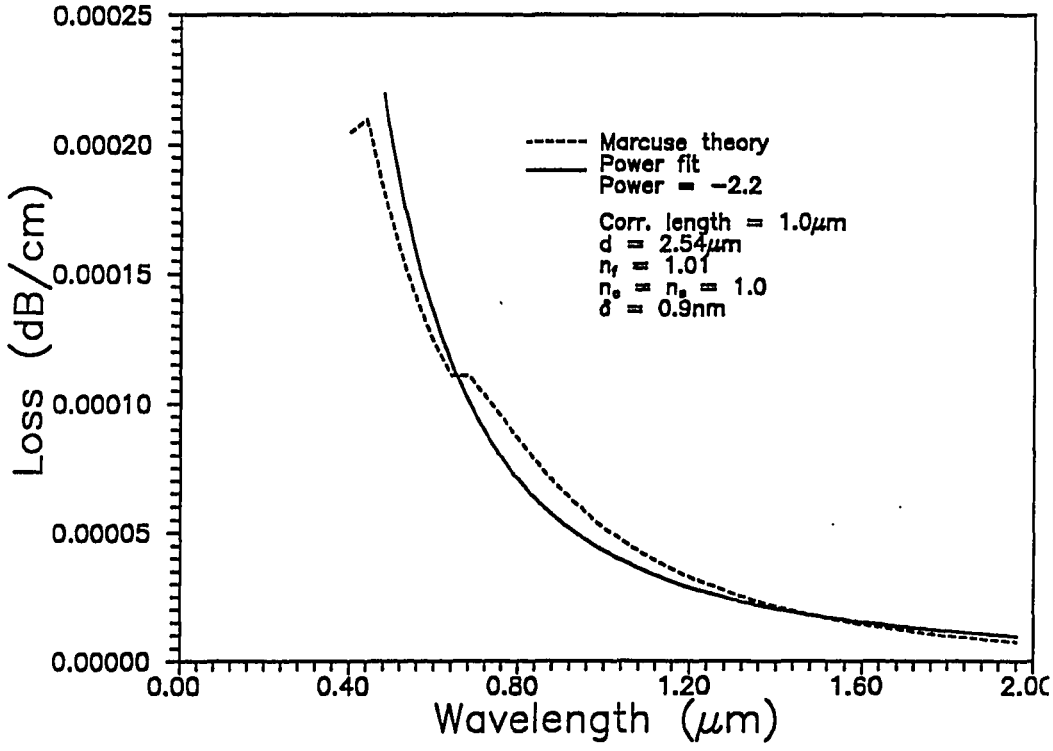

Figure 2.9. Losses caused by surface scatter from a waveguide with n_f = 1.01 as a function of wavelength.

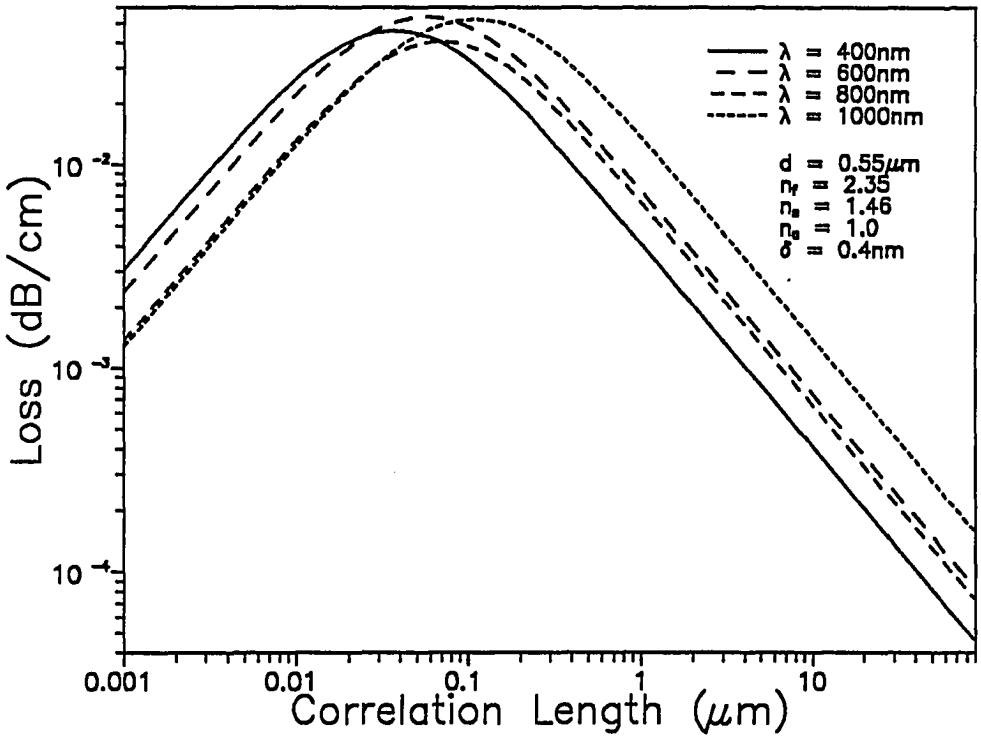

Figure 2.10. Loss versus surface correlation length for a ZnS (n_f = 2.35) thin film waveguide.

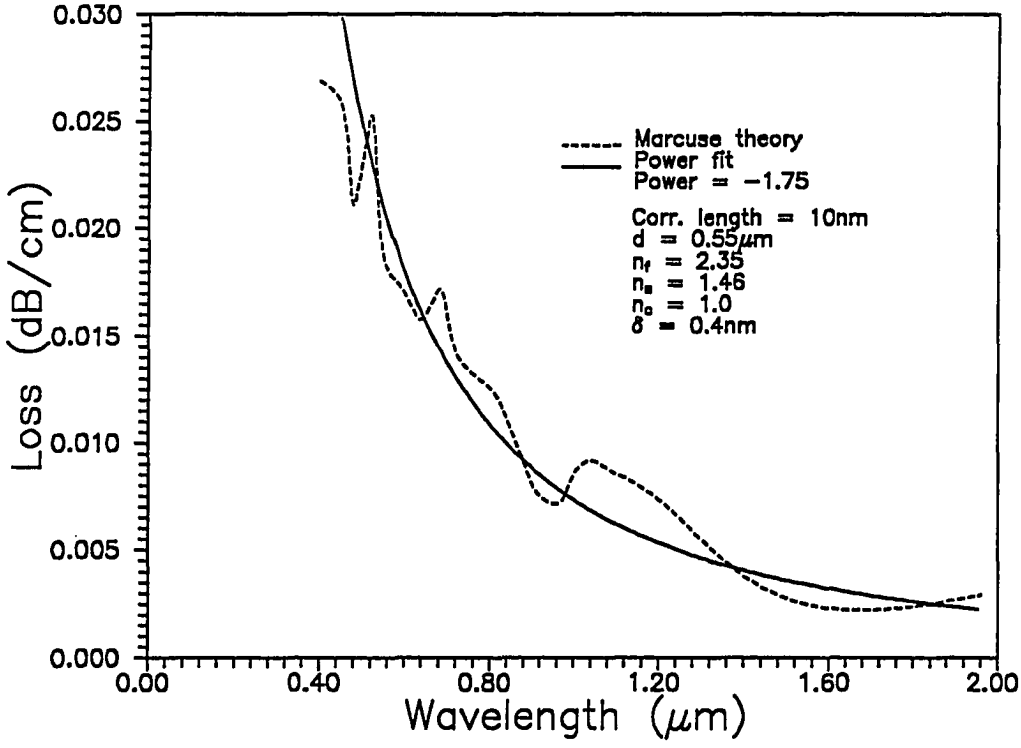

Figure 2.11. Loss versus wavelength for a ZnS thin film waveguide.

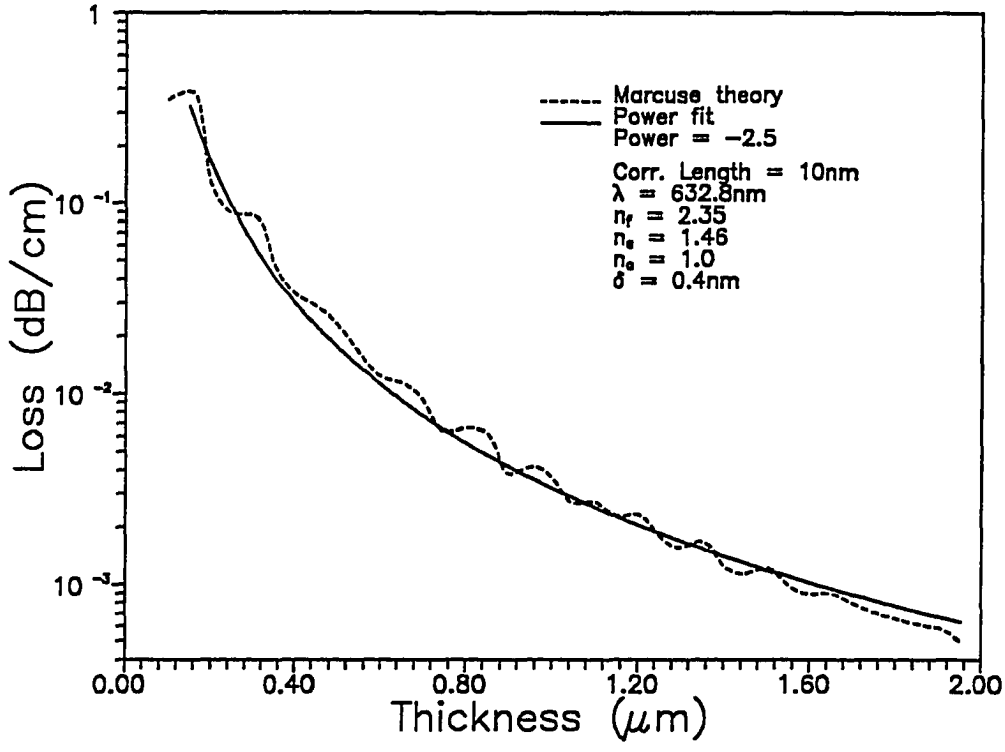

Figure 2.12. Loss versus thickness for a ZnS thin film waveguide.

wavelength as would be expected from true Rayleigh scattering. This is more evident in figure 2.11 where loss is plotted as a function of wavelength. A power fit to the data shows that overall, losses decrease as $1/\lambda^2$ but there are large deviations from this fit. The higher losses at particular wavelengths may be attributed to resonances associated with the leaky modes of the radiation fields (Marcuse, 1974; Findakly, Garmire, and Moon 1979). The same resonant behavior can be observed in figure 2.12 of loss versus thickness.

Even if the theoretical calculations are an underestimation by an order of magnitude, the losses for ZnS waveguides are apparently not dominated by scattering from the film/substrate interface. The majority of the losses must therefore be caused by the microstructure of the film, which may have a columnar or grain like structure that may lead to enhancement of the surface roughness at the film/air interface. The nucleation and growth of the film may also introduce index fluctuations within the film that can also introduce significant waveguide losses. Whether surface or volume effects dominate total losses will depend on material, deposition method, and guided mode field distribution. Volume effects are easily observed in ion-exchanged semiconductor doped glass waveguides, where a soda-lime or borosilicate glass is doped with small grains of CdS_xSe_{1-x}. Those crystallites increase waveguide losses from < 0.1 dB/cm to 3.0 dB/cm (Gabel, 1988).

At present, apparently because of the complexity involved, no theory describing the out-of-plane scatter from a polycrystalline film has been found. However, several studies relate interface roughness and index inhomogeneities to the angular distribution of scattered light. A two-dimensional approach to the angular scattering from interface roughness presented by Hall in 1980 was later expanded to three dimensions (Hall, 1981). Both the theories show that the angular distribution

of light scattered out of the waveguide is not uniform, but is single lobed and peaks in the forward scattered direction. The exact angle of the peak is dependent on the correlation length of the waveguide surface. Bradley and Hall (1982) show that the angular distribution of scattered light from a sputtered Corning 7059 glass waveguide agrees with the above theories.

The scattering from slab waveguides having refractive index fluctuations is studied using a stationary phase method by Miyanaga, Imai, and Asakura (1978). They show that strong multiple peaks in the forward direction occur in the substrate region when the correlation length of refractive-index inhomogeneities in the direction of guided light propagation is much greater than the wavelength of light. By combining perturbation and stationary phase methods, scattering from both index inhomogeneities and surface roughness was treated (Miyanaga, Asukara, and Imai 1979, 1980). The results show that for a waveguide with refractive index 1.01 surrounded by air and $d/\lambda = 10.0$, the effect of index inhomogeneities is pronounced in comparison with that of surface roughness. Therefore the scattering pattern is determined primarily by the correlation length of refractive index fluctuations. The correlation between both imperfections in asymmetric waveguides is also described. It is found that the degree of correlation between the imperfections does not affect the power radiated into the cover while it slightly modifies the power radiated into the substrate.

A simpler geometry, with cylindrical columns, has been used to calculate the in-plane scatter (Modavis and Hall, 1984; Hall, 1985). They employed a Green's function approach to determine the in-plane scatter from both surface roughness and refractive index fluctuations. For the case of a slab waveguide (glass surrounded by air and quartz) in which the relative surface roughness δ/d is

comparable to the relative refractive index fluctuation $\Delta n/n_g$, it was found that in-plane scattering caused by index fluctuations dominated surface scattering by at least an order of magnitude.

Absorption Processes

Absorptive losses are usually caused by a photon-electron interaction at a resonance or band edge. These losses are extremely wavelength dependent, strong at some wavelengths and nearly nonexistent at others. Absorption may also be caused by a departure from perfect film stoichiometry and structure. This may result in increased absorption across the visible spectrum.

Band edge absorption is well understood and is described in detail in any introductory solid state physics text (eg. Kittel, 1976). Photons with energy greater than the band gap of a semiconductor crystal will be absorbed, producing electron transitions from the valence band to the conduction band. This absorption will continue as long as either donor states exist near the conduction band or acceptor states exist near the valence band. For high intensities, the number of accepter or donor states will decrease and this absorption will saturate.

Material impurities can also contribute to absorption. These losses are usually extremely wavelength dependent and are caused by resonances with vibrational and rotational states of the impurity ion. These resonances typically occur in the near infrared and near ultraviolet. OH^- ions, for example, absorb at 725, 950, 1250, and 1390 nm. Deviations from perfect stoichiometry will affect material absorption by modifying the band structure and possibly introducing unfilled or dangling bonds. This will most likely shift the band edge in a semiconductor toward longer wavelengths and lengthen the tail, causing an increase in absorption through the visible spectrum.

Mode Dependence

So far, both volume and surface loss mechanisms have been discussed, but no mention has been made of their dependence on the modal properties of the guide. Because the electric field interacts *differently* with volume and surface mechanisms, measurement of the modal losses can yield information on the dominant loss mechanisms. The scattering strength is a function of the overlap integral of the scatterer, guided field, and radiated field. Thus, for surface roughness, the guided mode field strength at the interface is the most important, while for volume scattering and absorption, the power distribution within the guide will determine the loss. Therefore, it is possible to estimate the effects that different loss mechanisms will have on the modal properties by examining the field profiles of the different modes. The solutions to Maxwell's equations for guided modes (equation 2-8) show that the field amplitudes at the waveguide interfaces are higher for the higher order modes (figure 2.13). The field is also less confined within the waveguide as the mode number is increased (figure 2.13). That is, there is more power propagating in the substrate and superstrate for the higher order modes. Therefore, if the losses are caused solely by surface scattering the losses should be larger for the higher order modes and should follow the solid line in figure 2.13. If, on the other hand, the losses are caused solely by volume mechanisms such as absorption and internal scattering, the losses should decrease with increasing mode number and should follow the dashed line. For most waveguides, both surface and volume mechanisms will contribute to total waveguide loss and the modal dependence of the loss will deviate from the curves of figure 2.13.

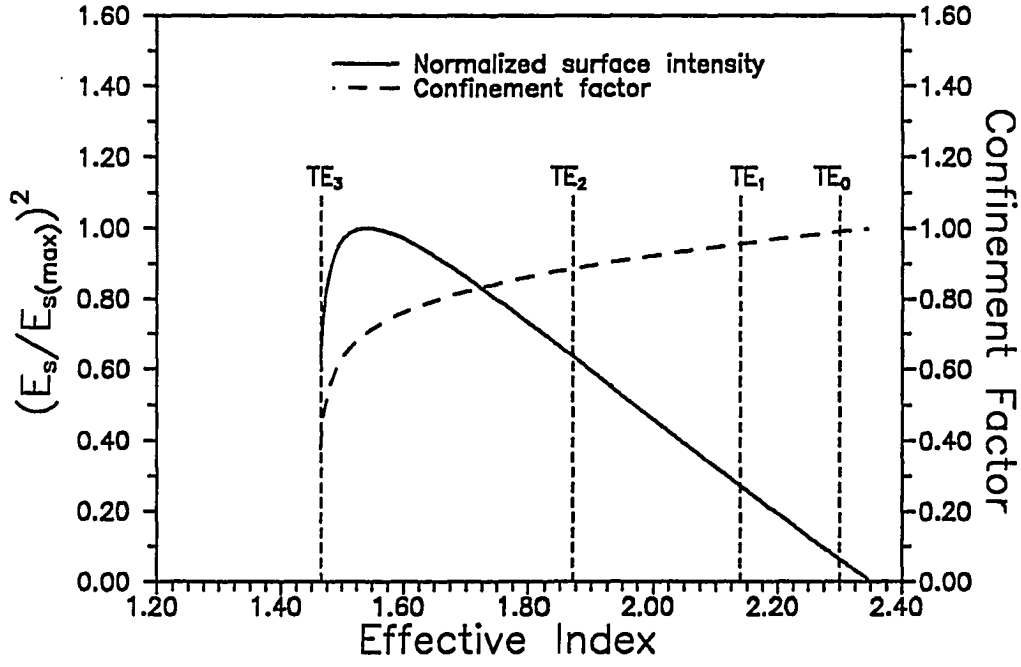

Figure 2.13. Normalized surface intensity and confinement factor versus waveguide effective index for a ZnS (n = 2.35) thin film waveguide of thickness 0.55μm, sufficient to support four TE modes. Surface intensity (solid line) is determined from equations 2-13 and 2-14. Confinement factor (dashed line) is determined from equation 2-17). Vertical lines show effective indices of the guided modes.

Thin Film Microstructure

When thin film materials were first used for the development of optical filters, it was assumed that the properties of the film were identical to those of a thin slab of bulk material. Deviations in optical performance, and the development of high resolution microscopies such as scanning electron microscopy, transmission electron microscopy, and scanning tunneling microscopy showed that this is not the case. In fact, the structure of a thin film can vary significantly from the bulk and this variation may affect the optical and mechanical properties of the film. Refractive index is usually reduced, but may be higher for some semiconductor materials, and the films may have higher losses, less stability, and reduced durability. The previous sections describe the various mechanisms that introduce losses in a thin film. The results presented in chapter 4 of this dissertation suggest that losses for vacuum deposited ZnS films are not dominated by substrate surface roughness, but result from the films internal microstructure.

This section presents a description of thin film microstructure and how it contributes to waveguide scattering losses. The microstructure of a film can usually be described by either a polycrystalline or columnar structure. Because research on these structures has been extensively reported in the literature, only the features that introduce losses will be described. The interested reader is directed to the literature for more information (Chopra, 1969; Pliskin, 1977; Macleod, 1986; Maissel and Glang, 1970).

Columnar Structure

Electron microscopy has shown that vacuum deposited thin film layers have a predominantly columnar structure with the columns growing nearly normal to the substrate (Pearson, 1970; Lissberger and Pearson, 1976; Pulker and Jung, 1971; Guenther and Pulker, 1976). This microstructure is directly attributable to the deposition conditions as shown by Movchan and Demchishin (1969), and Thornton (1974) who investigated the effects of substrate temperature and residual gases on the structure of evaporated and sputtered films, respectively. Those results show that the ratio of substrate temperature to the melting temperature of the evaporant is an important parameter. For ratios less than 0.3, the structure of the film is very columnar with the columns running parallel to the direction of growth. Increasing the ratio will increase adatom mobility resulting in higher film density. Further increase of the ratio will eventually lead to a film with bulk density. Increased residual gas pressure also induces a more pronounced columnar growth.

Because the melting points of the most common thin film materials are high, the substrate temperature is usually a small fraction of the evaporant melting point. Therefore, unless special procedures, such as ion assisted deposition or ion beam sputtering, are employed, the films invariably exhibit a columnar structure. The columns, usually cylindrical in shape, are tens of nanometers in diameter and are separated from each other by voids which run completely across the film. Although the melting point of ZnS (2100K) suggests that ZnS films will exhibit a pronounced columnar structure for ambient temperature depositions, ZnS is unusual in that Zn and S dissociate, which changes the kinetics. Therefore, it may be more appropriate to use the melting temperatures for the constituents (388K for S and 692K for Zn) which indicate that ZnS films will have a higher density. The

columnar structure makes the film porous and the packing density p, defined as:

$$p = \frac{\text{volume of solid part of film (i.e. columns)}}{\text{Total volume of film (i.e. voids plus columns)}} , \qquad 2\text{-}32$$

is a measure of that porosity. The packing density is usually in the range of 0.75 - 1.0 for thin film materials, and most often 0.8 - 0.95. This exposes large areas of the film to the surrounding environment, and water molecules may penetrate the film. At low humidities, water forms an adsorbed layer over the surfaces of the columns while at higher humidities the voids are filled with liquid water caused by capillary condensation.

The process of water adsorption may be reversed by heating the film and water molecules will be desorbed from the film. An important consequence of the desorption process is a resultant change in the refractive index of the film. The film refractive index, n_f, may be approximated by

$$n_f = pn_m + (1-p)n_v , \qquad 2\text{-}33$$

where n_m is the refractive index of the columns, n_v is the refractive index of the voids, and p is the packing density of the film. The void index will usually take on a value between 1.0 and 1.33, depending on the amount of water adsorbed by the film. Effects of water adsorption on the refractive index of ZnS films have been observed by Svensson (1988) and Roche, Bertrand, and Pelletier (1976). Svensson used an Ar ion laser coupled into a 1.0 μm thick ZnS waveguide to observe the effects of nonlinear distributed coupling. It was found that if the laser power was held constant, there was a relatively large and slow decrease of the output power with time. This was apparently caused by a decrease in the input coupling efficiency resulting from a small change in film refractive index. The

refractive index change was attributed to the desorption of water caused by heating of the film by the Ar ion laser. Similar index variations were observed by Roche, Bertrand, and Pelletier, (1976), but the authors were cautious in attributing the effect to a water desorption process.

Variations in refractive index and water adsorption are not the only effects associated with columnar structure. The voids between the columns can also introduce losses caused by scattering. Because the columns introduce refractive index inhomogeneities, losses will result from both in-plane and out-of-plane scattering, as was discussed previously. The columnar structure can also introduce out-of-plane scattering caused by a departure from the flat surfaces of the ideal film. Such departures can be caused by the roughness of the substrate or the columnar structure of the film that results in a nodular appearance of the film boundaries. If the atomic mobility at the substrate during deposition is small, the rms deviation in film thickness , δ, introduced by the columnar structure may be described by Poisson statistics and is given by

$$\delta = \sqrt{d} \ , \qquad 2\text{-}34$$

where d is the film thickness (Chopra, 1969). Usually some surface diffusion of the film atoms after impingement is possible. This has the effect of reducing surface roughness by filling in the valleys and leveling the peaks. It has been shown experimentally that the losses in conventionally deposited Al_2O_3 films are dominated by the enhanced surface roughness introduced by the columnar growth of the film (Binh, Netterfield, and Martin, 1985). For ZnS films, however, there is no evidence of increased surface roughness from interferometric topology (WYKO) or SEM measurements.

Thin films that exhibit columnar structure and low packing densities also exhibit tensile stress. This stress is caused by a coulombic attraction between adjacent columns. Usually the stress does not pose a problem to overall film performance. However, if the adhesion to the substrate is low, delamination may occur, and if the substrate is not flexible enough to compensate for the tensile stress, the film will crack and fissures may be observed. In some cases the stress failure may cause only microcracks at the substrate surface. These cracks may not be observable with optical microscopes, but could introduce large waveguide losses.

Thin films with high packing densities may exhibit compressive stress. To reduce the internal forces, the film must expand. Once again, the stress does not usually cause much of a problem unless it overcomes film adhesion. For compressive stress this will be observed by delamination and buckling of the film material.

To increase the film density and reduce the adverse effects caused by the columnar structure of the films, the mobility of the adatoms at the substrate during deposition must be increased. The work of Movchan and Demchishin (1969) suggests that the density of films deposited onto heated substrates will increase with temperature because of the increased adatom mobility. Unfortunately, the substrate temperatures required to produce film densities close to that of the bulk are not feasible. It is possible, however, to increase the effective energy and momentum of the adatoms by bombarding the growing film with low energy ions (100 - 2000 eV). Essentially, the ions bombard the surface of a film and transfer energy and momentum to the atoms on the surface. This energy transfer allows the atom to move around on the surface and fill surface voids, which results in a denser film. In fact, ion-assisted processes produce films with excellent optical and mechanical

properties. Water adsorption is reduced and the refractive index is close to that of the bulk and does not change on exposure to the environment. Film densification also reduces the tensile stress.

Polycrystalline Structure

Some materials, such as ZnS, have a very high packing density (0.95 - 1.0) when deposited at ambient temperature and thus do not suffer as extensively from the problems inherent in films with lower packing densities. Most often, however, films with high packing densities have larger crystallites than films with lower packing densities. For example, at ambient temperature ZnS films have an average crystallite size of 15 nm while Al_2O_3 films have an average crystallite size of 1 nm. The crystallite size of these films increases with the surface mobility of adatoms and clusters during deposition (Chopra, 1969). Therefore the crystallite size should increase with increasing substrate temperature and deposition rate. Inversely, the crystallite size should decrease until the film becomes amorphous as the substrate temperature during deposition is decreased. Although polycrystalline films still exhibit a slight columnar structure, their optical and mechanical properties are usually governed by the crystalline structure.

The crystal structure of a thin film usually reproduces the structure of the bulk material. The size and orientation of the crystallites, however, can vary substantially depending on the adatom mobility during deposition. Crystallites are often preferentially oriented with respect to the substrate and are several tens of nanometers in diameter. The crystallites in our ZnS films, for example, are cubic and preferentially oriented with either the (220) or (111) crystal planes parallel to the substrate surface. The crystals are most likely randomly oriented within the plane, that is, they are rotated about an axis normal to the plane of the film.

Although the packing densities of polycrystalline films are high, they are not unity. Therefore these films still have voids that separate the crystallites. On exposure to the environment, water will be adsorbed into the film as was described in the previous section. The effects of water adsorption, however, are not as pronounced for polycrystalline films because of their high density.

As was discussed previously, the rms roughness of the film surface is a source of scattering losses. For films that grow preferentially along certain crystal faces, the roughness of the film surface will be enhanced as the surface mobility is increased (as compared to the decrease in rms roughness produced by the evaporation of amorphous films). This enhanced roughness will increase the waveguide losses. The crystallites within the film will also introduce losses. Because the film is built up of oriented grains that are separated by defects or voids, there are internal refractive index fluctuations which result in increased scattering. Unlike internal scattering from a film exhibiting columnar structure, out-of-plane scattering from polycrystalline films can be significant because the voids are not necessarily parallel to the direction of film growth.

To reduce waveguide losses in a polycrystalline film, the adatom mobility during deposition must be reduced. The most effective technique is to cool the substrate, but this may introduce other problems such as contamination. This will be discussed in more detail in chapter 4.

Recent Experimental Studies

Waveguides may be fabricated by modifying a thin layer of the bulk material through in-diffusion or ion-exchange, by spin coating a substrate with a liquid followed by heating to harden and anneal the coating, or by vacuum

depositing a thin film coating. The first two methods yield waveguides with the lowest losses but are limited by the availability of appropriate materials. The third method is the most versatile because of the many materials available, but the waveguides typically exhibit higher losses. The primary material in use for the fabrication of integrated electro-optic devices is Ti-diffused $LiNbO_3$, which can be fabricated with losses as low as 0.05 dB/cm (Suche *et al.*, 1985). For wavelengths between 0.4μm amd 4.0μm there is a minimum in the intrinsic absorption and the dominant loss is caused by scattering or impurity absorption (Korotky and Alferness, 1987). Vahey *et al.* (1980), report a strong dependence of in-plane scatter on the direction of propagation. This indicates that the dominant loss mechanism for Ti:$LiNbO_3$ waveguides is anisotropic refractive index fluctuations, rather than surface scattering.

For waveguides that have bulk-like properties it is possible to determine the dominant loss mechanism by determining the modal dependence of the loss. Losses of Ag ion-exchanged waveguides were studied in detail by Findakly and Garmire (1980). Fabrication involved depositing a thin silver film onto a soda-lime glass microscope slide and heating the sample to 300 - 350°C. The exchange process was continued for times ranging from a few minutes to several hours depending on the number of modes desired. Waveguide attenuation measurements were performed at several wavelengths to determine the dominant loss mechanism. Losses at 476 nm decreased from 15 dB/cm for the TE_0 mode to 4 dB/cm for the TE_{16} mode. This sharp decrease indicated that losses were dominated by volume effects introduced by the diffused silver, because the higher order modes had more power propagating outside the diffused region. Losses at 1.15 μm, however showed the opposite behavior. Losses increased from 0.1 dB/cm for the TE_0 mode to 0.5 dB/cm for the

TE_7 mode. This indicated that losses were dominated by scattering at the air-glass interface.

Spin coated films such as sol-gel films and other organic polymer coatings also exhibit low losses. The process involves spinning the substrate while applying the solution. The film is then baked at several hundred degrees for several hours. This yields a hard layer of uniform thickness with an extremely smooth upper surface so that losses are probably not dominated by surface scatter. Herrmann and Wildman (1983) used the sol-gel technique to deposit mixed oxide films of TiO_2/SiO_2. Loss measurements yielded losses of 0.25 dB/cm at 633 nm. The losses of the fundamental TE mode were found to increase with decreasing wavelength and followed a $1/\lambda^4$ behavior which is indicative of Rayleigh scattering. The losses were attributed to microcrack formation at the film-substrate interface caused by a difference in the thermal expansion coefficients of the film and substrate.

Losses for several vacuum deposited thin film materials have also been studied. Once again, because of the inhomogeneities and anisotropies of these waveguides, it can be difficult to determine the exact cause of the losses. With carefully designed experiments and close examination of film microstructure it is possible to determine dominant mechanisms and in some cases improve guide performance. Henry, *et al.* (1987) reported low losses in Si_3N_4 channel waveguides in the near infrared. The guides were deposited onto oxidized silicon wafers with a 5.0 μm oxide layer. A CVD SiO_2 overlayer of 3.0 μm was then applied after etching a channel. To determine the loss mechanism, waveguide transmission spectra were measured by end-fire coupling light from a tungsten source into and out of the guide. The wavelength dependence was then determined with a grating spectrometer and a cooled Ge detector. Two absorption bands were observed at

1.40 and 1.52 μm with associated losses of 2.24 and 1.18 dB/cm, respectively. These losses are associated with O-H absorption in the CVD SiO_2 layer and Si-H in the Si_3N_4 film. By annealing the film for 1 hr at 1200 ^{0}C the losses were reduced to 0.3 dB/cm. The remaining losses were attributed to surface scattering.

Several studies have used post deposition laser annealing to improve waveguide performance (Dutta, Jackson, and Boyd, 1981; Dutta, *et al.*, 1981; Dutta, *et al.*, 1982). Their first studies were performed on ZnO films sputtered onto oxidized silicon wafers. Laser annealing was achieved by scanning a focused CO_2 laser across the waveguide surface. Losses were reduced from several dB/cm to 0.01 dB/cm. Because ZnO is optically transparent at 10.6 μm, they attributed the decrease to annealing at the film-substrate interface. In their second study CO_2 laser annealing was used in conjunction with a surface coating to reduce the losses in sputtered 7059 glass waveguides. The surface coating is a spin coated Ti-doped SiO_2 film with a refractive index slightly less than that of the waveguide. Losses were reduced from 7.9 to 2.4 dB/cm after applying the index matching layer. The losses of a laser annealed film with initial losses of 1.4 dB/cm were reduced to 0.4 dB/cm after applying the surface coating. The loss of this film prior to laser annealing was 7.2 dB/cm, indicating that the glass waveguides have significant contributions to overall loss from both surface and volume scattering. In the third paper laser annealing was applied to Si_3N_4, Nb_2O_5, and Ta_2O_5 films. In all cases, some improvement in waveguide performance was observed. These studies show that post deposition laser annealing is a valuable technique for reducing losses in thin film waveguides.

Depositions of several oxide materials (Al_2O_3, ZrO_2, CeO_2, and Ta_2O_5) with different ion-beam parameters were performed by Binh *et al.* (1985). The losses of

the films without IAD were all in excess of 10 dB/cm at 633 nm. In all cases losses decreased with O_2 ion-bombardment. The lowest losses (1.5 dB/cm) were observed in an Al_2O_3 ion-assisted film using 1200 eV O_2 ions. It should be noted that although the dominant loss mechanism appeared to be volume scattering, the losses increased with increasing mode number. This is inconsistent with the results of Findakly and Garmire (1980) for ion-exchanged waveguides. Therefore the losses were most likely caused by the enhanced surface roughness introduced by the columnar structure of the film. It should be noted, however, that IAD is not necessary for the deposition of low loss Al_2O_3 waveguides. By depositing Al_2O_3 in a backpressure of O_2, losses of approximately 1.0 dB/cm have been reported (Suits, 1988). It has been suggested that films deposited without the presence of O_2 may be oxygen defficient, resulting in absorption and increased waveguide losses.

It is not necessary to measure the propagation losses in a waveguide to determine the dominant scattering mechanism. By measuring the angular distribution of the scattered light along a short section of the waveguide and comparing it to theory, it may be possible to separate volume from surface scattering. This method was used to examine sputtered 7059 glass waveguides (Imai, Koseki, and Ohtsuka, 1981; Imai, Ohtsuka, and Koseki, 1982). It required measuring the angular distribution of both air and substrate radiation. Theoretical distributions were determined for both surface and volume scattering using the known refractive index and thickness of the film. These calculations assumed that the surface and volume correlation lengths were the same and that there was some correlation between the two imperfections. This was a reasonable assumption if shadowing effects caused by a columnar structure were responsible for the rough surface. The results from the theory were then weighted and summed to match the

experimental results. For a sputtered 7059 glass waveguide with total losses of 4.0 dB/cm for the TE_0 mode at $\lambda = 0.6328$ μm, their results indicated that surface scatter is five times larger than volume scattering.

The above studies of losses in deposited waveguides indicate that it may be difficult, but not impossible, to determine the dominant loss mechanism. It is possible, however, to improve waveguide performance by altering the deposition parameters or by post deposition techniques such as thermal annealing, once the dominant loss mechanisms are known. The main focus of this dissertation research is to determine the dominant loss mechanisms in ZnS waveguides and adapt the deposition technique to reduce total film attenuation.

CHAPTER 3

FABRICATION AND CHARACTERIZATION OF ZnS WAVEGUIDES

The main objective of this research is to determine the effects of film microstructure on the propagation of optical energy. To this end, it is necessary to have control and monitoring capability over ZnS deposition conditions. ZnS was chosen as the material to be studied for several reasons. First, ZnS has a very high refractive index (n = 2.35) and a wide transparency band (0.4 - 13 μm) which makes it an important material for the fabrication of thin film filters. This high index also makes it possible to deposit a relatively thin waveguide that will support multiple modes which allow accurate determination of film refractive index and thickness. Second, ZnS exhibits a strong thermal nonlinearity that can be used to demonstrate nonlinear and bistable integrated optical devices. Finally, although the films studied are not single crystal, there is a potential to fabricate short wavelength laser diodes in epitaxial layers.

Besides monitoring the deposition parameters, several techniques are employed for characterization because it is also necessary to determine accurately the microstructure and light propagation properties of the film. A waveguide technique is employed to determine the total attenuation of the film. This technique is capable of measuring attenuation levels very accurately because the measurement is made over several millimeters. Because the direction of propagation of the incident light differs for guided wave and transverse measurements, measurements of the total attenuation may be different. Measurements of the intensity absorption

coefficient, α, of less than 0.23 cm^{-1} (1.0 dB/cm) are possible using waveguiding techniques (Weber, Dunn, and Leibolt, 1973; Okamura, *et al.*, 1983, 1985; Himel and Gibson, 1986). Film microstructure is determined by x-ray diffraction (XRD) and chemical composition is ascertained by Rutherford backscattering (RBS). Surface profiles are determined with a WYKO optical profiler. This chapter discusses the deposition and monitoring capabilities of the vacuum system used for this study, as well as the characterization methods used.

Thin Film Deposition

Vacuum System

Thin films of ZnS were prepared by both thermal evaporation and ion-beam sputtering (IBS) in a viton-sealed, diffusion-pumped vacuum system with an 18" cylindrical glass bell jar (figure 3.1). The system utilizes a 4" oil diffusion pump backed with a mechanical pump. The diffusion pump and bell jar are separated by a chevron baffled liquid nitrogen cold trap that was filled prior to all depositions. This tends to reduce carbon and oxygen contamination of the film. The system also has a stainless steel cylindrical collar with several 2-3/4" conflat flanges for the attachment of monitoring equipment. System pressure is monitored with both thermocouple and ion gauges while the foreline pressure is monitored with a thermocouple gauge. The system can easily achieve a base pressure of 3.0×10^{-6} Torr, with 7.0×10^{-7} Torr possible if the system is baked to further reduce water content.

The system contains two thermal sources for material evaporation. For the majority of the depositions only one source is necessary. The second source is only used with an empty boat for bakeout of the system. Initial depositions used a Ta boat, but it was later determined that better reproducibility was acheived with an

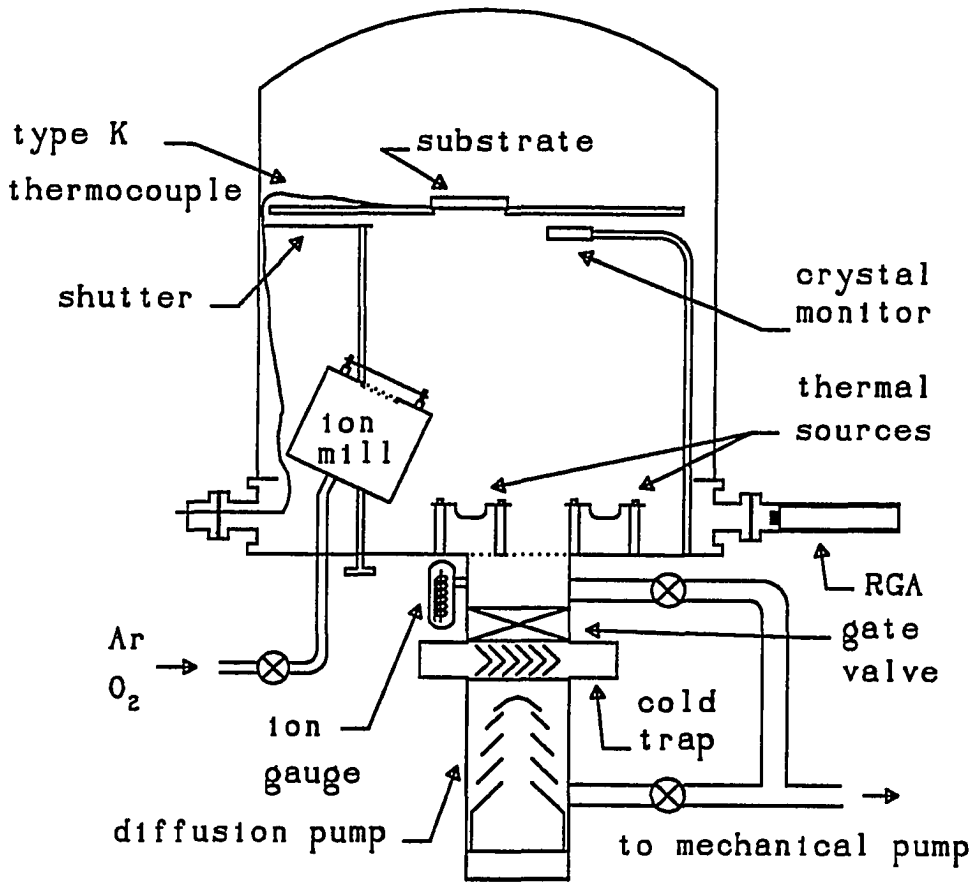

Figure 3.1. Schematic of diffusion pumped vacuum system.

alumina crucible heated with a tungsten crucible heater. The source material is "Patinal" ZnS purchased from EM Chemical that is approximately 99.99% pure. The system also has an Ion Tech 1.0" Kaufman-type ion gun that is used for ion-precleaning the substrate and performing ion-assisted deposition (IAD) and IBS studies.

As will be shown in chapter 4, the microstructure of the film is strongly dependent on the deposition conditions. For this reason it is necessary to monitor and control the deposition process. Approximate deposition rate and thickness are recorded with an Inficon XTM quartz crystal oscillator. Although the crystal monitor could be corrected for different deposition geometries by adjusting the tooling factor, perfect calibration is not possible because the substrate and crystal temperatures are different. After the film thickness is accurately measured, the exact deposition rate is determined by multiplying the average measured deposition rate by the ratio of actual film thickness to recorded thickness. Substrate temperatures are monitored with a chromel/alumel thermocouple that is clamped in close proximity to the substrate for films deposited at ambient temperature. For the films deposited onto liquid nitrogen cooled substrates, knowledge of the exact substrate temperature is critical. Therefore, the thermocouple is attached directly to the substrate with a small bead of indalloy #4 solder. Substrate cooling is acheived using a liquid nitrogen feedthrough and flexible stainless steel tubing attached to a copper block. Substrate temperature can be more accurately controlled by inserting a copper heater block between the cooling block and substrate. Two thin stainless steel shims had to be inserted between the cooling and heating blocks to impede heat transfer from the heater block to the cooling block (figure 3.2). Good thermal contact between the layers is achieved with Apiezon H grease. The substrate

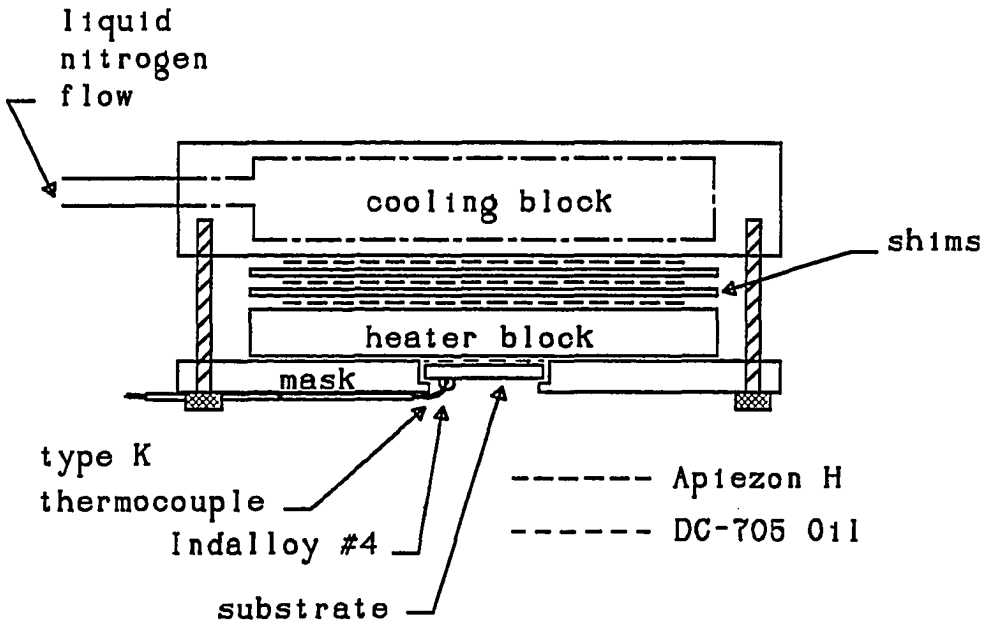

Figure 3.2. Schematic of combined cooling and heating block.

holder assembly allows for accurate control of substrate temperature from -100 to 500°C, but also increases the time required to reach thermal equilibrium. For studies where temperature control is not necessary, the substrates are not clamped but just rest in a mask.

Residual gas pressure also plays an important role in the film microstructure. Two bleed valves are available for the introduction of gases. One is dedicated to H_2S while the other is connected to both Ar and O_2. The second valve could easily be connected to other gas cylinders. The bleed valves are Vacoa MV-25 series that can introduce backpressures as low as 10^{-9} Torr. Ar was introduced for the IAD and IBS films while O_2 was introduced to determine its effect on film microstructure. H_2O partial pressures are reduced by baking the system before deposition while higher pressures can be achieved by partially closing the gate valve. Unfortunately, these methods changed the partial pressures of other gases as well. Partial pressures were initially monitored with a Spectramass 1000 residual gas analyzer but current experiments utilize an Inficon Quadrex partial pressure controller (PPC). The PPC is separated from the chamber with a butterfly valve to avoid the deposition of material onto the filament. The valve is opened only when the PPC is being used.

Substrates

Two different substrate materials are used for this research. The majority of the waveguides are deposited onto silicon wafers with a 1.0 μm oxide layer. Initially the substrates were supplied by Dr. Fred Hickernell at Motorola, but recently a supply was purchased from the Semiconductor Processing Corporation. These substrates have an extremely well polished surface with an rms surface roughness of 0.4 nm, as was measured on a Wyko Topo-2D optical profiler using a

20X objective. The lateral resolution of the profiler at that magnification is 1.0 μm. Therefore, these roughness measurements are an average over a relatively large area. Although other films are deposited onto 1.0 mm thick fused silica microscope slides purchased from Esco products, silicon substrates are preferred for several reasons. First, the surface polish of the silicon is more uniform than that of conventionally polished silica. The silica slides have more scratches and digs and may suffer from subsurface damage. This is readily observed in the scattered light streak from a guided mode. The scattering is more uniform for guides deposited onto silicon wafers. Second, because the silicon is opaque, the signal to noise ratio for the loss measurements is much higher because scattered light from other surfaces is significantly reduced. For the films deposited onto silica, black tape attached to the back of the substrate does help. Finally, charging of the substrate during RBS measurements is much less of a problem when silicon substrates are used. On occasion films are deposited onto pyrolized carbon substrates so that estimates of film oxygen content can be made from RBS measurements.

The method of substrate cleaning is dependent on the substrate material. The oxidized Si wafers are cleaned with methanol in an ultrasonic cleaner for 15 minutes. When removed from the beaker, the wetting pattern is observed. If it is uniform over the entire substrate, the substrate is dipped into the methanol and blown dry with dry N_2. Nonuniform wetting indicates that there is still organic contamination of the surface and the ultrasonic rinse is repeated. Once dry, the substrates are examined under reflection from the room lights. If there is significant scatter from dust particles, the cleaning process is repeated. Only if the substrates are extremely dirty is any scrubbing as described below, necessary.

The silica substrates, however, seldom arrive clean and a more laborious

cleaning is required. First, the substrate is scrubbed with Liquinox soaked cotton and rinsed thoroughly under hot water. It is then cleaned with distilled water in an ultrasonic cleaner for 15 minutes. This step is repeated twice. The final steps are identical to those described above for the silicon. The entire process is repeated if necessary.

Deposition Procedure

Once the substrates are clean, they are placed in the mask or clamped to the combined cooling/heating block, depending on the deposition being performed. For films being deposited onto cooled substrates, the thermocouple is soldered directly to the substrate with indium solder #4. This solder is used because of its good wetting of glass and because good contact is possible without using flux. The thermocouple is attached near the edge of the substrate to allow for the longest propagation length possible. In some cases, the thermocouple is attached to the stainless steel plate that supports the mask (see figure 3.1). Proper operation of the quartz crystal monitor is then verified and the heater block leads are connected if necessary. For the earlier depositions a new Ta boat with new ZnS source material was installed, while for current depositions the alumina crucible is emptied of the old ZnS and filled with new source material. The use of new source material for each deposition is absolutely necessary to prevent both Ta contamination from the boat and non-stoichiometric films. Stainless steel shields are then put in place to prevent material from depositing onto the glass bell jar. The bell jar is lowered and the air inlet valve closed. The liquid nitrogen trap is filled and the bell jar is roughed out to approximately 100 millitorr before opening the gate valve. The system pumpdown is continued until the pressure reaches 4.0×10^{-6} Torr.

At this stage the exact deposition procedure depends on the deposition

parameters required. The system may be baked, the substrate may be heated or cooled, gases may be bled into the system, or the substrate may be ion-precleaned for example. The exact procedures will be discussed further in chapter 4. There are, however, certain procedures which are the same. These are described here. Once the proper deposition parameters are set and recorded, the ZnS is slowly preheated until a deposition rate of about 0.8 nm/s is achieved. That rate is maintained for approximately two minutes to burn off any contaminants. The substrate is shuttered from exposure for the outgassing procedure. The deposition rate is then stabilized at 0.4 nm/s and the shutter is opened. Deposition continues until the desired thickness of 0.55 μm is obtained. This thickness is chosen so that the waveguide will support three TE modes for accurate determination of refractive index and thickness. With the deposition completed, the system is shut down and the gate valve closed. The films are removed after the vacuum system reaches ambient condition, usually the following day.

Characterization

A variety of techniques are used to determine film characteristics such as refractive index, crystal structure, and propagation losses. This research concentrates on detecting small changes in the optical performance of ZnS films; therefore a sensitive method for measuring the optical losses must be used. Waveguide loss measurements are extremely sensitive to small changes in the film microstructure. Waveguide techniques are also used to determine the refractive index and thickness of a thin film.

Thickness and Refractive Index

The ZnS films are initially examined under a microscope at a magnification of 200X to determine film quality. If the films have a high pinhole density, no further characterization is performed because these films invariably have excessive losses. Some films exhibit adhesion failure caused by excessive film stress and are useless for waveguiding. Both compressive and tensile stress failure patterns are observed.

A rutile coupling prism with refractive indices of 2.872 (TE mode excitation) and 2.584 (TM mode excitation) is clamped in place on the waveguide for prism coupling. Both the waveguide and prism base must be free of dust in order to get close contact, which is readily observed as a contact spot on the prism base. The waveguide assembly is then mounted on a Klinger rotation and translation assembly that has its rotation axis aligned with the polarized beam from a HeNe laser (figure 3.3). TE and TM mode selection is possible by rotating the polarizer. Initially, measurements were made with a single line HeNe laser with output at 633 nm. Currently, however, a multiline HeNe is available with output at 543, 594, 611, and 633 nm. X-Y translation stages are mounted to the top of the rotation stage while a lab jack provides for vertical translation. A vertical tilt stage is used for precise alignment of the sample when loss measurements are required. The prism coupler is translated until the coupling spot is aligned with the rotational axis, which eliminates constant realignment of the coupler as it is rotated. The assembly is rotated to excite the individual modes and the coupling angles for each mode are recorded for determination of film refractive index and thickness.

The index and thickness are determined numerically by solving the transverse resonance condition (equation 2-4) for each guided mode. For a given

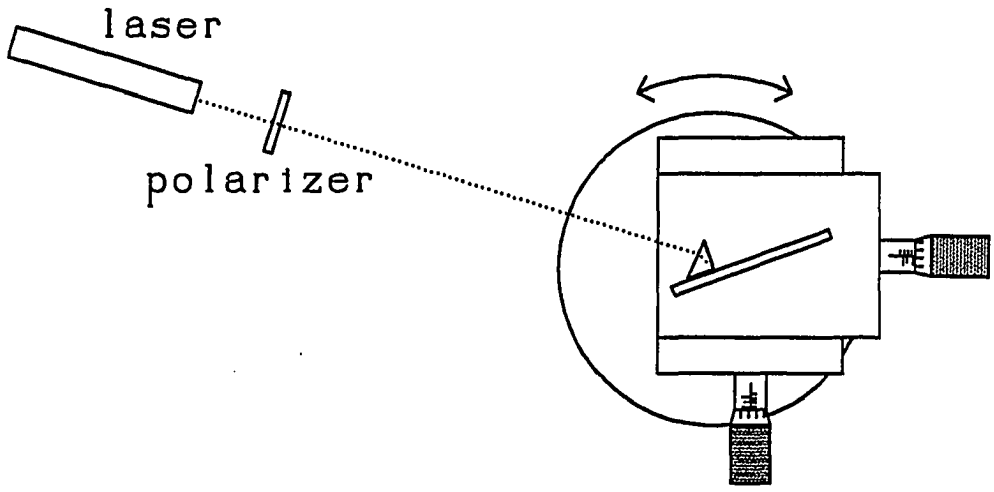

Figure 3.3. The experimental set-up for determining film refractive index and thickness from modal measurements.

coupling angle there exists a complete set of [refractive index, thickness] ordered pairs that form a single curve. By plotting the curves for at least two modes, the index and thickness may be determined by the intersection of the curves (figure 3.4a). If three or more modes are used for the calculation, there may be some deviation in the crossover points (figure 3.4b). This may be caused by measurement error or by inhomogeneities within the film. For our set-up, coupling angles for ZnS films can be measured to an accuracy of 20 - 30', which results in refractive index and thickness measurements accurate to three decimal places. Measurements of n and d should be made for each polarization (TE and TM) because the film may exhibit birefringence. Material dispersion can also be observed by measuring the refractive index at several wavelengths. The results for two films deposited under different conditions are shown in figure 3.5. The solid line is for a film deposited at ambient temperature while the dashed line is representative of films deposited onto cooled substrates. The lower indices for the cooled films suggest that the films have a low density. The films deposited at ambient temperatures actually have indices slightly higher than that reported for bulk ZnS. This may be a caused by interstitial defects which lead to greater than bulk density and compressive stress.

Loss Measurements

Several techniques for measuring waveguide losses have been developed, but all have certain disadvantages. Techniques that monitor the total throughput require the use of prisms, gratings, or end-fire couplers to couple light into and out of the waveguide (Weber, Dunn, and Leibolt, 1973; Won, Jaussaud, and Chartier, 1986; Brannon, 1986; Arutunyan and Galoyan, 1986). The output must be measured at several different locations along the waveguide to get a reasonable

a)

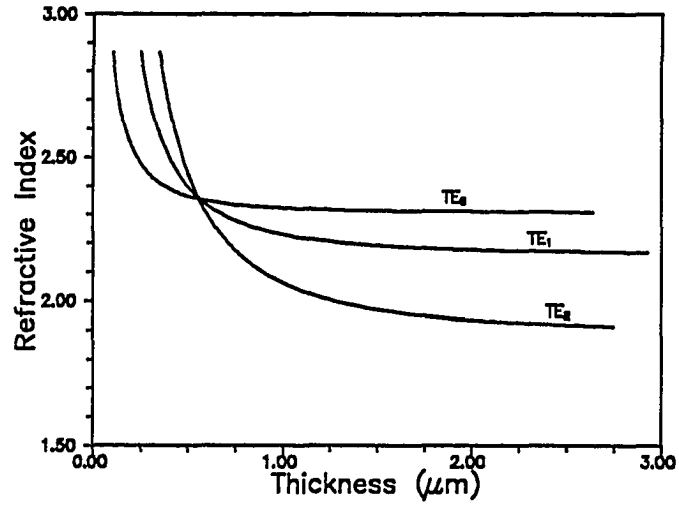

b)

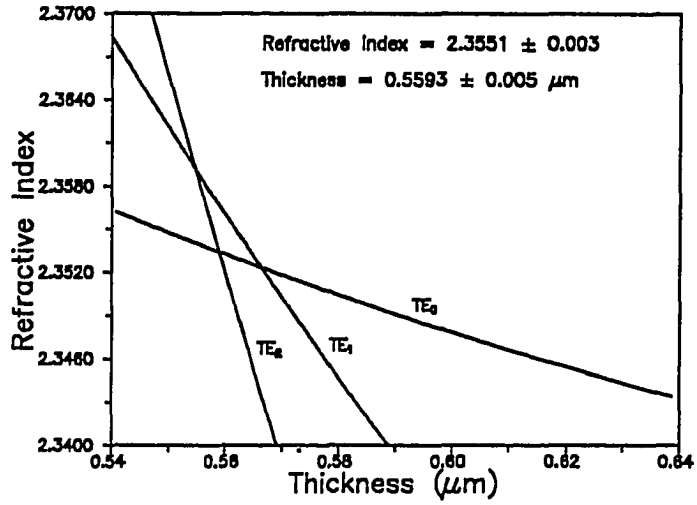

Figure 3.4. Graphical solution for calculating film refractive index and thickness from modal measurements. a) n versus d for a ZnS waveguide which supports three TE modes and b) enlargement of region where curves intersect. Measurement accuracy is determined from the standard deviation of the intersections.

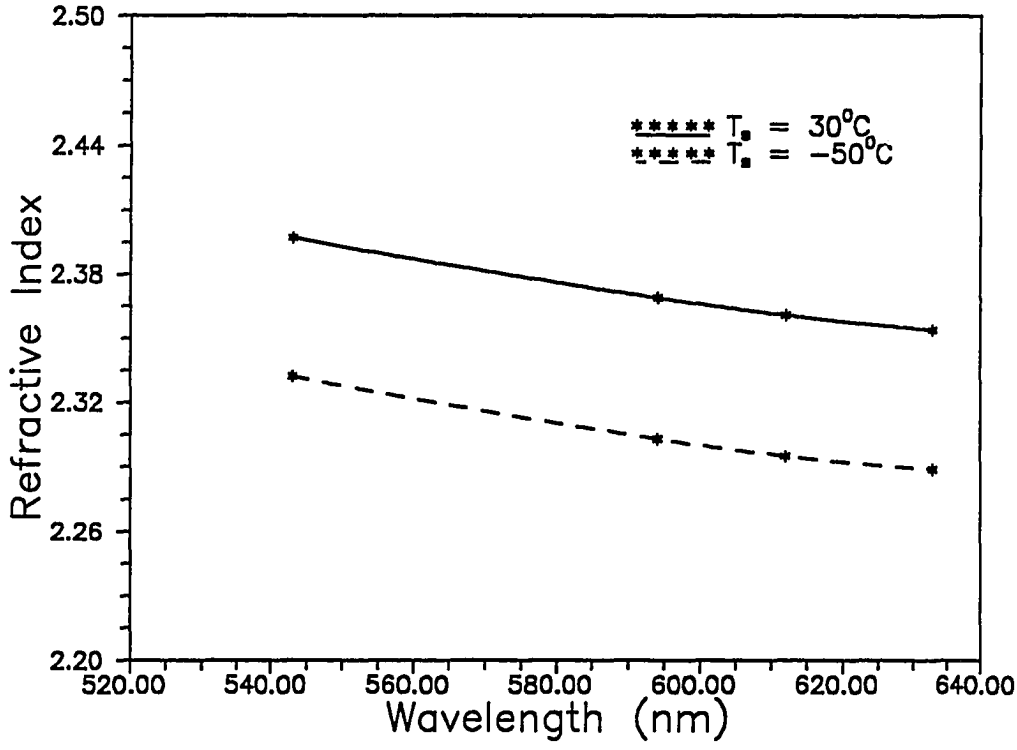

Figure 3.5. Refractive index versus wavelength for two ZnS films deposited at different substrate temperatures.

estimate of the loss. The most common and simplest technique is the two prism method where the output prism is clamped at several different points along the waveguide. This technique is highly susceptible to error because the coupling efficiency can not be well controlled. To reduce the effect of coupling efficiency, Won *et al.* (1986) developed a three prism technique, and a sliding prism method was developed by Weber *et al.* (1973). For the sliding prism method an output prism, coupled to the waveguide through an index matching fluid, is slid along the guide while pressure is applied to maintain a constant coupling efficiency. Although highly accurate, this system is difficult to implement. Both of those techniques are likely to damage the waveguide surface.

Several loss measurement techniques have been developed that exploit film absorption. Haegele and Ulrich (1979) use a sliding Hg electrode to measure the pyroelectric voltage that results from absorption in Ti:$LiNbO_3$ in-diffused waveguides. Although the technique is capable of measuring losses less than 1.0 dB/cm it is only useful for pyroelectric materials. Rather than depending on the pyroelectric effect to reflect temperature increases, Jackel and Veselka (1984) extended the technique of Haegele and Ulrich to directly measure waveguide temperature by immersing a chromel-constantan thermocouple in the mercury. The method is also capable of measuring losses less than 1.0 dB/cm with 0.08 dB/cm precision. Allen *et al.* (1979) employed a calorimetric technique to show that absorption losses of out-diffused $LiNbO_3$ waveguides are two orders of magnitude less than total waveguide losses, suggesting that the predominant loss mechanism is scatter. Hickernell, *et al.* (1988) uses a photothermal deflection technique (PTD) to measure total waveguide attenuation. Because the PTD signal depends on the gradient and not on the light intensity itself, the contribution of an absorption

center to a PTD data point is significantly less than the contribution of a scattering center to a scattered light data point. Therefore, for low loss waveguides the PTD technique may yield more accurate results than techniques that measure the scattered light.

Techniques that measure the out-of-plane scattered light are the most widely used because they are accurate and will not damage the waveguide (Goell and Stanley, 1969; Dutta, *et al.*, 1982; Okamura, *et al.*, 1983, 1985; Bernardi, Loffredo, and Morasca, 1986; Himel and Gibson, 1986). They do, however, have their limitations. First, If the loss is caused primarily by absorption, the scattered light may be overwhelmed by background scattering. Second, because the method assumes a uniform distribution of scatterers, point defects may yield inaccurate results. Finally, alignment of the fiber or detector used to make the measurements is critical.

One approach uses a single optical fiber that is scanned along the scattered light streak (Goell and Stanley, 1969; Dutta, *et al.*, 1982). The optical fiber must be aligned accurately along the direction of the propagating beam and must be maintained at a constant distance from the waveguide. Dutta *et al.* (1982) use a 10X scanning microscope incorporating a 50 μm diameter optical fiber probe within the eyepiece. This allows precise positioning of the fiber with respect to the waveguide surface. The microscope is defocused by 3 mm to reduce the effect of scattering centers. Several transverse scans of the fiber probe are made at different positions along the streak. Although loss measurements as low as 0.01 dB/cm have been reported, the measurements are difficult and time consuming. Another approach employs a CCD camera interfaced with a microcomputer (Okamura *et al.*, 1983, 1985). This method yields high resolution two-dimensional profiles of the

light streak. The data may be filtered to reduce the effects that scattering centers may have on a least squares fit. Although accurate and much easier to align than the scanning fiber, it can be expensive to set up and can only be used for measurements at wavelengths < 1.0 μm.

The technique used for this research also measures the out-of-plane scatter, but it combines the better attributes of the above two methods (Himel and Gibson, 1986). It utilizes a coherent (or image forming) fiber bundle to image the streak away from the waveguide, and a detector to scan the image to determine the waveguide loss. The system is automated and data is acquired and processed with an IBM PC. The system is accurate, easy to align, and can be set up inexpensively.

Figure 3.6 is a schematic of the loss measurement system. The light from a 7 mw unpolarized Melles Griot HeNe laser is polarized and passes through a beamsplitter. The polarizer allows for selection of TE or TM polarized light. For measurements at other wavelengths, the PMS multiline HeNe laser is used. This laser is internally polarized so that only TE modes can be excited. The light reflected from the beamsplitter is monitored by an internally chopped Laser Precision RQP 546 silicon radiometer and used to normalize the signal, thereby eliminating the effect of laser power fluctuations. The unreflected beam passes through a chopper operating at 1000 Hz and is focused with a 30 cm focal length lens onto a prism/film coupler that is mounted on the stage described in the previous section. A coherent fiber bundle is placed in close proximity to the waveguide to form an image of the scattered light streak at a remote detector plane.

The fiber bundle presently in use was purchased from Collimated Holes Inc. and is a 20 mm wide by 3 mm thick composite of seven 3 mm square by 20.3 mm long rods. The large area of the fiber bundle permits complete coverage of the light

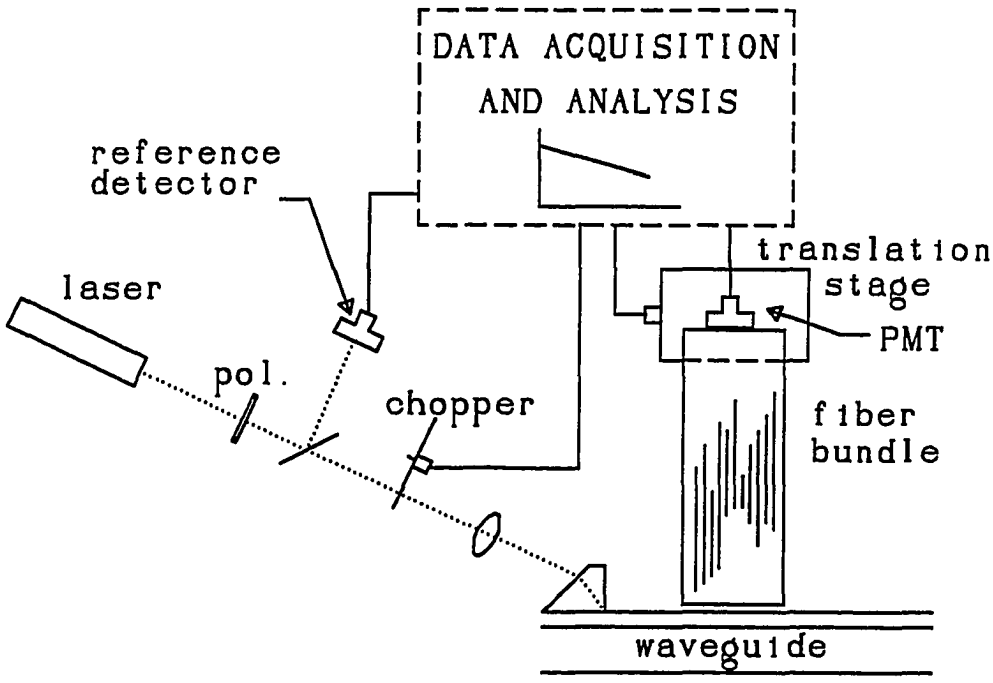

Figure 3.6. Schematic of equipment for measuring the mode propagation losses in planar optical waveguides.

streak, simplifying alignment in the transverse direction. The individual fibers are 25 - 50 μm in diameter with a numerical aperture (N.A.) of 0.66. The fibers are separated by cladding doped with light absorbing EMA to reduce the effect of fiber crosstalk. The high N.A. of the fibers allows more of the scattered radiation to be delivered to the detector than would be the case for a lens system. However, the fiber bundle must be parallel to the plane of the waveguide for loss measurements to be accurate. To prevent damage to the waveguide or bundle during alignment, lens tissue is inserted between the two as the fiber bundle is moved into position. Uniform friction on the tissue between the guide and bundle indicates accurate alignment. The process is repeated at the detector end of the bundle. Because of the large imaging area of the bundle and its proximity to the waveguide; accurate, reproducible, and rapid visual alignment is possible.

By imaging the streak away from the waveguide, several detection schemes are possible. The simplest and most economical approach is to scan a photodiode or photomultiplier tube (PMT) longitudinally along the fiber bundle. For visible measurements, a Hamamatsu 25 mm diameter end-on PMT is mounted in an aluminum housing attached to an Aerotech stepper-motor-controlled translation stage. Resolution is achieved by placing a slit between the fiber bundle and PMT. The slit was fabricated in-house by using a cylindrical lens to focus the beam from a high power Nd:YAG laser onto a piece of 5.0 mil thick BeCu foil. The resulting slit width averaged 40 ± 10 μm. The chopped PMT output, I(z), the DC reference signal from the radiometer, I_{ref}, and the chopper reference signal are all input into a Princeton Applied Research model 5707 Lock-in amplifier (LIA), and the ratio of scattered intensity to laser intensity is recorded as the detector is scanned. Once aligned, the entire measurement process is computer controlled with a National

Instruments GPIB interface board that is installed in an IBM PC. The detector is scanned in 100 μm steps for a total distance of 1.0 - 2.0 cm and the ratio output from the LIA is sampled five times at each point. Although the ratio signal may be displayed directly on the LIA, the numerator and denominator must be transmitted across the GPIB interface bus separately. This results in higher accuracy.

The resolution of the system is determined by the size of the individual fibers, the width of the slit at the detector, the bundle to waveguide and detector separations, and the N.A. of the fibers (figure 3.7). This resolution may be approximated by

$$R = d + w + 2(s_1 + s_2)\tan\theta, \qquad 3\text{-}1$$

where

d = fiber diameter

w = detector slit width

θ = acceptance angle of fibers

s_1 = waveguide to fiber bundle separation, and

s_2 = detector to fiber bundle separation.

For the present system $d = 25$ μm, $w = 40$ μm, $s_1 = s_2 \cong 25$ μm, and $\theta = 41^0$ (N.A. = 0.66); thus $R \cong 160$ μm.

To determine the waveguide loss, a least squares fit to $10\log_{10}(I(z)/I_{ref})$ is performed. In some cases manipulation of the data is required prior to the linear fit because of large peaks in the output caused by scattering from defects and index inhomogeneities. To remove these peaks from the data, a median window (Frieden, 1983) with an adjustable window width is used. Figure 3.8 is a plot of loss versus distance for a waveguide with several defects. The two lines represent least

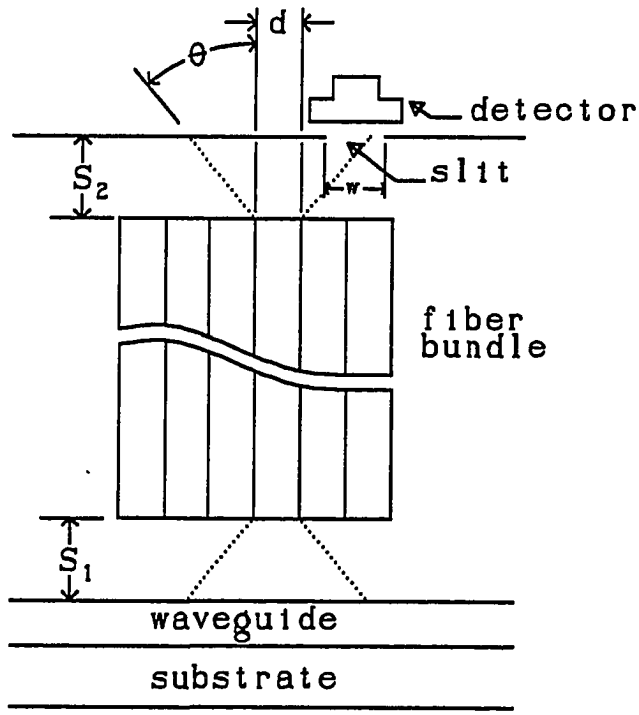

Figure 3.7. Diagram of resolution related parameters.

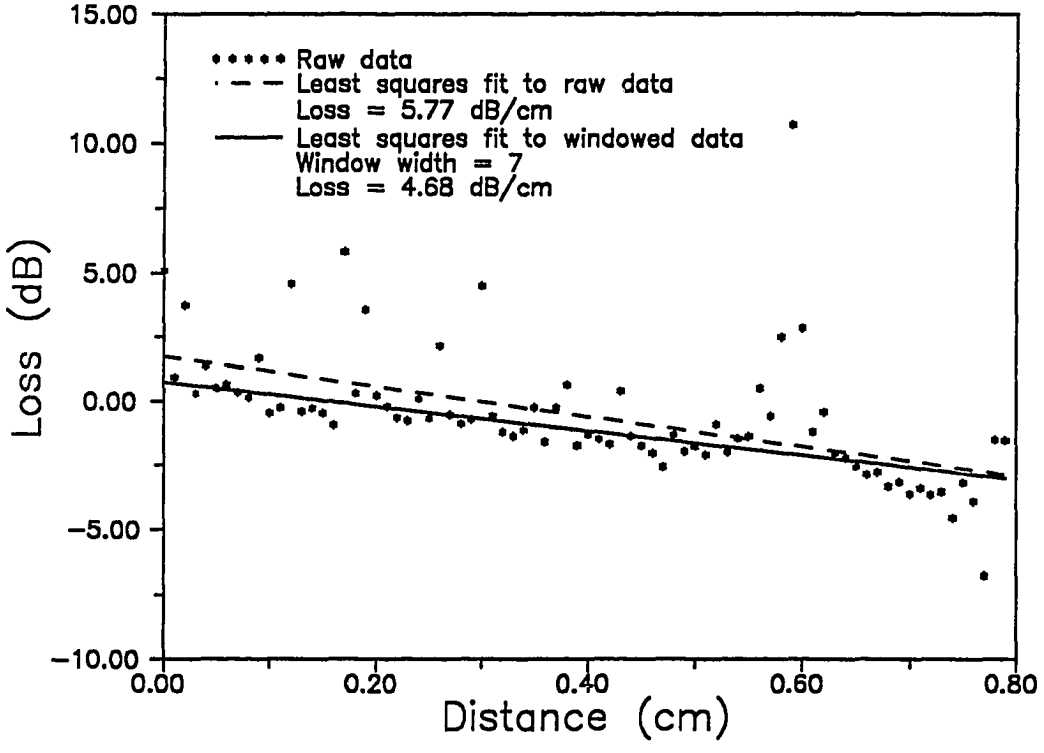

Figure 3.8. Plot of loss versus distance for a waveguide with several defects. Least squares fit to windowed data (solid line) yields more accurate result than least squares fit to raw data (dashed line).

squares fits to the raw (solid line) and windowed (dashed line) data. The fit to the windowed data is more representative of the actual loss.

To determine the capabilities and limitations of the system, losses at λ = 633 nm were measured for several different types of waveguides. A summary of results is given in table 3.1. An important requirement for any measurement system is repeatability. This was determined by making multiple measurements of the same waveguide both before and after removing and realigning the fiber bundle. All of the measurements agreed to within 2.0%.

The first waveguides tested were fabricated by Allan Gabel using ion-exchange of K for Na in a Schott soda-lime glass doped with small amounts of CdS_xSe_{1-x} (Gabel, 1988). These waveguides have low losses (typically less than 1.0 dB/cm) and were measured to determine if the system is capable of measuring losses less than 1.0 dB/cm. The exchange of Na ions with more massive ions such as K causes a slight densification of the glass. This in turn produces an increase in the material refractive index which is dependent on the K concentration. Because ion-exchange is a diffusion process, the dopant concentration will decrease with depth, yielding a gradient index layer with a higher refractive index near the surface. Waveguides with two TE and two TM modes were prepared in both unpolished and polished substrates by immersing the glass in molten KNO_3 at 400°C for 1.5 hr. The measured losses for the TE_0 modes in these guides were 10.9 and 3.6 dB/cm, respectively. Measurements of the rms surface roughness were made on the two samples with a WYKO Topo-2D optical profiler. As shown in figure 3.9, the roughness of the unpolished substrate (δ = 1.0 nm) is twice that of the polished sample (δ = 0.46 nm). If the waveguide losses were caused entirely by surface roughness, the quadratic dependence on the rms roughness (equation 2-26) would

Table 3.1. Measured losses for the TE modes of several planar waveguides.

Waveguide	d (μm)	n	Sample	mode	Loss (dB/cm)	Comments
Ion-exchanged glass	4.72	1.53	1	TE_1	10.9	Unpolished
			2	TE_0	4.9	Polished
			2	TE_1	3.6	Polished
			3	TE_1	0.85	Polished
Sputtered ZnO	0.64	2.00	4	TE_0	1.49	
			4	TE_1	2.42	
			4	TE_2	5.90	
			4	TE_1	2.95	Different input coupling site
Evaporated ZnS	0.55	2.35	5	TE_0	11.5	
			6	TE_0	10.2	Ar backpressure 8.0×10^{-5} Torr
			7	TE_0	17.3	IAD for first 60 nm
			8	TE_0	6.75	O_2 backpressure 1.0×10^{-7} Torr
			9	TE_0	< .4	Substrate temperature -50°C

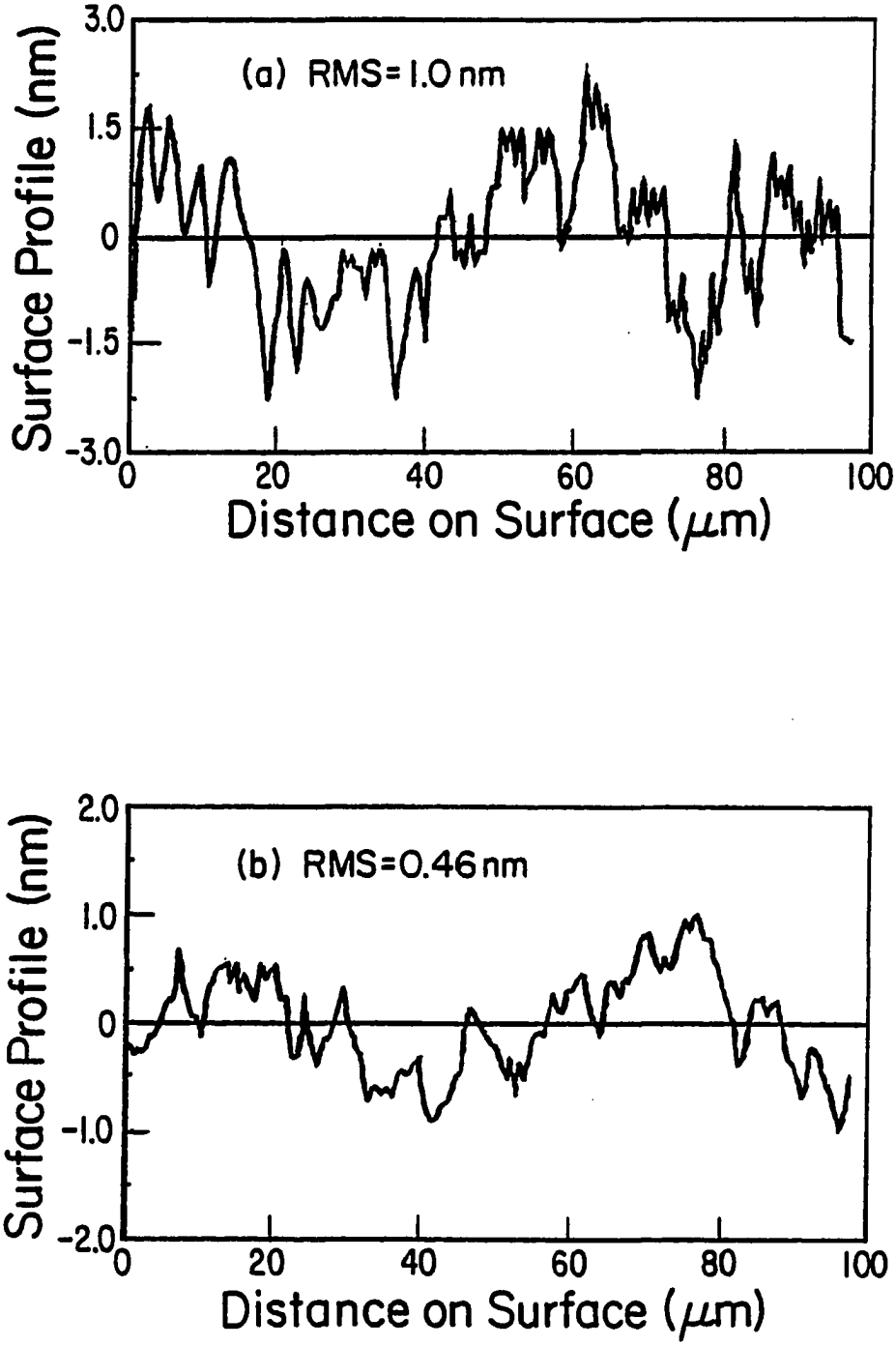

Figure 3.9. Surface roughness for a) unpolished and b) polished semiconductor doped glass substrates.

predict a fourfold decrease in the waveguide loss for the polished sample. Because there are absorptive and internal scattering contributions to the loss, the measured loss ratio of 3.0 is not unreasonable. In fact, the losses for the polished guide are lower for the higher order modes indicating that the losses are now dominated by volume mechanisms such as internal scattering and absorption from the CdS_xSe_{1-x} crystallites. The lowest losses measured for these ion-exchanged waveguides was 0.85 dB/cm. This does not appear to be the limit of the measurement system. The system should be capable of measuring even lower losses provided the scattering out of the waveguide is uniform. Therefore, accurate determination of waveguide loss is limited by the quality of the guide, not the measurement system.

A relatively low loss ZnO waveguide was also tested. The film was rf magnetron sputtered by Rance Fortenberry onto a quartz substrate (Fortenberry, 1986). The results are also listed in table 3.1. The losses increased from 1.49 dB/cm for the TE_0 mode to 5.9 dB/cm for the TE_2 mode. This indicates that the losses are dominated by surface scattering. In chapter 2 it was shown that the theoretical losses caused by scatter from the film/substrate interface are much less than 1.0 dB/cm; therefore the losses for the ZnO films are probably caused by increased surface roughness at the film/air interface that was introduced during film growth. Variations observed in the losses measured at different locations can probably be attributed to inhomogeneities in the waveguide because measurements were repeatable to greater accuracy.

Losses were also measured for several ZnS films. While the majority of the waveguides have measured losses of $\cong$ 10 dB/cm, waveguides deposited onto substrates cooled with liquid nitrogen have losses $<$ 1.0 dB/cm. These are the lowest losses reported for ZnS waveguides. These results are discussed in detail in

the following chapter.

Transverse Angular Distribution of Scattered Light

For films deposited onto oxidized silicon substrates an interference effect is observed for light scattered transversely to the direction of propagation (figure 3.10). This effect is not observed for films deposited onto quartz substrates. The effect can be described by examining the optical path taken by light that is scattered from a point on the film/air interface. The geometry is shown in figure 3.11a. Light scattered from a point source will reflect from both the film/oxide and oxide/silicon interfaces, which will result in interference. The resulting fringes may be described as fringes of equal inclination (Hecht and Zajak, 1974) where the relative phase shift is

$$\delta = \frac{4\pi n_f}{\lambda_0} d\cos\theta_t \pm \pi \ . \qquad 3\text{-}2$$

The resulting intensity distribution may be described by

$$I = I_1 + I_2 + 2\sqrt{I_1 I_2}\cos\delta \ , \qquad 3\text{-}3$$

where I_1 and I_2 are the reflected intensities from the film/SiO_2 interface and the SiO_2/Si interface, respectively. I_1 and I_2 must be determined from the Fresnel reflection coefficients. As θ_t increases, the critical angle will be reached for light reflecting from the film/air interface. Because this is the upper surface reflection and light will be totally internally reflected, interference will no longer occur in the cover region. As shown in figure 3.11b, once the critical angle is reached light will be trapped in the film layer and either a guided, radiation or leaky mode will be excited.

The experimental data is taken by attaching a flexible 0.25" diameter fiber

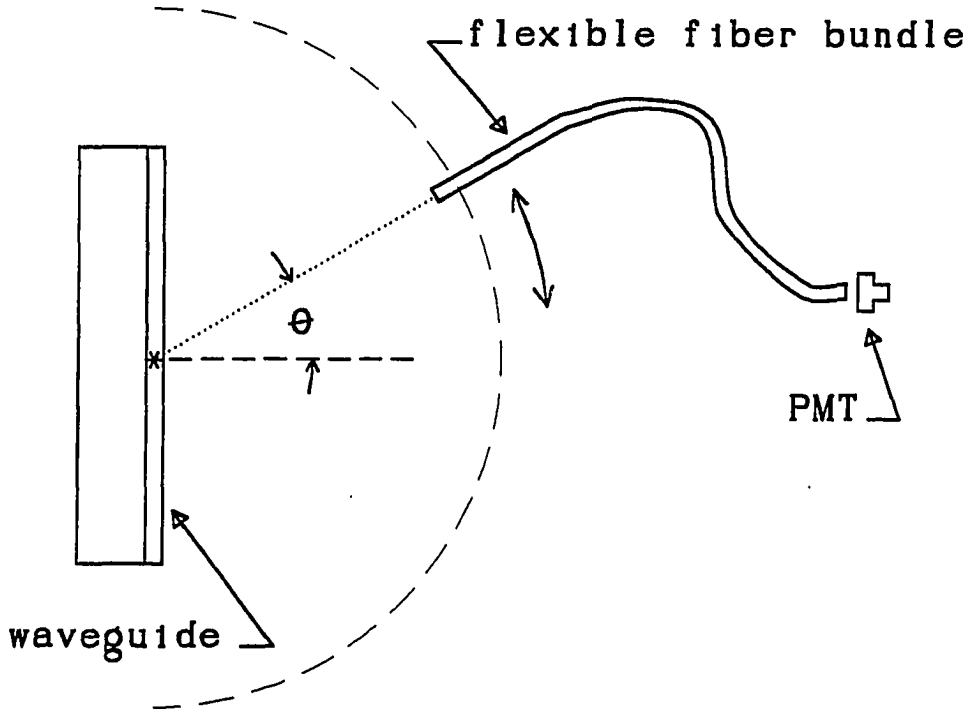

Figure 3.10. Geometry for measuring the transverse angular dependence of scattered light. Guided mode energy is propagating normal to the page.

bundle to a rotation stage. The stage is aligned with the sample so that a transverse angular scan can be taken. The output of the fiber bundle is input to a PMT connected to the LIA. A reference signal is also used to normalize the data for laser intensity fluctuations. Data is taken manually in 5 degree steps. The results of both theory and experiment are shown in figure 3.12. The oxide layer thickness (1.01 μm) is selected to most closely match the experimental data. For simplicity, the Fresnel coefficients are not included in the theoretical calculations and only incident angles less than the critical angle are considered.

Once the transverse scan was completed, the ZnS film was removed by immersing the sample in a 10% solution of HCl. The SiO_2 layer was removed from half of the sample so that the oxide layer thickness could be determined with a Tencor Alpha Step 100. The measured thickness was 1.01 μm within the accuracy of the instrument.

X-ray Diffraction

X-ray diffraction measurements are made by J. A. Ruffner (see references) to determine the crystalline properties of the ZnS films. For a crystalline film, diffraction peaks are observed when reflected x-rays interfere constructively from parallel planes within the crystal. Those peaks occur when the Bragg law

$$m\lambda = 2d\sin\theta, \qquad 3\text{-}4$$

is satisfied, where d is the plane separation, θ is the incident angle of the x-rays, m is the diffracted order, and λ is the x-ray wavelength. For the case of ZnS, which is a polycrystalline film, x-ray diffraction measurements can be used to determine the crystal structure and preferential orientation of the crystallites. It is also possible to get an approximate measure of the grain size.

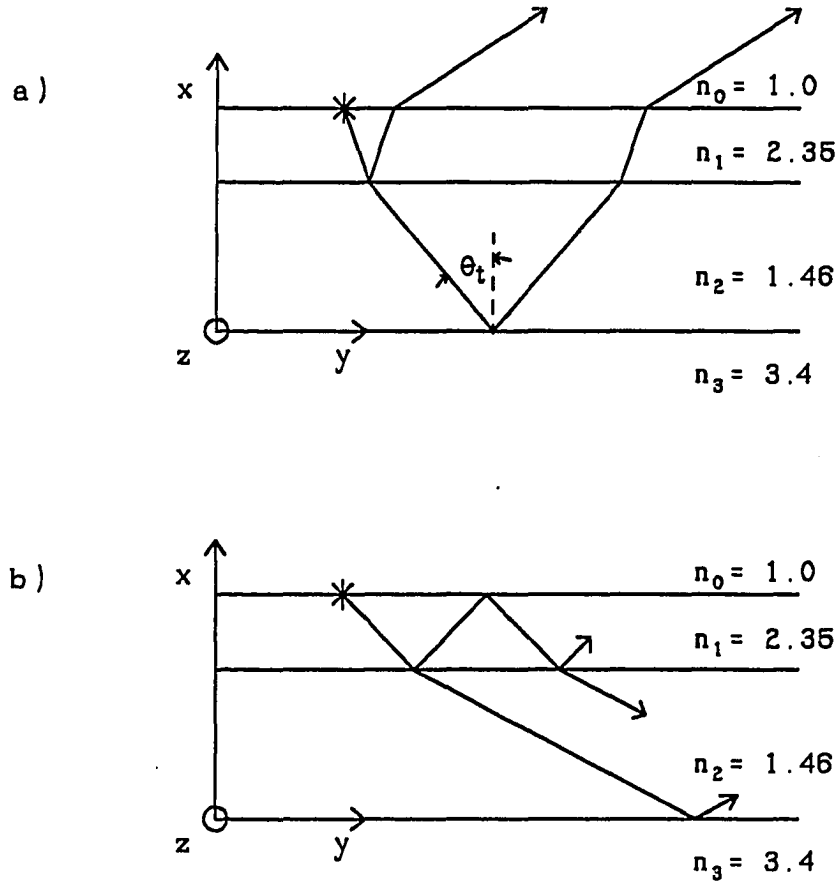

Figure 3.11. Fringes of equal inclination caused by light scattering from the upper surface of the film. a) θ_t less than critical angle and b) θ_t greater than critical angle.

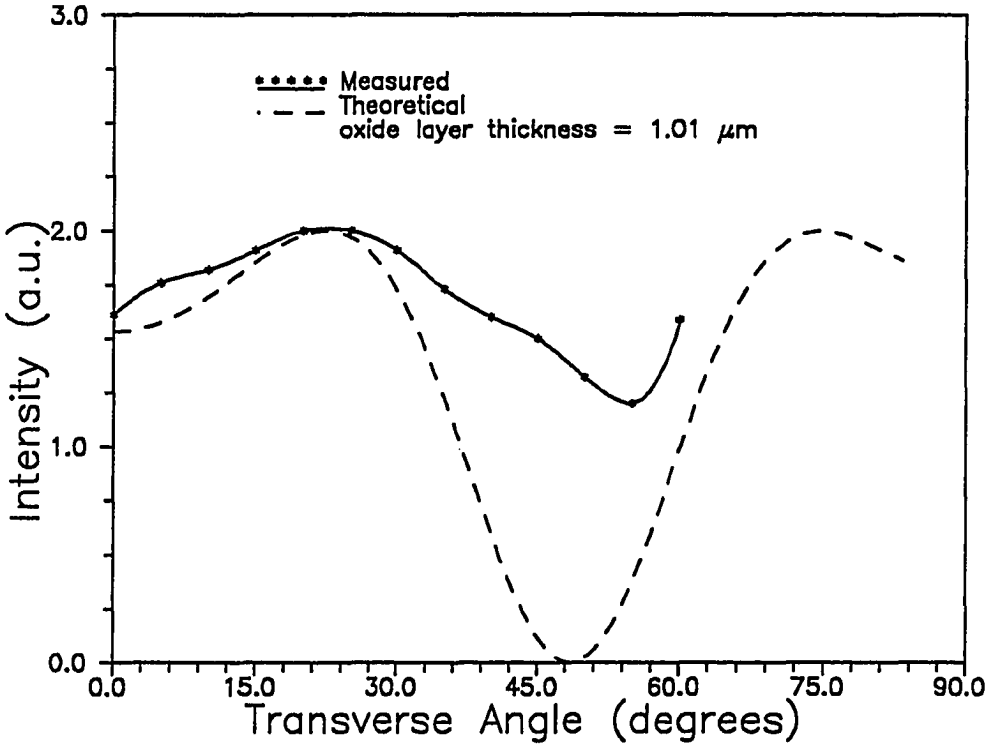

Figure 3.12. Theoretical and measured intensity distributions as a function of transverse scattering angle. Best match of experiment to theory achieved for an oxide thickness of 1.01 μm.

Diffraction peaks will not be observed at all of the angles that satisfy the Bragg condition because some crystalline planes will interfere destructively with others. That is, some peaks will be "disallowed". The combination of constructive and destructive interference will modulate the amplitudes of those peaks that are allowed. The crystal structure of the film may be determined by locating all the diffraction maxima and comparing them to the allowed peaks for the various crystal structures. To determine if the crystallites are preferentially oriented, the relative strengths of the peaks for the film are compared to those of a random powder sample. Any deviation from the relative peak heights of a random sample indicates that there is some preferred orientation, but the degree can be difficult to determine.

For polycrystalline films, the crystallite size is related to the width of the diffraction peak by the Scherrer equation (Maissel and Glang, Chapter 9, 1970). For a Bragg-Brentano θ-2θ x-ray diffractometer the relationship is

$$C = \frac{\lambda}{\Delta(2\theta)\cos\theta}, \qquad 3\text{-}5$$

where C is the average crystal size, $\Delta(2\theta)$ is the angular FWHM of the diffraction peak, and θ is the diffraction angle. The Scherrer equation shows that larger crystals have narrower diffraction peaks. Because the width of the diffraction peak is affected by nonuniform stresses in a film, the calculated crystal sizes are only approximate.

Rutherford Backscattering

To determine film stoichiometry and impurity levels, Rutherford backscattering measurements are made by J. A. Leavitt, L. C. McIntyre, M. D. Ashbaugh, and J. G. Oder (see references). This technique consists of bombarding a sample with high energy (≅ 2 MeV) helium nuclei and monitoring the nuclei that are elastically backscattered to determine the mass and number of the atomic species within the film. A sample RBS spectrum from a ZnS film is shown in figure 3.13. Because momentum must be conserved, the highest backscattered energy is the result of scattering from the most massive atoms in the film. As the incident beam of nuclei propagates through the film it loses energy through interaction with electrons. This results in a spread in energies for each species within the film. To keep the substrate scattered signal from overwhelming the film signal, a low mass substrate such as carbon should be used.

RBS measurements yield accurate information on the total number of an atomic species per square centimeter. The ZnS film stoichiometry can be determined easily by comparing the number of counts in the Zn and S peaks. By assuming bulk density for ZnS, it is also possible to estimate the film thickness. The actual film density may be determined by taking the ratio of the RBS thickness estimate to the actual film thickness. RBS measurements show that almost all of the films deposited for this project are stoichiometric. Some of the films deposited onto cooled substrates, however, appear to deviate substantially from perfect stoichiometry. These films were deposited onto fused silica and were damaged by substrate charging during the RBS measurements. Therefore, the data may be unreliable. For this research the measurement uncertainties are approximately 1%. For samples deposited onto SiO_2 instead of pyrolized carbon, oxygen impurity levels

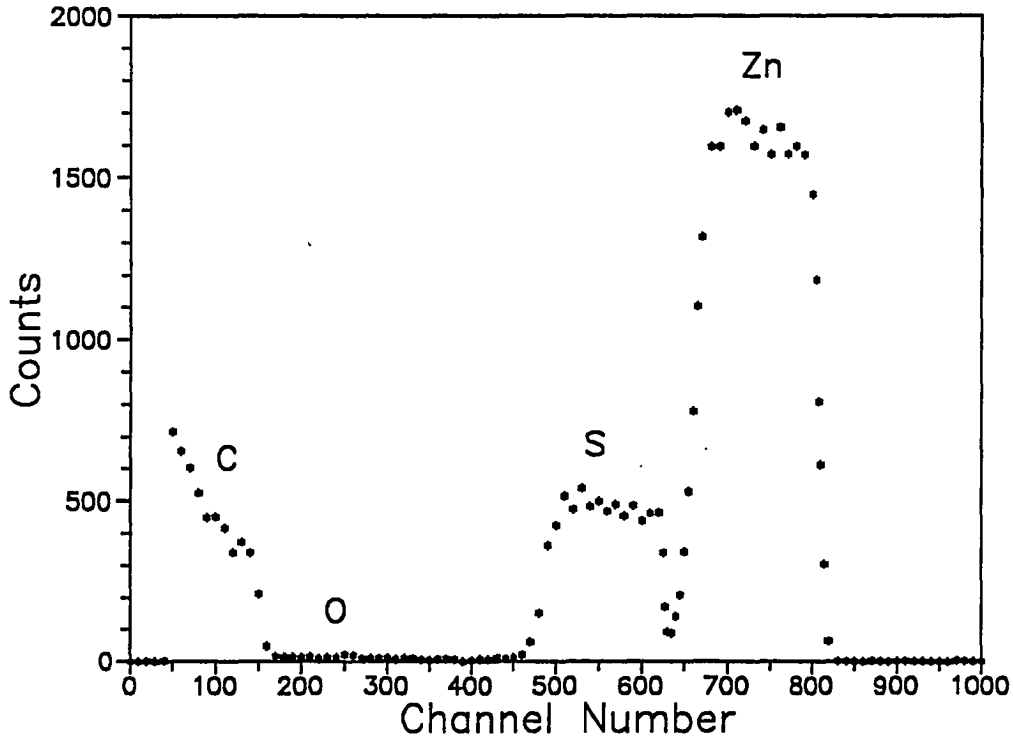

Figure 3.13. Sample Rutherford backscattering spectrum.

could not be determined. This is not considered a problem because typical oxygen impurities are less than 1%.

Surface Roughness

Surface profiles are measured on a WYKO TOPO-2D phase shifting interferometric optical profiler. This technique provides a linear scan of the sample at a magnification of 20X over a distance of 660 μm. The surface is imaged onto a linear CCD array with 1024 pixels. This yields a lateral resolution of 1.0 μm. The roughness measurements are repeatable to approximately 0.01 nm and WYKO claims that roughness measurements of less than 0.1 nm are possible. The silicon wafers used for these experiments had a measured roughness of 0.4 nm. This is an average of several scans taken at different points on the substrate.

The basic limitation of the WYKO is that the measured roughnesses are actually averages over a pixel size of 1.0 μm. This means that any high frequency defects on the surface will be averaged out, thus yielding an inaccurate indication of the rms roughness. Therefore, it is somewhat risky to use the roughness data collected to interpret experimental results.

CHAPTER 4

EXPERIMENTAL RESULTS AND DISCUSSION

The preceding chapters discussed the microstructure of thin film coatings and how that structure may contribute to overall waveguide losses through refractive index fluctuations and enhanced surface roughness. Recent experiments designed to determine the dominant loss mechanisms for a variety of materials were also discussed. These showed that the dominant loss mechanisms are strongly dependent upon the material and methods of fabrication. Once the dominant loss mechanisms are determined, the fabrication method may be altered in an attempt to improve waveguide performance.

This chapter presents the results of similar studies on ZnS waveguides. Once it was determined that the waveguide losses are not dominated by scattering from the film/substrate interface, a systematic study to determine the dominant loss mechanisms was performed. This included depositing coatings at different residual gas pressures and substrate temperatures. Initial studies indicate that the losses can be attributed to the polycrystalline structure of ZnS films. The losses increase with increasing grain size as a result of both volume scattering and scattering from enhanced surface roughness. To reduce the size of the crystallites, films are deposited onto liquid nitrogen cooled substrates. This has the effect of reducing adatom mobility at the surface, which yields amorphous films with the lowest reported losses for ZnS waveguides (Himel, Ruffner, and Gibson, 1988). Unfortunately, these films also have a lower refractive index and increased in-plane

scattering. This indicates that the films have a lower packing density and possibly enhanced columnar structure compared to films deposited at ambient temperature. The low packing density is also evidenced by a change in the stress from compressive to tensile for the films deposited onto cooled substrates.

Microstructure versus Substrate Effects

Although the calculations in chapter 2 indicate that the losses of ZnS waveguides are theoretically dominated by film microstructure, a preliminary experiment was performed to determine if this actually is the case. If the losses are dominated by substrate scatter, small changes in the film microstructure would not significantly affect the losses. Therefore, this project requires that the losses introduced by substrate roughness be negligible.

The waveguide scattering theories predict a quadratic dependence for loss as a function of surface roughness (see for example Marcuse, 1969; Ames and Hall, 1983). If waveguide losses are dominated by scattering from the film/substrate interface, this quadratic dependence should be observed for waveguides deposited onto substrates with different roughnesses. To determine if there are any substrate effects, ZnS films were deposited onto substrates with rms roughnesses ranging from 0.2 - 0.7 nm. The parameters for the various substrates used are listed in table 4.1. Several ZnS films were deposited using different substrates and the same deposition parameters (table 4.2). Additional ZnS source material was added to the boat prior to each deposition and an oxidized silicon wafer substrate was used in each deposition as a control. The results of these depositions, shown in figures 4.1 and 4.2, are not as expected.

Figure 4.1 is a plot of loss versus surface roughness and it is obvious that there is no quadratic dependence. In fact, the losses as a function of surface

Table 4.1. Substrate properties.

Substrate	RMS roughness (nm)	Measurement technique	Polish
Oxidized Si Wafer	0.4	WYKO optical profiler	Prime
Zerodur	0.2	Talystep	Float
Fused Quartz	0.7	WYKO	
SAW polished Quartz	0.3	WYKO	
BK7	0.3	WYKO	Superpolish

Table 4.2. ZnS deposition parameters.

Base pressure	4.0 x 10^{-6} Torr
Source holder	Ta boat or Al_2O_3 crucible
Source material	Patinal ZnS (EM Chemical)
Source purity	99.99%
Source/substrate distance	26 cm
Deposition rate	0.4nm/s
Film thickness	550.0 nm

roughness appear to be random, suggesting that the losses are caused by something other than substrate roughness. By plotting the losses for the films deposited onto the control substrates in the order in which they were deposited (figure 4.2), an interesting trend is observed. The losses increase with each successive deposition. The losses for films deposited onto the control substrates are comparable to the losses for films deposited onto the substrates being tested. For comparison (between figures 4.1 and 4.2), the individual data points have been labeled according to deposition order. Rutherford backscattering (RBS) measurements show that the films are stoichiometric and contain small amounts of Ta. The first film contains a small amount of Ta (< 1%), but the contamination increases with subsequent runs. Apparently reusing the ZnS source material and the Ta boat results in Ta contamination of the evaporant. This is evidenced by a darkening of the source material. The Ta contamination most likely contributes to overall waveguide losses by introducing absorption. Although this absorption may be negligible for most filter applications, these results show that it is a major contributor to overall waveguide losses. To avoid Ta contamination, a different source holder should be utilized.

The above experiment suggests that the dominant loss mechanism for ZnS waveguides is something other than scattering from the substrate interface. Even without introducing absorption the losses of these waveguides (8.0 dB/cm) are significantly higher than that predicted from Marcuse's surface scattering theory (< 1.0 dB/cm). The majority of the losses are caused by defects in the internal microstructure of the film, or by an enhanced surface roughness at the film/air interface.

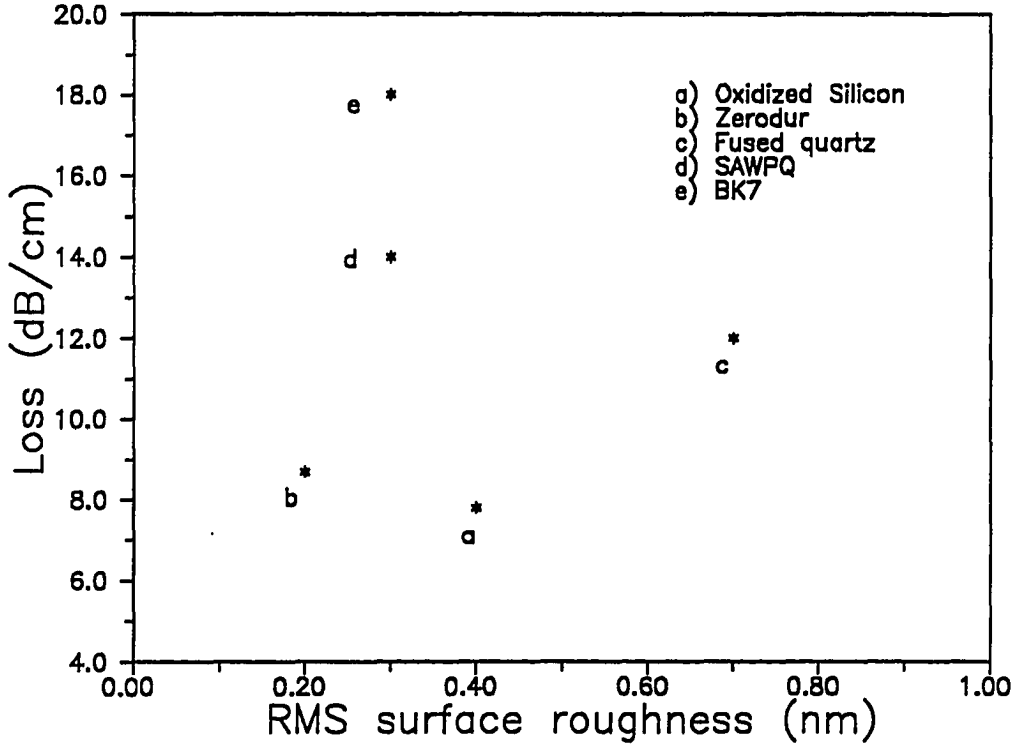

Figure 4.1. Loss versus substrate rms surface roughness for ZnS waveguides.

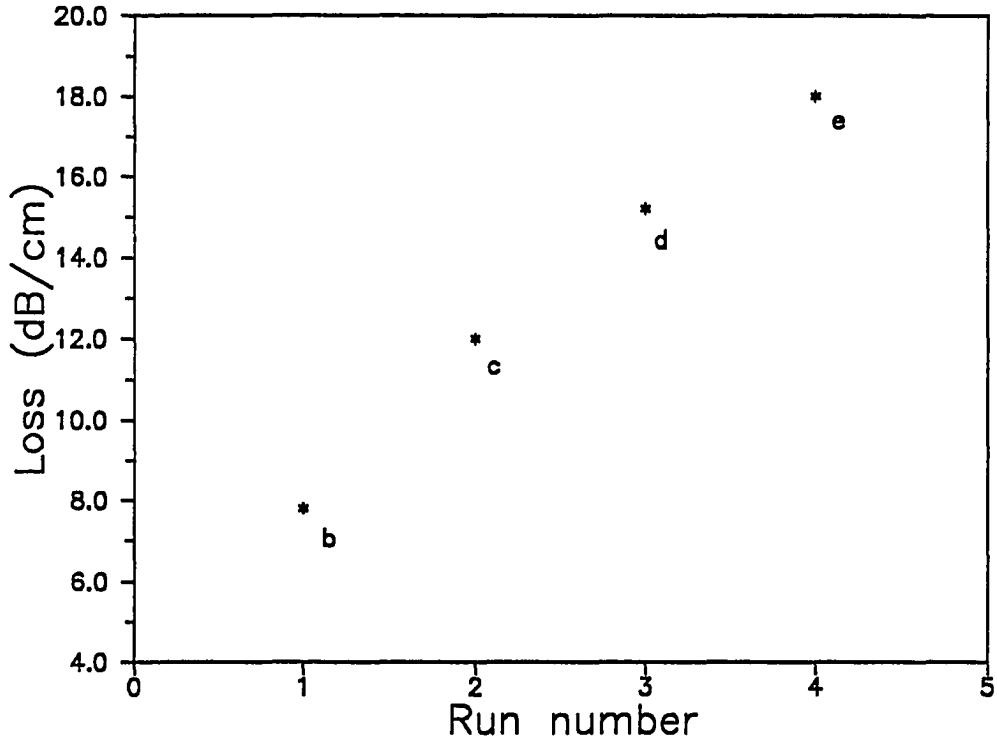

Figure 4.2. Loss versus deposition order for ZnS waveguides deposited onto oxidized Si control substrates with used Ta boat and source material. Labels correspond to films in figure 4.1.

Predeposition Requirement

Early in the project it was noticed that if the deposition system had not been used for several days or if some other material had been deposited, the first ZnS waveguide deposited would exhibit higher losses. The losses are as much as 3.0 dB/cm higher than the losses for successively deposited films (≅ 8 dB/cm, see figure 4.3). For the first film plotted in figure 4.3, ZnS was deposited from a new Ta boat after the system had not been used for several days, while the other four films were deposited (also from new Ta boats) on successive days. To eliminate this problem, a pre-deposition (or "muck-up" run) is performed prior to each series of depositions to condition the system. ZnS is evaporated in the vacuum system using the same parameters shown in table 4.2, but no substrate is installed. The system is then opened to air and prepared for an actual film deposition.

Reproducibility

To determine repeatability, three series of depositions were performed using the deposition conditions listed in table 4.2. Each series consisted of three successive depositions using substrates cleaved from a single 3" diameter oxidized silicon wafer. Because the Ta boats cause film contamination, each series of depositions used a different source holder. The trial source holders included quartz and alumina crucibles, and molybdenum boats. A new Mo boat was used for each of the three depositions while the crucibles were used repeatedly after they were "burned-in". The "burn-in" consists of heating the crucible under vacuum for 2 hours to outgas any impurities. This is achieved by installing a crucible filled with Patinal ZnS in a tungsten crucible heater, pumping down the system to 4.0×10^{-6} Torr and heating the crucible until a deposition rate of 0.8 nm/s is reached. This

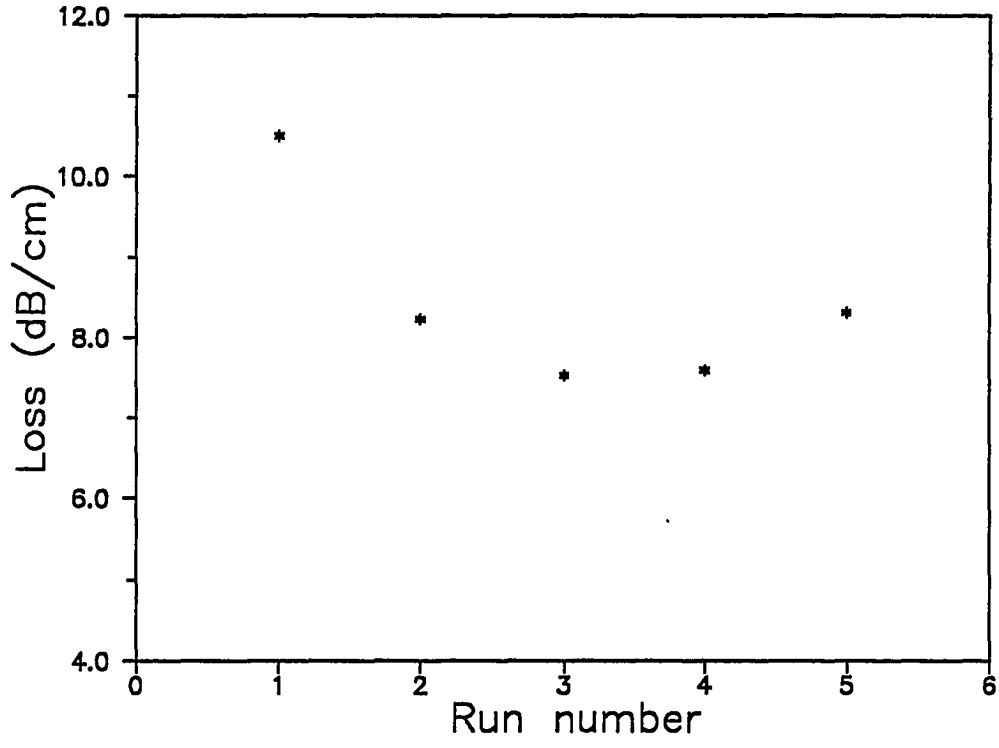

Figure 4.3. Loss versus deposition order for ZnS waveguides deposited with new boat and source material.

rate is higher than that of a normal deposition so that no impurity outgassing will occur at the actual deposition rate of 0.4 nm/s. Once the vacuum system had been preconditioned as described above, three successive depositions were performed for each of the source holders. In all cases the measured losses are approximately 9.0 ± 1.0 dB/cm and the RBS data showed no measurable impurities. Therefore, any of the source holders are useable for the project. The alumina crucible was selected because it yields a steadier deposition rate than the other two holders. In fact, a rate of 0.4 ± 0.02 nm/s can be maintained for the entire deposition without adjusting the power source. The other two holders require constant adjustment to maintain a rate that fluctuated by 0.1 nm/s.

Effects of Residual Gas Partial Pressures

Once repeatability was established, a systematic study of other effects on waveguide losses was possible. To more accurately determine and control the processes that affect waveguide losses, the Spectramass 100 residual gas analyzer (RGA) was installed on the deposition system. Although the RGA total pressure readings differ from those of the ion gauge, they are self consistent. Once it was determined that Ta contamination introduced absorption, it was suspected that residual gases in the vacuum system could also be incorporated into the film and cause an increase in absorptive losses. To reduce the effects of residual gases on waveguide performance, it is necessary to deposit the films in a pressure less than 4.0×10^{-6} Torr which is the basepressure used for most of the depositions. For the diffusion-pumped system in use, that pressure is attainable only by baking out the system to outgas the residual gases. To perform the bakeout, the system is prepared as before for a deposition and a second thermal source (empty Ta boat) is installed in the system. The system is pumped down to a pressure of 4.0×10^{-6} Torr and

Ar is introduced through a Vacoa bleed valve until a pressure of 1.5×10^{-4} Torr is reached. The thermal conductivity of the Ar results in more uniform heating of the chamber, even in places where there is no direct irradiation from the Ta boat. The bakeout is continued for approximately one hour or until the system temperature reaches 120°C. This temperature is monitored with a type K thermocouple that is attached to an aluminum plate in close proximity to the substrate (figure 3.1). The system is then allowed to cool for several hours until ambient temperature is reached, then the Ar is shut off. The bakeout results in an order of magnitude decrease in the H_2O partial pressure from 3.0×10^{-6} to 4.0×10^{-7} Torr. The O_2 partial pressure of 4.0×10^{-8} Torr, however, is essentially unchanged. The effects on waveguide losses are not as expected. Instead of lower losses, the film deposited in a baked out system has significantly higher losses (16.5 dB/cm). This prompted further studies into the effects of H_2O and O_2 backpressures during film preparation (Himel, Ruffner, and Gibson, 1987).

Depositions were made by varying O_2 pressures for successive depositions. O_2 was introduced into the vacuum system through the Vacoa bleed valve until the desired partial pressure, indicated by a Spectramass 100 RGA, was reached. O_2 pressures varied from 3.0×10^{-8} to 1.0×10^{-6} Torr. The results of these studies are shown in figure 4.4 which is a plot of loss versus O_2 backpressure for two different H_2O partial pressures. The lower curve represents films deposited in a base pressure of 4.0×10^{-6} Torr and it shows a strong dependence on O_2 partial pressure, while the upper curve represents films deposited at 4.0×10^{-7} Torr. Although there are only two data points for the upper curve, it appears to have a dependence on O_2 partial pressure similar to that of the lower curve. The initial decrease in losses with increasing O_2 pressure may result from oxygen bonding to

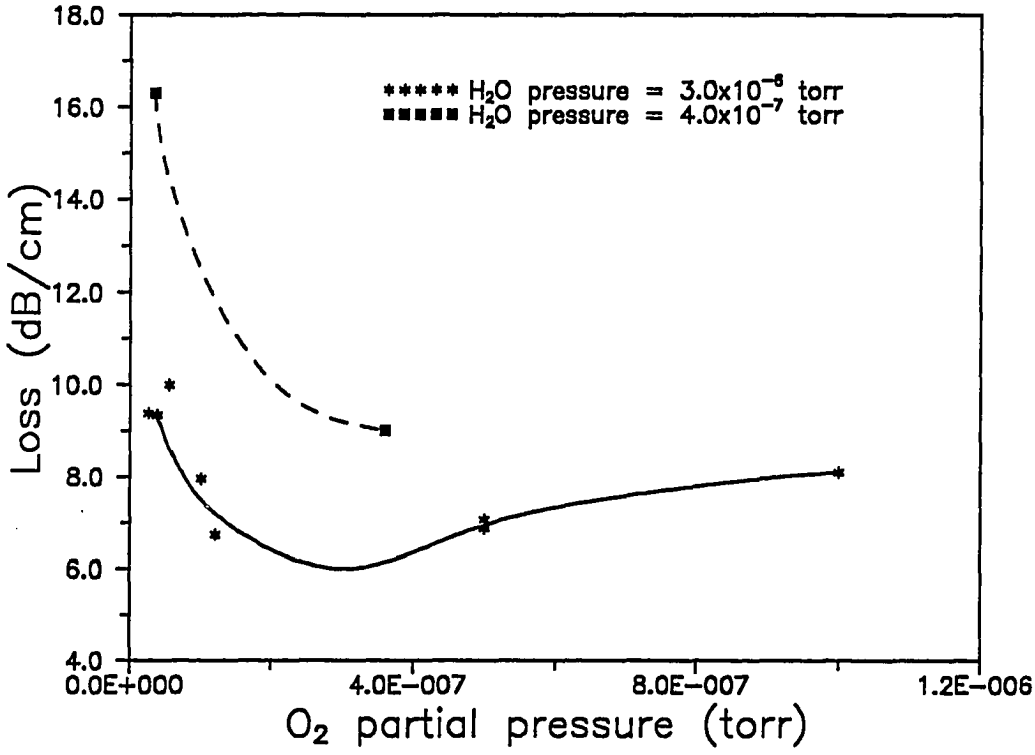

Figure 4.4. Loss versus O_2 partial pressure for two H_2O partial pressures.

dangling Zn bonds at grain boundaries. This would reduce absorption and yield lower overall losses. The initial decrease could also result from molecular ZnO filling in voids between ZnS grains. The theories for scattering from index variations shows that loss is proportional to M^2 where M is the rms index variation (Miyanaga, *et al.*, 1978, 1979, 1980; Hall, 1985). Therefore, incorporating ZnO (with a refractive index of 2.0) into film voids instead of air or water should lower waveguide losses. It may be possible to determine which of these effects is responsible for the reduction of losses by examining the RBS results. The RBS data give a maximum value for the number of free carriers present in the film. The zinc-to-sulfur ratio for these films is 1.00 to within 1%. Therefore the maximum number of free carriers, N, caused by a 1% difference in stoichiometry is $10^{16}/cm^3$. The loss introduced by the free carriers may be described by

$$\text{Loss (dB/cm)} = 10\sigma N \log_{10} e \,, \qquad 4\text{-}1$$

where σ is the free carrier absorption cross-section. Using a cross-section of 10^{-18} (Van Stryland *et al.*, 1985) yields a maximum loss of 0.04 dB/cm. Free carrier absorption is not the only absorpive mechanism resulting from a lack of stoichiometry that may introduce losses. Cluster formation of the excess constituent is also possible. To estimate losses introduced by cluster formation of 1% excess Zn, a Bruggeman effective medium (Wood and Ashcroft, 1977; Hickey, 1987) calculation was performed. The calculation yields losses of 2.1×10^4 dB/cm at a wavelength of 633 nm. Because losses of this magnitude have never been observed in ZnS waveguides, it is reasonable to assume that excess Zn or S does not form clusters. Therefore, the reduction in losses is most likely caused by the reduction in the refractive index difference between the crystallites and voids resulting from the

incorporation of ZnO into the film voids.

The interaction of O_2 and H_2O with Zn and S at the substrate could also modify crystallite growth or columnar structure. As O_2 partial pressure is increased, losses show a slight increase that could result from enhanced columnar growth caused by oxygen incorporation into the film. The increase could also be caused by microcracks at the film/substrate interface resulting from an increase in the internal stresses of the film (Bovard, 1988). RBS measurements show that the ZnS films are stoichiometric with 1-2% oxygen content. However, the percent concentrations are only accurate to 1% so that any small change in the oxygen impurity level would not be apparent from RBS measurements.

The x-ray diffractometry (XRD) measurements are the most revealing of the tests performed and can be used to explain why the films deposited at lower base pressures have higher losses. XRD indicates that the films are polycrystalline and have the zinc-blende (cubic) structure. ZnS can form in both cubic and hexagonal crystal structures, but preferential orientation within the films may complicate structure identification. The allowed diffraction peaks and their associated angles and intensities for both structures are shown in table 4.3 and a typical XRD scan is shown in figure 4.5. By comparing the peaks observed in the scan to the allowed angles in table 4.3, it is possible to determine the structure of the crystallites. ZnS peaks are located at 28.6^0, 47.6^0, and 56.3^0. Although these peaks correspond closely to allowed peaks for both cubic and hexagonal structures, several allowed high intensity peaks for the hexagonal structure are never observed. Therefore, it is highly probable that the crystal structure is cubic.

Figure 4.6 is a plot of waveguide loss as a function of crystallite size. The grain size is determined by measuring the full width at half maximum of a

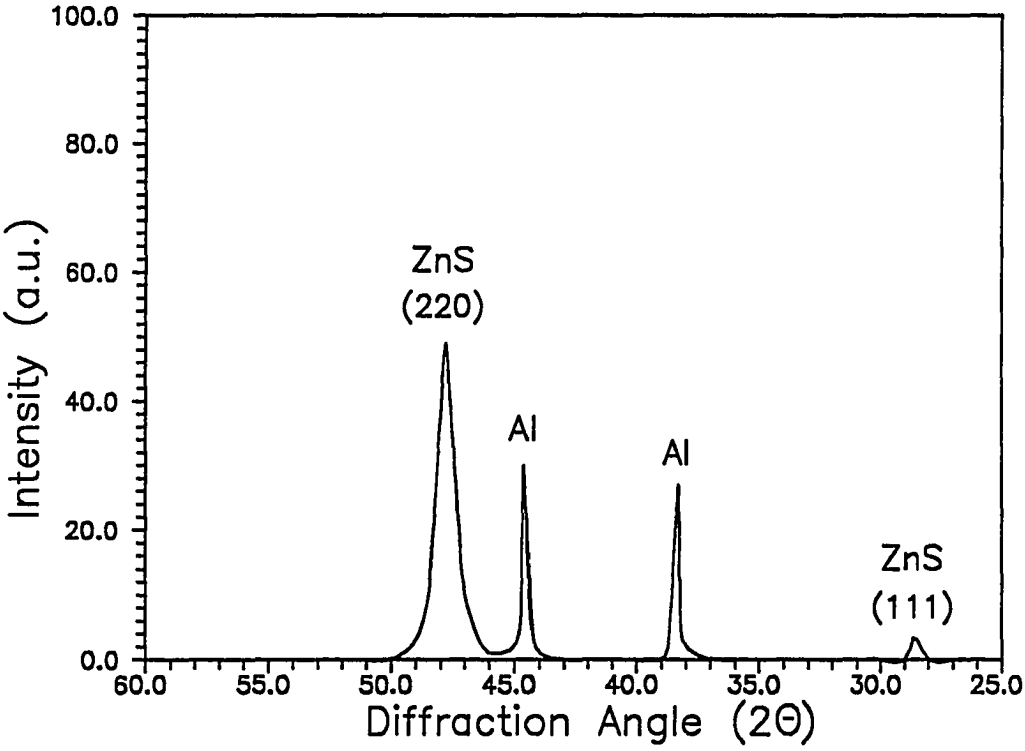

Figure 4.5. X-ray diffraction spectrum for ZnS film deposited in a base pressure of 4.0 x 10^{-6} Torr.

Table 4.3. Crystalographic data for cubic and hexagonal ZnS (Swanson and Fuyat, 1967).

	hkl	d	2θ	I/I_1
Cubic ZnS	111	3.123	28.6	100
	200	2.705	33.1	10
	220	1.912	47.6	51
	311	1.633	56.3	30
	222	1.561	59.2	2
Hexagonal ZnS	100	3.309	26.9	100
	002	3.128	28.5	86
	101	2.965	30.6	84
	102	2.273	39.7	29
	110	1.911	47.6	74
	103	1.764	51.8	52
	200	1.654	55.6	10
	112	1.630	56.5	45
	201	1.599	57.6	12

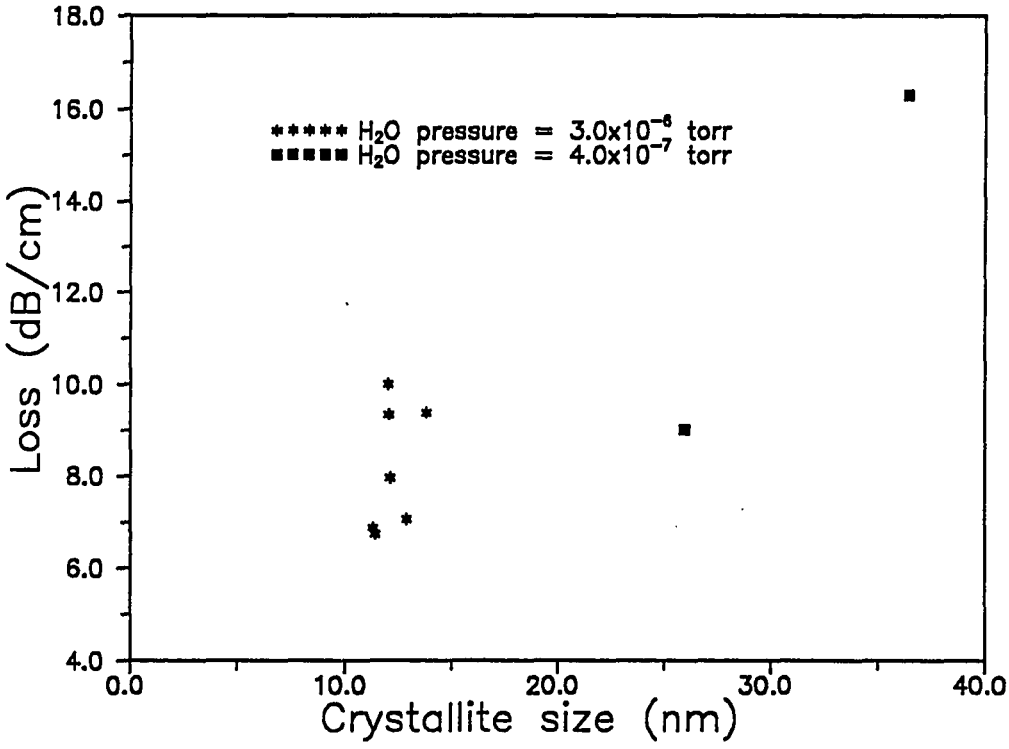

Figure 4.6. ZnS waveguide losses versus average crystallite size.

diffraction peak and using the Scherrer equation (equation 3-5). The waveguides deposited in an H_2O partial pressure of 3.5×10^{-6} Torr all have (220) crystal planes preferentially oriented with the substrate surface. Grain sizes range from 12.0 to 14.0 nm while losses vary from 6.7 to 10.0 dB/cm. The 10.0 dB/cm waveguide also has a significant number of (111) oriented grains present. These grains have an average size of 25.6 nm and could be responsible for the higher losses of this guide. The films deposited at a lower base pressure (4.0×10^{-7} Torr) had (111) crystal planes oriented with the substrate surface. These films have larger average grain sizes and consequently higher losses. These results suggest that the presence of H_2O at the substrate surface during deposition may play an important role in preferential orientation leading to smaller crystallites or retardation of crystal growth, which results in lower losses.

Mode Dependence of Waveguide Loss

As discussed in chapter 2, the modal dependence of waveguide loss can give insight into whether the losses are caused by surface scattering, volume mechanisms, or some combination of both. Figures 4.7 and 4.8 show the losses of a ZnS film deposited at ambient temperature for several TE and TM modes at $\lambda = 0.6328$ μm. The losses increase significantly for the higher order modes, which suggests that losses resulting from surface scattering are dominant or become dominant for the higher order modes. Although the substrate surface has a very low rms roughness (0.4 nm), the roughness at the upper surface of the film may be much greater as a result of the polycrystalline nature and preferential growth along crystal planes. Because the fields for the different modes sample the volume of the film differently (figure 2.3), it may be possible to see the same modal dependence of loss in the absence of surface scattering if there were large inhomogeneous layers parallel to

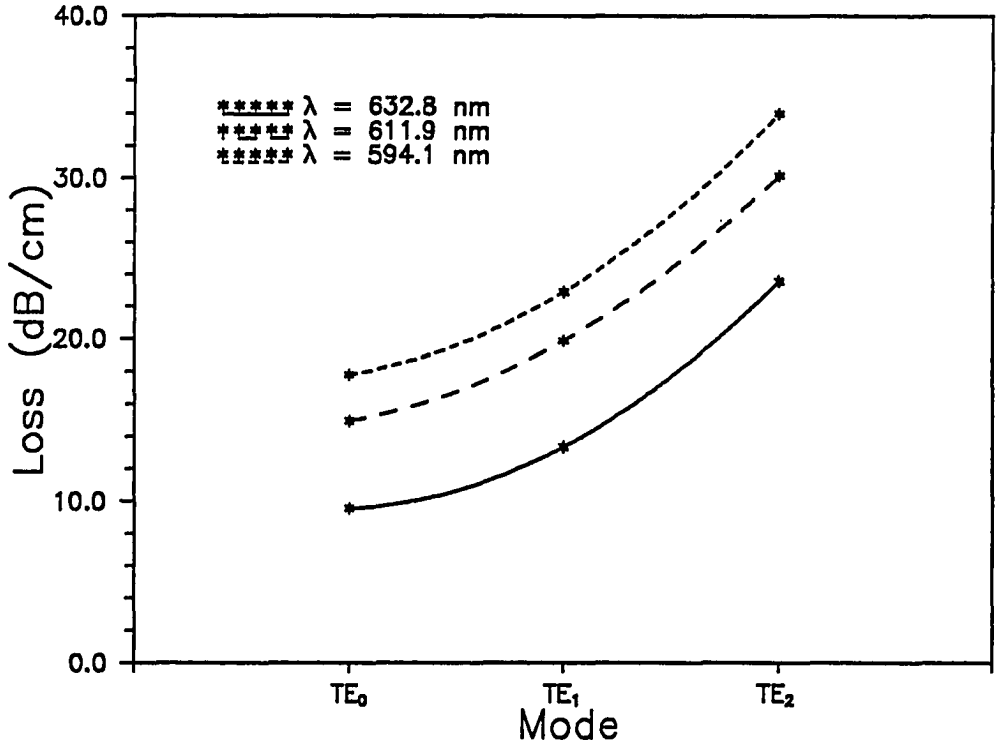

Figure 4.7. Waveguide loss versus TE mode number for different wavelengths.

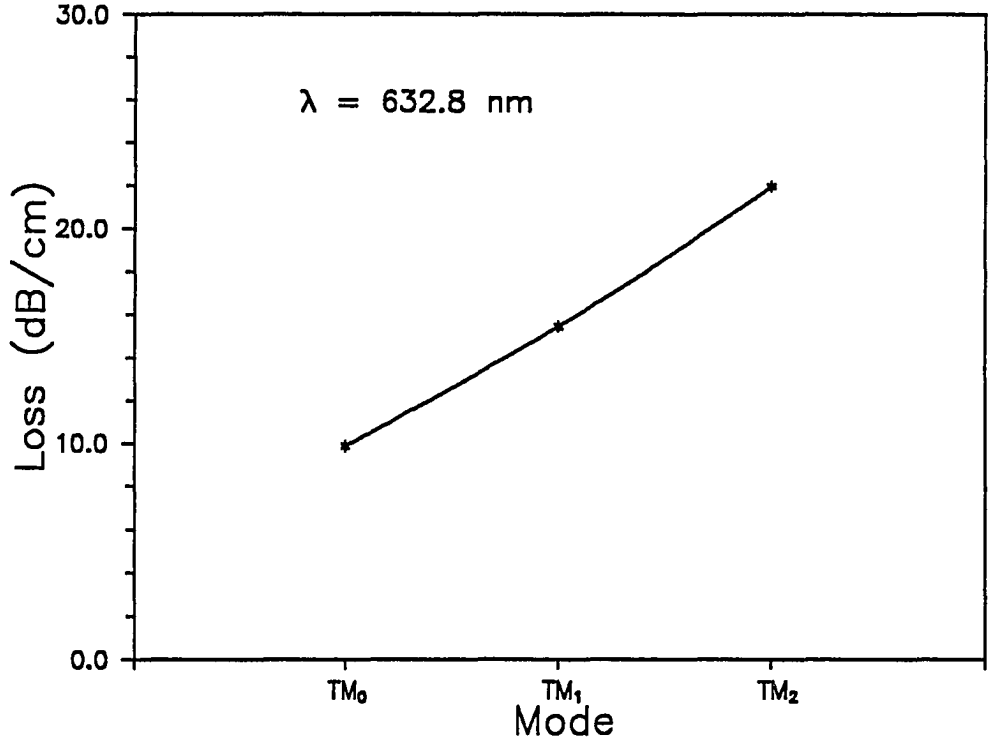

Figure 4.8. Waveguide loss versus TM mode number.

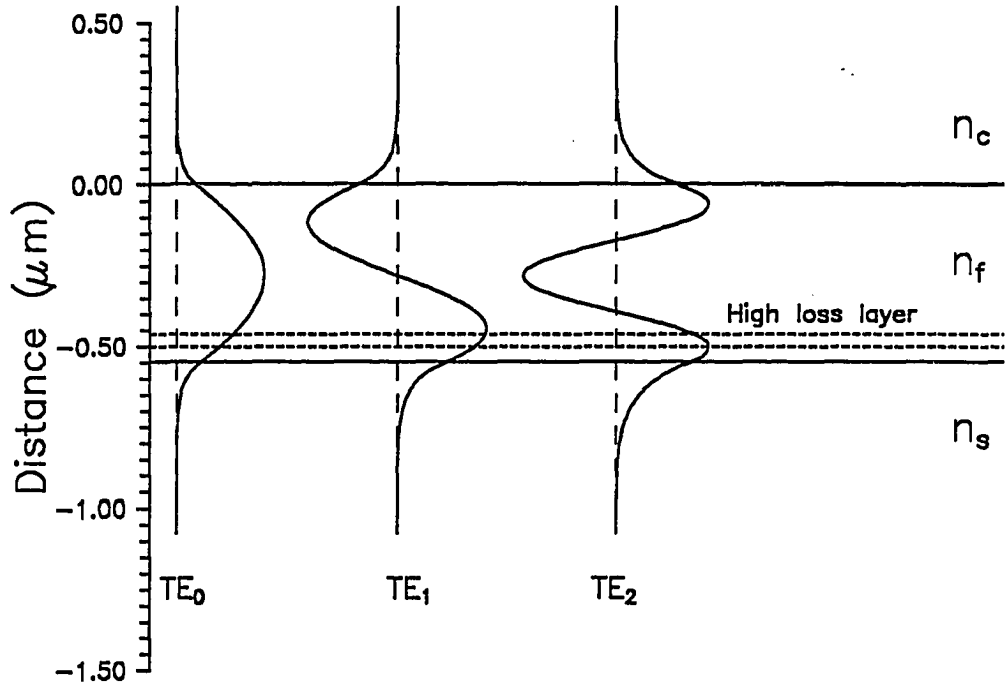

Figure 4.9. Model of a film with a high loss layer that may contribute to higher losses for higher order modes.

the substrate within the film. For example, figure 4.9 shows a model of a film with a high loss layer that may contribute to higher losses for the higher order modes, because the electric field within the defect layer increases for higher order modes. All of the films deposited at ambient temperature have the same modal dependence. Since it is highly unlikely that each film contains an identical defect layer, the losses are most likely caused by surface scattering or a combination of surface and volume scattering. Initial film nucleation will introduce a defect layer at the substrate surface, but this will most likely contribute to surface scattering.

By comparing the measured losses of several guided modes to the theoretical dependence of loss on surface electric field intensity and confinement factor, it is possible to separate volume and surface losses (Channin, Hammer, and Duffy, 1975). The losses for three modes of a ZnS waveguide (same waveguide described in figures 4.7 and 4.8) along with the calculated electric field intensity (equation 2-13) and confinement factor (equation 2-17) are plotted in figure 4.10. The calculated curves are normalized to the measured loss of the TE_0 mode. In the absence of volume losses the measured losses for increasing mode number should increase with surface field intensity (solid line), while losses resulting solely from volume mechanisms should decrease with confinement factor (dashed line). It is clear from figure 4.10, however, that neither case is observed. The losses are obviously a combination of volume and surface effects.

For a waveguide that supports three guided modes for example, volume and surface losses can be determined by solving the following set of three equations:

$$L_0 = L_{s,0} + L_{v,0} \qquad 4\text{-}2$$

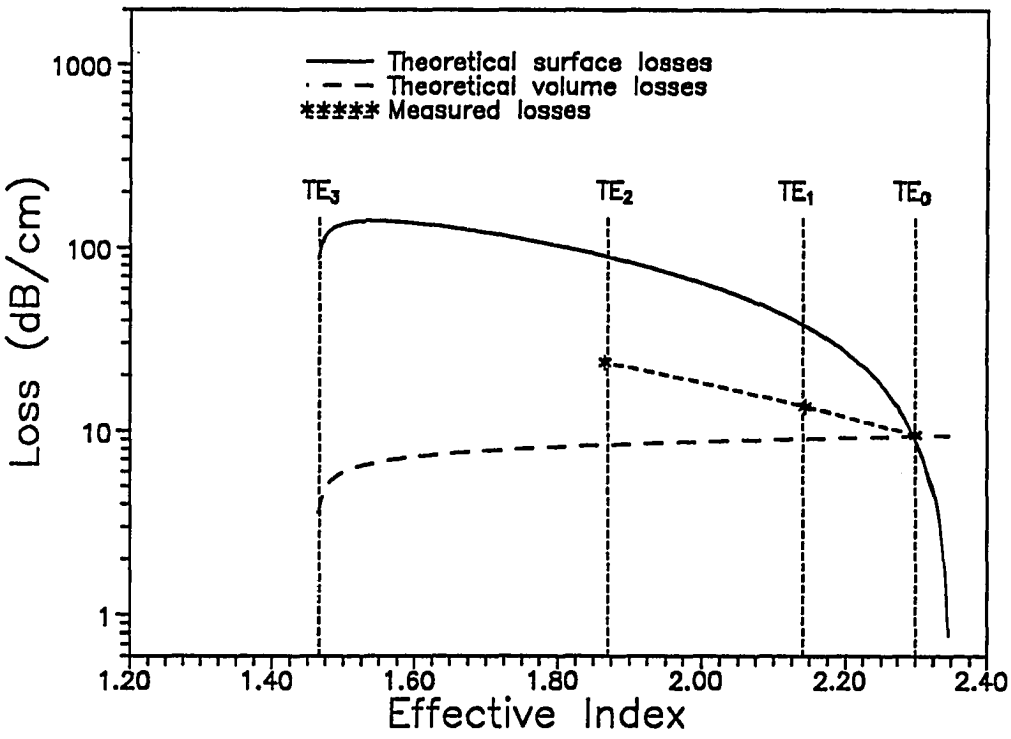

Figure 4.10. Theoretical and experimental dependence of waveguide loss on effective index. Losses introduced solely by surface scattering increase with mode number (solid line) while losses resulting from volume scattering and absorption decrease with mode number (dashed line). Measured losses (asterisks and dashed line) do not follow either theoretical curve. Vertical lines show effective index of the guided modes.

$$L_1 = L_{s,1} + L_{v,1} = \left[\frac{E_{s,1}}{E_{s,0}}\right]^2 L_{s,0} + \frac{\Gamma_1}{\Gamma_0} L_{v,0} \qquad 4\text{-}3$$

$$L_2 = L_{s,2} + L_{v,2} = \left[\frac{E_{s,2}}{E_{s,0}}\right]^2 L_{s,0} + \frac{\Gamma_2}{\Gamma_0} L_{v,0} \,, \qquad 4\text{-}4$$

where L is the loss. The subscripts s and v refer to surface and volume parameters, respectively, and the numeric subscript corresponds to the mode number. These equations assume that surface and volume losses are not cross-correlated, that there is no multiple scattering, and that total waveguide losses may be described by a linear superposition of volume and surface effects.

The losses of the three lowest order TE modes for several ZnS waveguides deposited at ambient temperature with total losses for the TE_0 mode ranging from 3.0 - 10.0 dB/cm are plotted in figure 4.11. The solutions to equations 4-2 - 4-4 are shown in table 4.4. For all of the waveguides tested the losses introduced by surface scattering are approximately 1.5 dB/cm for the TE_0 mode. This is independent of the total waveguide loss. For the TE_0 modes of the three higher loss samples (a-c), the volume losses exceed surface scattering, while for the TE_0 mode of the lowest loss sample (d), volume and surface losses are equal. Losses caused by surface scattering, however, increase with increasing mode number and are substantially higher than volume losses for the TE_2 mode. These results suggest that the major effect of changing deposition conditions is a reduction of volume losses.

Wavelength Dependence of Waveguide Loss

Figure 4.12 is a plot of loss versus λ for the same waveguide described in figures 4.7 and 4.8. These measurements were made with a PMS tunable HeNe laser that was internally polarized so that only TE measurements could easily be taken. If the losses are strictly caused by Rayleigh-like scattering, losses should

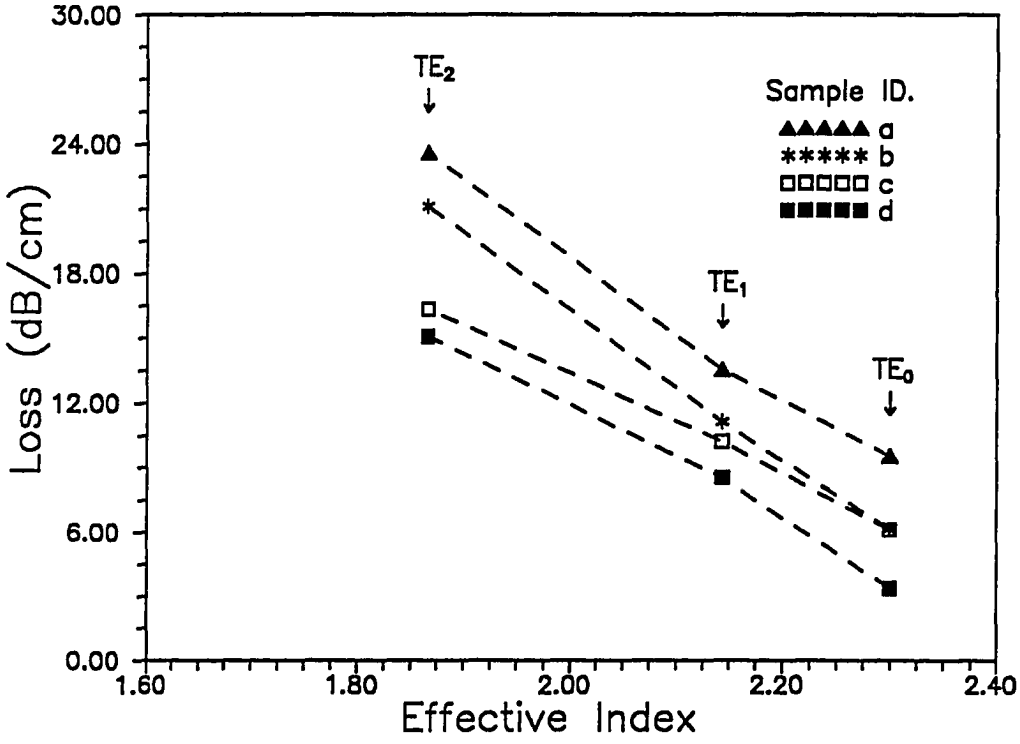

Figure 4.11. Loss versus effective index for several ZnS waveguides.

Table 4.4. Magnitude of volume and surface losses for several ZnS. Sample letters correspond to labeled points in figure 4.11.

Sample	Mode	Meas. Loss	L_v	L_s	Calc. Loss
a	TE_0	9.55	8.20	1.35	
	TE_1	13.55	7.93	5.62	
	TE_2	23.58	7.32	13.52	20.84
b	TE_0	6.14	4.51	1.63	
	TE_1	11.14	4.36	6.78	
	TE_2	21.12	4.03	16.29	20.31
c	TE_0	6.11	4.76	1.35	
	TE_1	10.22	4.60	5.62	
	TE_2	16.35	4.25	13.50	17.75
d	TE_0	3.37	1.72	1.65	
	TE_1	8.54	1.66	6.88	
	TE_2	15.08	1.53	16.54	18.07

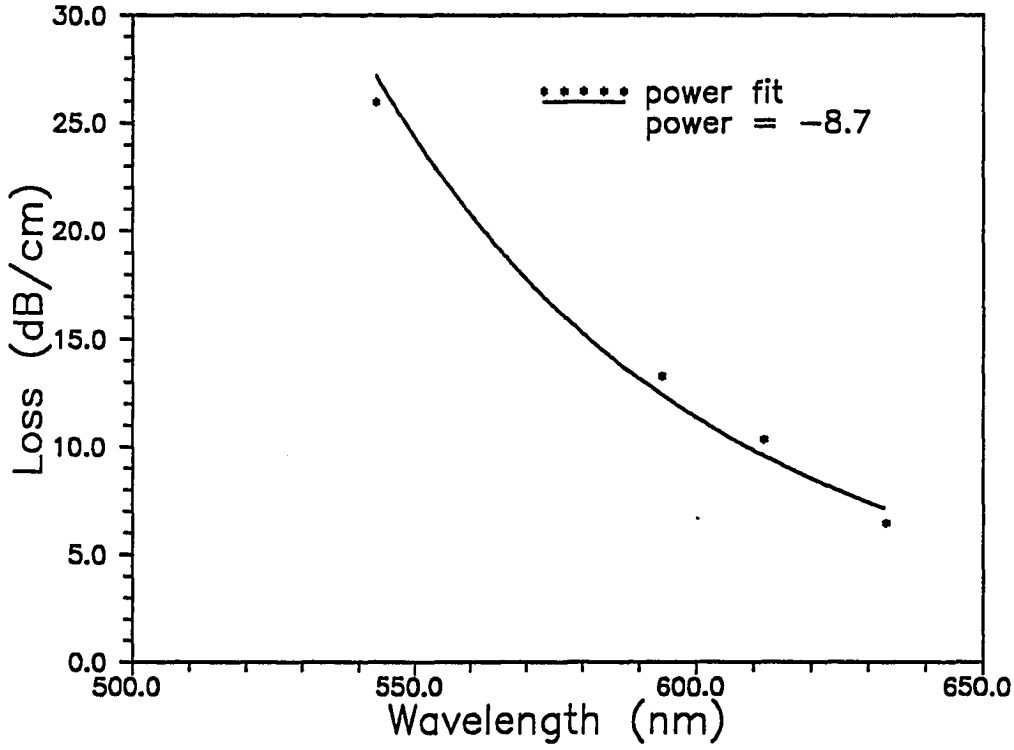

Figure 4.12. Loss versus wavelength for a ZnS waveguide deposited at ambient temperature.

exhibit approximately a $1/\lambda^4$ dependence. True Rayleigh scattering is only observed for the case of plane waves interacting with molecularly sized particles. Therefore, deviations from a $1/\lambda^4$ dependence are expected because of the modal field distributions that occur within a waveguide. This dependence is expected for both volume and surface scattering. A power fit to the measured losses, however, show a much stronger $1/\lambda^9$ dependence. The absorption of bulk ZnS results in losses of 3.0 dB/cm at λ = 633 nm and only increases slightly to 3.2 dB/cm at 543 nm (Palik, 1985). This suggests that absorption may not be responsible for the $1/\lambda^9$ behavior. It should be noted, however, that films deposited onto cooled substrates have losses less than 1.0 dB/cm. Thus the bulk absorption properties do not accurately describe absorption in ZnS thin films and any conclusion based on bulk properties may be inaccurate.

Effects of Substrate Temperature

Once it had been determined that the losses are primarily caused by the polycrystalline structure of the film, it was possible to modify the deposition process to produce films with smaller crystallites. The crystallite size is dependent on adatom surface mobility which increases with temperature. Therefore, an increase in substrate temperature during deposition should result in larger grains. This result was confirmed in a related study performed by Ruffner (1988). Several films were deposited at different substrate temperatures ranging from -110°C to 300°C. The results of XRD measurements are plotted in figures 4.13 and 4.14. As expected the grain size decreases with decreasing substrate temperature (figure 4.13) and films deposited onto cooled substrates (< -50°C) were amorphous as determined by XRD. Aside from grain size, preferential orientation is also affected by changes in substrate temperature (figure 4.14). For films deposited at ambient temperature

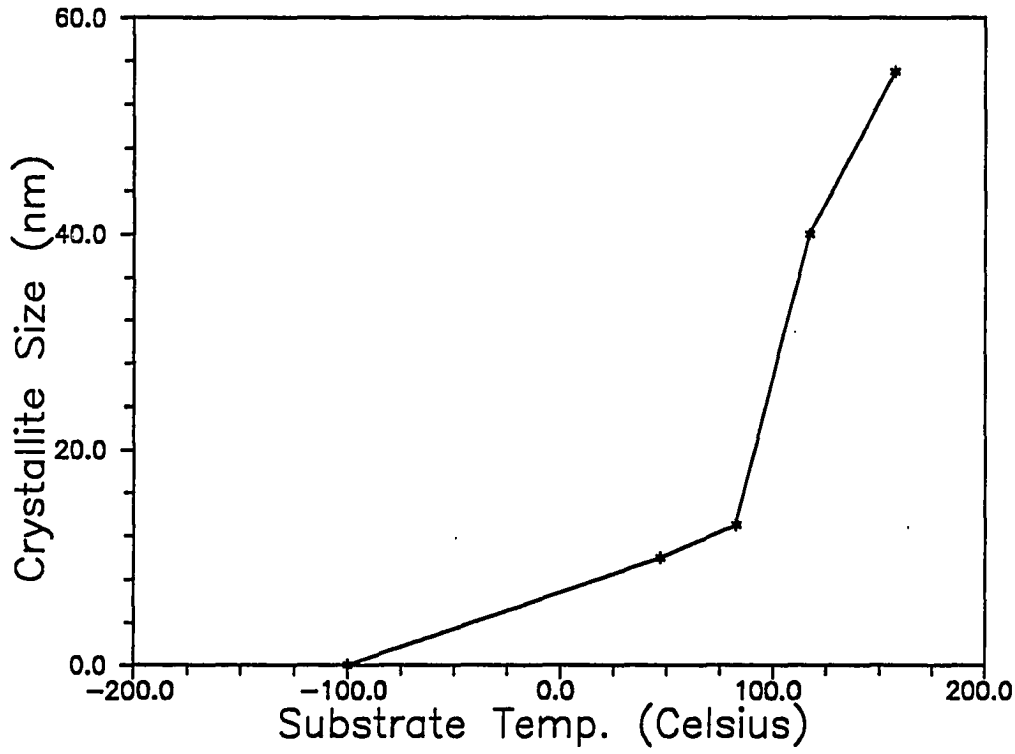

Figure 4.13. ZnS crystallite size versus the substrate temperature during deposition (Ruffner, 1988).

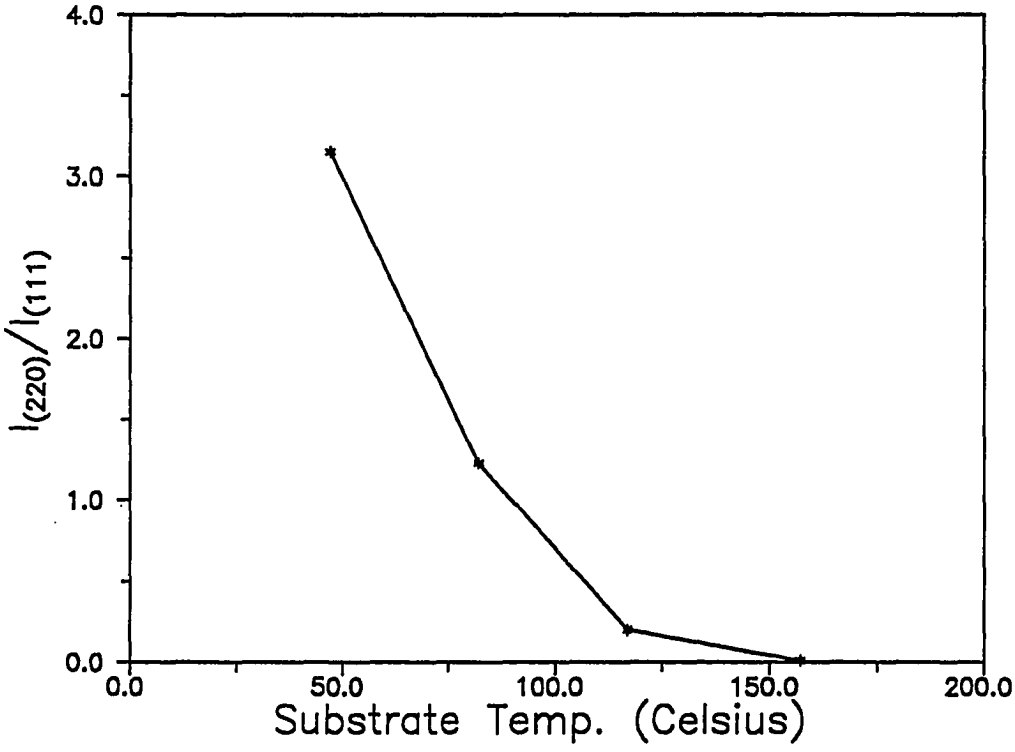

Figure 4.14. Ratio of (220) to (111) peak intensities for ZnS films versus substrate temperature during deposition (Ruffner, 1988).

the majority of the crystallites are oriented with (220) crystal planes parallel to the substrate. As the substrate temperature during deposition is increased a gradual change from (220) to (111) preferred orientation is observed. This orientation shift is similar to that observed when the H_2O partial pressure during deposition is decreased. Whether the orientation shift is caused by a change in substrate temperature or H_2O pressure is uncertain and warrants further study.

Deposition onto Cooled Substrates

The above experiments show that it is possible to make amorphous ZnS films by depositing onto cooled substrates. This procedure has not been exploited previously because it was expected that contaminants will condense onto the substrate prior to deposition. As the substrate warms to room temperature, the water or condensed oil will act as a separation layer and promote delamination of the film. In fact, cooling of the substrate holder does lead to a significant reduction in system pressure (from 4.0×10^{-6} to 1.5×10^{-6} Torr), indicating that the cooling block is acting as a getter. Because the substrate cools less rapidly than the copper block, however, it should be less contaminated.

The first films were deposited onto fused silica substrates that were tightly clamped to a liquid nitrogen cooling block. These films exhibited adhesion failure as shown in figure 4.15. This pattern is representative of tensile stress which is not seen in conventionally deposited ZnS films. Compressive stress is more common in ZnS films (Wenz and Hoffman, 1977; Laugier, 1981; Nesmelov, Lazareva, and Gusev, 1984) but tensile stress has been observed for ZnS deposited at high base pressures (Pulker and Maser, 1979).

To improve film adhesion, the substrates are ion-precleaned immediately prior to deposition. The substrate is cooled by flowing liquid nitrogen through the

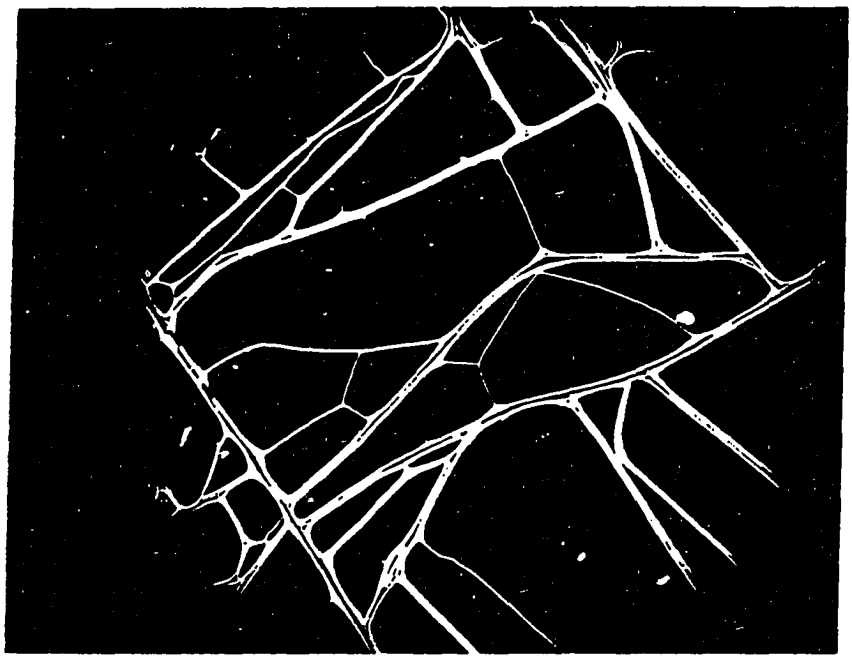

Figure 4.15. Tensile stress failure of ZnS film deposited onto liquid nitrogen cooled substrate.

cooling block. Meanwhile, the substrate temperature is monitored with a thermocouple that has been soldered with indalloy #4 to the fused silica substrate. After the substrate temperature reaches equilibrium, the ZnS source material is preheated to a deposition rate of 0.8 nm/s and outgassed for 2 to 3 minutes before the rate is reduced and stabilized at 0.4 nm/s. The source is then shuttered closed and Ar is bled into the system to a pressure of 1.0×10^{-4} Torr. The substrate is then ion-precleaned with the Kauffman type ion source for 60 seconds with a beam voltage of 600 eV and a beam current of 10.0 mA. The source is shuttered open as the ion-beam is shut off. Deposition continues until the XTM indicates that 500.0 nm has been deposited. The film is removed after it has warmed to ambient temperature. Although the films exhibit improved adhesion, they have a large variation in thickness (50 - 100 nm) across the 1" x 1" surface. This thickness variation is an effect of the low thermal conductivity of fused silica. The substrate edges are clamped tightly to the cooling block, and so are cooled more efficiently than the center of the substrate, resulting in a thermal gradient. When two thermocouples were attached to a substrate, one in the center and one at the edge, a 20°C temperature difference was observed on a substrate clamped tightly to the cooling block.

There are two possible ways to eliminate the thermal gradient. The first is to use a substrate, such as silicon, that has a much higher thermal conductivity than fused silica. The second is to improve the thermal contact so that it would be uniform across the entire substrate. The second is accomplished by attaching the substrate to the cooling block using capillary action from a drop of DC-705 diffusion pump oil. A mask is lightly clamped over the substrate to keep it from falling off. This technique is used for films deposited onto both oxidized silicon

wafers and fused silica. Films deposited on these substrates are uniform.

To determine the temperature dependence of waveguide loss, films were deposited at several different substrate temperatures. The results shown in figure 4.16, indicate that as the substrate temperature during deposition is decreased, the losses decrease until they reach a minimum of less than 1.0 dB/cm for λ = 633 nm at a substrate temperature of -50°C. These losses are lower than any previously reported for ZnS (Al-Douri, 1986). However, if the substrate temperature is too cold (< -70°C), the losses increase significantly. In fact, the losses for a film deposited at -90°C are so high that they can only be estimated at about 100 dB/cm. Although the high loss films look continuous to the naked eye, examination with a 100X magnification microscope reveal that they are not. The film deposited at -75°C has a very high density of pinholes while the film deposited at -90°C has microcracks. The cracks are caused by tensile stress failure, while the pinholes can be caused by either tensile stress failure or adhesion failure resulting from substrate contamination. These results suggest that the optimum substrate temperature for low losses is between -40 and -60°C. The losses for the lowest loss waveguide were measured for different wavelengths and modes as shown in table 4.5. Because the waveguide was deposited on a fused silica substrate, losses were difficult to measure accurately because of nonuniform scattering from scratches and subsurface defects. Therefore, accurate measurements could only be made for higher order modes and shorter wavelengths. Once again, this is a limitation of the waveguide and not the measurement technique. It should be noted that losses that could not be measured are probably lower than 0.44 dB/cm, which is the lowest measurable loss for this waveguide. Because of the measurement inaccuracy for this particular waveguide, the wavelength and mode dependence of loss could not

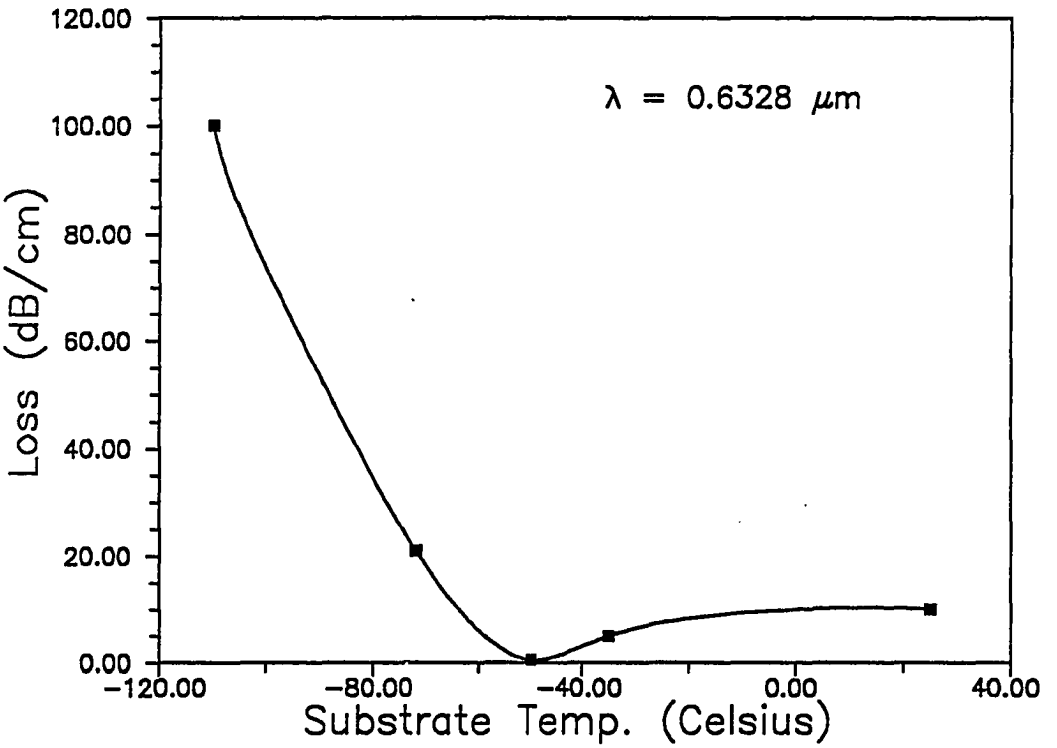

Figure 4.16. Loss versus substrate temperature during deposition for ZnS waveguides.

Table 4.5. Losses of different modes and wavelengths for a ZnS waveguide deposited onto a substrate cooled to -50°C.

Mode \ λ	633	611.9	594.1	543
TE_0	-	-	-	4.4
TE_1	-	-	0.44	3.86
TE_2	-	0.5	2.40	6.35

be reliably determined.

Several measurements suggest that the densities of these films are much lower than the bulk density of ZnS. Figure 4.17 is a plot of refractive index as a function of substrate temperature (Ruffner, 1988). For films deposited at ambient temperature the refractive index is slightly higher than the bulk index, indicating compressive stress. For films deposited at lower temperatures, the refractive index is significantly lower than that of the bulk material. This may be caused by a low packing density or by the incorporation of other materials such as ZnO. A low packing density is suspected because of the tensile stress observed in these films. However, SEM examination does not show columnar structure. This does not rule out the existance of columnar structure because the column diameters could be less than the SEM resolution (50-60 nm).

The in-plane scattering for waveguides deposited at lower temperatures is higher than that for films deposited at ambient temperature. Although no quantitative measurements have been made, this is easily observed by looking at the light exiting from the end of the waveguide. The in-plane scattering theories (Modavis and Hall, 1983; Hall, 1985) show that in-plane scattering is dominated by scattering from refractice index fluctuations within the film. The larger the refractive index fluctuation, the larger the in-plane scatter. This also supports the theory that the films have a low packing density that results from enhanced columnar structure or increased porosity.

Svensson reported effects of water desorption on nonlinear prism coupling in ZnS waveguides (Svensson, 1988). These films were deposited to a thickness of 500 nm at ambient temperature. IAD was used for the first 100.0 nm to improve film adhesion. The beam from a high power Ar ion laser was coupled into the

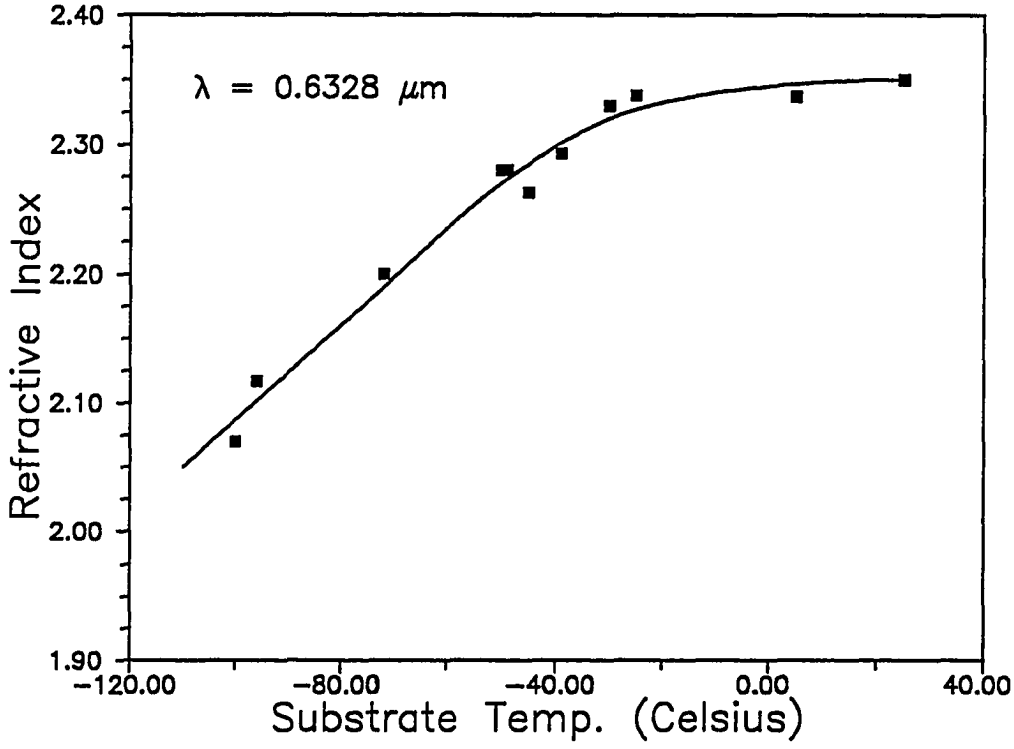

Figure 4.17. Refractive index versus substrate temperature during deposition for ZnS waveguides (Ruffner, 1988).

waveguide with a grating coupler and the output coupled light from a second grating was monitored with a detector. For a constant input power (≅ 1.0 W), the output coupling power decreased with time. This was evidence of a change in the film refractive index. This could be attributed to a thermal nonlinearity or possibly to the desorption of water from the film voids as the sample was heated. The latter was suspected because the thermal nonlinearity of ZnS has a response time of a few microseconds and the film did not recover for several hours or days.

More dramatic instabilities are observed for the films deposited onto cooled substrates. In an attempt to repeat Svensson's nonlinear measurements on the low loss waveguides, a similar set-up is used to couple the light from an Ar ion laser into and out of the waveguides. For low laser powers (10 mW) a well defined light streak and small output coupling spot are observed (figure 4.18a), while for higher powers (≅ 100 mW) the streak fanned out in the plane of the waveguide (figure 4.18b). Because the beam intensity in the plane of the waveguide is roughly gaussian, differential water desorption may occur. That is, more water will be desorbed where the light intensity is highest. This will introduce a refractive index gradient in the plane of the film which will act as a lens to spread out the light (Stegeman, 1988). Once the laser power is reduced or turned off, the film will recover within several days. Although these measurements are purely qualitative, the lower the refractive index, the more pronounced the refractive index gradient and the longer it takes for the film to recover. By performing these measurements with the sample in an evacuated chamber, most of the water contained in the film should desorb and the effects of differential water desorption should be eliminated.

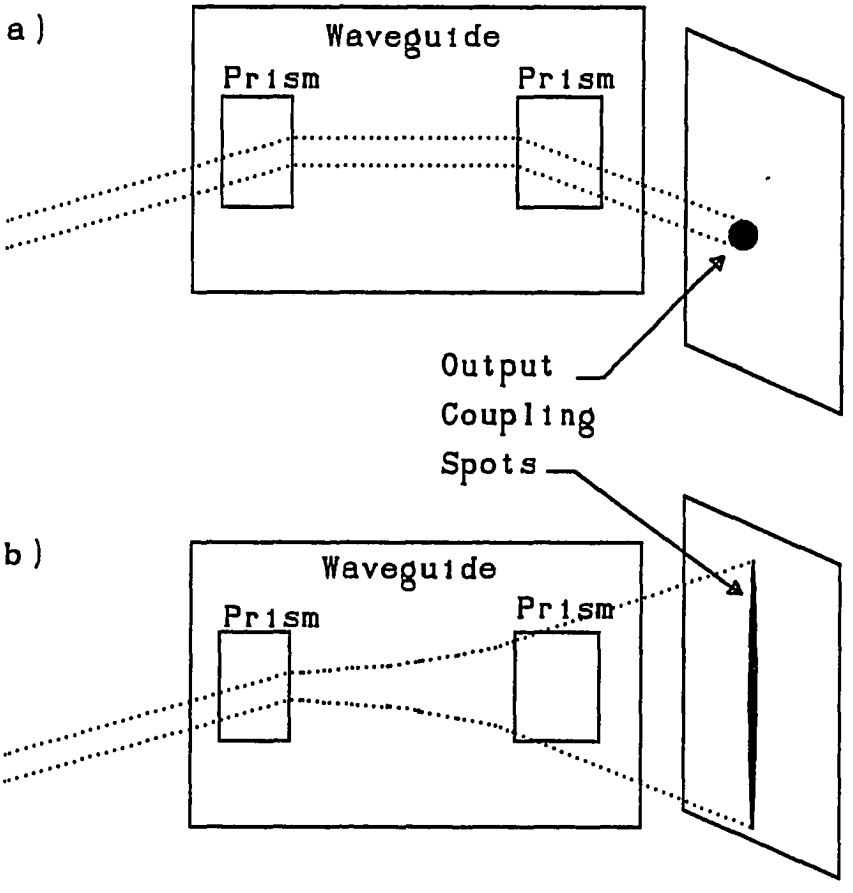

Figure 4.18. Scattered light profiles for a) low input power and b) high input power for a ZnS waveguide deposited onta a cooled substrate.

Summary

Effects of deposition conditions on ZnS film microstructure have been studied and compared with measurements of waveguide loss and refractive index. The results show a dependence of loss on O_2 and H_2O partial pressures. XRD measurements suggest that the higher losses for films deposited at lower H_2O partial pressures can most likely be attributed to larger crystallites. A decrease in volume scattering caused by the incorporation of ZnO into film voids is observed for depositions in O_2 backpressures. By measuring the losses of several modes for waveguides deposited at ambient temperature, it was determined that losses for the TE_0 mode caused by surface scattering are approximately 1.5 dB/cm, regardless of total waveguide losses. For the lowest order mode, volume losses exceed or equal surface losses while the losses of the higher order modes are dominated by surface scattering. By depositing films onto substrates cooled with liquid nitrogen, films with smaller crystallites and thus lower losses were fabricated. The losses of these films are less than 1.0 dB/cm and are lower than any previously reported for ZnS. Although these waveguides have low losses, they are extremely porous, as evidenced by a low refractive index. Attempts to observe nonlinear prism coupling failed because of differential water desorption. Ion-assisted deposition in conjunction with substrate cooling may yield low-loss and dense ZnS waveguides.

CHAPTER 5

CONCLUSION

ZnS thin-film coatings are used extensively in optical devices over a wide spectral range (Macleod, 1986). Currently, the majority of applications require the fabrication of multiple layer stacks to modify the transmitted or reflected spectrum of an optical element. Furthermore, both high reflectivity and high power applications require coatings with extremely low scatter and absorption, which can make characterization of the coatings exacting. Scattering and absorption losses in ZnS coatings are affected by the microstructure of the film, which is a direct result of deposition conditions (Al-Douri, 1986; Himel, Ruffner, and Gibson, 1987, 1988). Accurate determination of these losses at or near normal incidence is difficult because the light interacts with the film for only a few micrometers. As a result, losses are low and difficult to measure. If a waveguide geometry is used, however, the optical path may be several centimeters and losses as low as 0.01 dB/cm can be measured.

In this work a waveguide technique was used to determine the refractive index, thickness, and propagation losses of vacuum deposited ZnS thin films. The losses were determined by coupling a multiple line HeNe laser into a ZnS waveguide with a prism coupler and measuring the scattered light as a function of propagation distance along the film. A coherent fiber bundle was used to image this scattered light streak to a remote detector plane that was scanned with an apertured photomultiplier tube. The losses of the waveguide were compared to the

chemical composition and microstructure, which were determined from Rutherford backscattering and x-ray diffraction measurements, respectively.

By characterizing ZnS films fabricated under a variety of deposition conditions it is possible to determine the dominant loss mechanisms. Once the dominant loss mechanisms are understood, the deposition conditions can be modified to reduce their effects on the total losses. For example, early studies showed that evaporation of ZnS from used Ta boats resulted in losses that are significantly higher than the losses of films deposited from new Ta boats or Al_2O_3 crucibles. The losses are up to 9.0 dB/cm higher and result from Ta contamination of the film. Although these higher losses may be insignificant for many thin film applications, a source holder that does not contaminate the sample should be used for applications where absorption must be minimized, such as in high power laser mirrors or integrated optics. Currently an Al_2O_3 crucible is being used because it yields a steady deposition rate, and subsequent RBS measurements have not revealed any film contamination.

The effects of Ta contamination prompted studies into the effects of residual gas contaminants such as H_2O and O_2 on waveguide losses. The largest effect observed was an increase in waveguide losses with decreasing H_2O partial pressure. The losses for films deposited in an H_2O pressure of 4.0×10^{-7} Torr were 7.0 dB/cm higher than the losses for films deposited in an H_2O pressure of 3.0×10^{-6} Torr. XRD measurements showed an increase in the average grain size and a change in the preferential orientation of the grains for films deposited at lower H_2O partial pressures. The higher losses could be attributed to either an increase in surface scattering caused by an increased surface roughness for larger crystallites, or an increase in volume scattering. Increasing the O_2 pressure, however, had a

different effect on losses. A decrease in volume scattering caused by the incorporation of ZnO into film voids resulted in lower total losses for films deposited in a higher backpressure of O_2. The losses decreased because scattering is dependent on the index difference between ZnS and the interstitial material. Therefore, void filling with ZnO should result in lower volume scattering than void filling with air or water.

Although the above results suggest that the losses are dominated by the polycrystalline structure of the films, they do not show whether the losses are dominated by volume or surface scattering. Because the solutions to Maxwell's equations show that the surface field intensity increases and the confinement factor decreases with increasing mode number, it should be possible to separate volume effects from surface effects. By measuring the propagation losses of several TE modes and comparing them to the interface field intensity and the modal confinement factor, it is possible to quantitatively determine the volume and surface losses. The results show that, for ZnS waveguides deposited at ambient temperature in a base pressure of 4.0×10^{-6} Torr, the losses caused by surface scattering are approximately 1.5 dB/cm for the TE_0 mode and about 15 dB/cm for the TE_2 mode. The remaining losses (2 - 8 dB/cm for the TE_0 mode) can be attributed to volume scattering which decreases slightly with increasing mode number. These results show that losses for the lowest order mode are typically dominated by volume scattering while losses for the higher order modes are dominated by surface scattering.

Once it was determined that losses are dominated by the polycrystalline structure of the film, the deposition parameters were modified to produce films with smaller crystallites. By depositing onto substrates cooled with liquid nitrogen, the

adatom mobility was reduced and resulted in amorphous films. The optimum substrate temperature was found to be -50°C, which resulted in losses of less than 0.5 dB/cm for the TE_0 mode at λ = 633 nm. These losses are lower than any previously reported for ZnS. However, further reduction of the substrate temperature during deposition resulted in an increase in waveguide losses. Examination of the film under a microscope showed that the film had crazed as a result of tensile stress. ZnS films usually exhibit compressive stress as a result of their high packing density, but the films deposited onto cooled substrates had a low refractive index, which is evidence of a low packing density and increased porosity. This increased porosity may have resulted in tensile stress.

Further evidence of the increased porosity was observed when nonlinear prism coupling was attempted. As the input power from an Ar ion laser was increased, the scattered light streak spread out in the plane of the waveguide. This is most likely a result of differential water desorption introducing a refractive index gradient that acts as a lens to defocus the beam. Because the transverse line shape of the input beam is guassian, the waveguide will heat up more where the intensity is highest, resulting in more water being desorbed from the center of the guassian field distribution. The effect was more pronounced for films with lower refractive indices. Eventually the films recovered but, in some cases, this took several days.

Although the films deposited onto cooled substrates have low losses, they exhibit other problems that must be solved before the coatings can be used for either filter or integrated optics applications. The density of the films must be increased to approach that of the bulk material without significantly increasing the losses. This may be possible by depositing onto cooled substrates in conjunction with ion-assisted deposition. Another possibility is to thermally anneal the film

after deposition. There is a good chance that these methods will increase film density but will also increase losses by introducing crystallinity.

There are several questions that arose throughout this research which remain unanswered. First, both a decrease in the water partial pressure and an increase in substrate temperature resulted in a change in the crystallite preferential orientation from (220) to (111) crystal planes oriented parallel to the substrate. It is still unknown whether this change is a result of temperature, H_2O partial pressure, or both. By performing an experiment in UHV where gas partial pressure and substrate temperature can be more accurately controlled, it should be possible to determine the cause of the orientation shift. Second, the wavelength dependence of waveguide loss is significantly different from that predicted by scattering theory. Rayleigh scattering predicts a $1/\lambda^4$ dependence and Marcuse's two-dimensional treatment of roughness-induced scattering predicts a $1/\lambda^2$ dependence. However, a $1/\lambda^9$ dependence was observed. This is probably caused by absorption resulting from the broadening of the band edge for ZnS films, but this needs to be verified.

Although we think that the $1/\lambda^9$ dependence is related to near-band-edge absorption, it is possible that scattering from the film microstructure is partially responsible. However, the current waveguide scattering theories, which suggest a $1/\lambda^{3-4}$ dependence, do not accurately describe scattering from a polycrystalline film. Because Rayleigh scattering theories assume that all of the scatterers are identical and widely spaced, they can not be used to describe systems that have a distribution of closely spaced non-identical scatterers (different sized grains). Although, linear superposition principles hold for the case of non-identical scatterers that are widely spaced, for the case of a polycrystalline film, correlated scattering within grains and between different grains must be accounted for. These

possible scattering effects as well as cross-correlation effects make developing this theory very challenging. Also, because the film microstructure exhibits index inhomogeneities that are large and discontinuous, theories that employ perturbation methods, which assume the index fluctuations are small and continuous, may not be applicable. Therefore, to accurately describe scattering from a polycrystalline film, the scattering theory must account for the following: large index variations, index discontinuities at grain boundaries, non-identical scatterers, correlated scattering from within grains and between different grains, and cross-correlations between surface and volume scattering.

Finally, the water desorption and nonlinear properties of the low-loss waveguides should be studied with the sample under vacuum. By measuring the coupling angles for the different modes before and after evacuating the sample cell, it should be possible to measure the change in refractive index of the film as water is desorbed. Once the water is desorbed from the entire film, nonlinear coupling measurements can be made. To facilitate coupling into and out of the waveguide, samples should be deposited onto substrates which have gratings etched into them.

At present, no experiments have been performed that compare waveguide scattering to measurements of the total integrated scatter (TIS) or the bidirectional reflectance distribution function (BRDF). TIS and BRDF measurements are used extensively to determine the scattering characteristics of thin films. Because the waveguide geometry samples the film microstructure differently than the TIS and BRDF geometries, the measurements may yield slightly different results. However, there should be some correlation between the results of the different measurements. To make waveguide loss measurements more useful to the coating industry, this correlation should be determined.

In conclusion, this work used a waveguide technique to accurately determine the propagation losses of ZnS thin films. By comparing the measured losses with the film microstructure, it was determined that the losses were dominated by scattering from the polycrystalline structure of the film. By depositing films onto cooled substrates, amorphous films with low losses were fabricated.

REFERENCES

A. A. L. Al-Douri, "The Influence of Substrate Temperature on the Optical Losses of ZnS Film," J. Vac. Sci. Technol. A. 4, 2477 (1986).

S. D. Allen, *et al.*, "Calorimetric Measurement of $LiNbO_3$ Waveguide Absorption Losses," Appl. Phys. Lett. 34, 435 (1979).

G. H. Ames and D. G. Hall, "Attenuation in Planar Optical Waveguides: Comparison of Theory and Experiment," IEEE J. Quantum Electron. QE-19, 845 (1983).

M. Arnz and H. E. Ponath, "Roughness-Induced Scattering and Attenuation of Guided Modes in Slab Waveguides," J. Opt. Soc. Am. A. 3, 2055 (1986).

E. A. Arutunyan and S. Kh. Galoyan, "New Method for Loss Measurements in Optical Waveguides," Opt. Comm. 57, 391 (1986).

L. N. Binh, R. P. Netterfield, and P. J. Martin, "Low-Loss Waveguiding in Ion-Assisted-Deposited Thin Films," Appl. Surf. Sci. 22,23, (1985).

M. Born and E. Wolf, *Principles of Optics,* (Pergamon Press, New York, 1980).

B. Bovard, Optical Sciences Center, University of Arizona, Tucson, Arizona 85721 USA (Personal communication, 1988).

E. Bradley and D. G. Hall, "Out-of-Plane Scattering from Glass Waveguides: Comparison of Theory and Experiment," Opt. Lett. 7, 235 (1982).

P. J. Brannon, "Improved Method of Measuring Optical Waveguide Propagation Losses," Appl. Opt. 25, 3596 (1986).

C. De Bernardi, A. Loffredo, and S. Morasca, "Optimum Conditions for Waveguide Loss Measurements by Scattered Radiation Detection at Visible and Near-IR Wavelengths," *Integrated Optical Circuit Engineering III,* Proc. SPIE 651, 259 (1986).

D. J. Channin, J. M. Hammer, and M. T. Duffy, "Scattering in ZnO-Sapphire Optical Waveguides," Appl. Opt. 14, 923 (1975).

K. L. Chopra, *Thin Film Phenomena,* (Robert E. Krieger, New York, 1979).

S. Dutta, H. E. Jackson, and J. T. Boyd, "Extremely Low-Loss Glass Thin-Film Optical Waveguides Utilizing Surface Coating and Laser Annealing," J. Appl. Phys. 52, 3873 (1981).

S. Dutta, *et al.*, "Scattering Loss Reduction in ZnO Optical Waveguides by Laser Annealing," Appl. Phys. Lett. 39, 206 (1981).

S. Dutta, *et al.*, "CO_2 Laser Annealing of Si_3N_4, Nb_2O_5, and Ta_2O_5 Thin-Film Optical Waveguides to Achieve Scattering Loss Reduction," IEEE J. Quantum Electron. **QE-18**, 800 (1982).

T. Findakly, E. Garmire, and H. T. Moon, "Comparison of Losses in Imperfect Surface-Diffused and Buried Optical Waveguides," Opt. Lett. **4**, 149 (1979).

T. Findakly and E. Garmire, "Reduction and Control of Optical Waveguide Losses in Glass," Appl. Phys. Lett. **37**, 855 (1980).

R. M. Fortenberry, *Nonlinear Optical Phenomena in Zinc Oxide Waveguides*, (Ph. D. Dissertation, University of Arizona, 1986).

B. R. Frieden, *Probability, Statistical Optics, and Data Testing*, (Springer-Verlag, New York, 1983).

A. H. Gabel, *Degenerate Four Wave Mixing in Semiconductor Doped Glass Waveguides*, (Ph. D. Dissertation, University of Arizona, 1988).

J. D. Gaskill, *Linear Systems, Fourier Transforms, and Optics*, (John Wiley and Sons, New York, 1978).

J. E. Goell and R. D. Stanley, "Sputtered Glass Waveguides for Integrated Optical Circuits," Bell Syst. Tech. J. **48**, 3445 (1969).

J. W. Goodman, *Introduction to Fourier Optics*, (McGraw-Hill, San Francisco, 1968).

K. H. Guenther and H. K. Pulker, "Electron Microscopical Investigations of Cross Sections of Optical Thin Films," Appl. Opt. **15**, 2992 (1976).

K. H. Haegele and R. Ulrich, "Pyroelectric Loss Measurement in $LiNbO_3$:Ti Guides," Opt. Lett. **4**, 60 (1979).

D. G. Hall, R. R. Rice, and J. D. Zino, "Simple Gaussian-Beam Model For GaAlAs Double-Heterostructure Laser-Diode-to-Diffused-Waveguide Coupling Calculations," Opt. Lett. **4**, 292 (1979).

D. G. Hall, "Effects of Waveguide Mode Asymmetry on the Laser Diode-to-Diffused Waveguide Coupling Efficiency," Appl. Opt. **18**, 3372 (1979).

D. G. Hall, "Comparison of Two Approaches to the Waveguide Scattering Problem," Appl. Opt. **19**, 1732 (1980).

D. G. Hall, "Scattering of Optical Guided Waves by Waveguide Surface Roughness: a Three-Dimensional Treatment," Opt. Lett. **6**, 601 (1981).

D. G. Hall, "In-Plane Scattering in Planar Optical Waveguides: Refractive-Index Fluctuations and Surface Roughness," J Opt. Soc. Am. A. **2**, 747 (1985).

D. G. Hall, "Theory of Waveguides and Devices," in *Integrated Optical Circuits and Components, Design and Applications*, ed. L. D. Hutcheson, (Marcel Dekker, New York, 1987).

E. Hecht and A. Zajac, *Optics*, (Addison-Wesley, Massachusetts, 1974).

C. H. Henry, *et al.*, "Low Loss Si_3N_4-SiO_2 Optical Waveguides on Si," Appl. Opt. 26, 2621 (1987).

P. P. Herrmann and D. Wildmann, "Fabrication of Planar Dielectric Waveguides with High Optical Damage Threshold," IEEE J. Quantum Electron. QE-19, 1735 (1983).

F. S. Hickernell, Motorola Government Electronics Division, Scottsdale Arizona, 85252 USA.

R. K. Hickernell, *et al.*, "Waveguide Loss Measurement using Photothermal Deflection," Appl. Opt. *27*, 2636 (1988).

C. F. Hickey, *Optical, Chemical, and Structural Properties of Thin Films of Samarium Sulfide and Zinc Sulfide*, (Ph. D. Dissertation, University of Arizona, 1987).

M. D. Himel and U. J. Gibson, "Measurement of Planar Waveguide Losses using a Coherent Fiber Bundle," Appl. Opt., 25, 4415 (1986).

M. D. Himel, J. A. Ruffner, and U. J. Gibson, "Propagation Losses of Thin Film Waveguides," *Integrated Optical Circuit Engineering V* 835, 32 (1987).

M. D. Himel, J. A. Ruffner, and U. J. Gibson, "Stress Modification and Reduced Waveguide Losses in ZnS Thin Films," Appl. Opt. 27, 2810 (1988).

R. G. Hunsperger, *Integrated Optics: Theory and Technology*, (Springer-Verlag, New York, 1984).

M. Imai, M. Koseki, and Y. Ohtsuka, "Light Scattering from a Glass Thin-Film Optical Waveguide," J. Appl. Phys. 52, 6506 (1981).

M. Imai, Y. Ohtsuka, and M. Koseka, "Scattering Pattern Measurement and Analysis of Sputtered-Glass Optical Waveguides for Integrated Optics," IEEE J. Quantum Electron. QE-18, 789 (1982).

J. L. Jackel and J. J. Veselka, "Measuring Losses in Optical Waveguides: a New Method," Appl. Opt. 23, 197 (1984).

N. S. Kapany and J. J. Burke, *Optical Waveguides*, (Academic Press, New York, 1972).

C. Kittel, *Introduction to Solid State Physics*, (John Wiley and Sons, New York, 1976).

H. Kogelnik, "Theory of Dielectric Waveguides," in *Integrated Optics*, ed. T. Tamir, (Springer-Verlag, New York, 1979).

S. K. Korotky and R. C. Alferness, "Ti:$LiNbO_3$ Integrated Optic Technology: Fundamentals, Design Considerations, and Capabilities," in *Integrated Optical Circuits and Components, Design and Applications*, ed. L. D. Hutcheson, (Marcel Dekker, New York, 1987).

M. Laugier, "Intrinsic Stress in Thin Films of Vacuum Evaporated LiF and ZnS using an Improved Cantilevered Plate Technique," Vacuum 31, 155 (1981).

J. A. Leavitt, L. C. McIntyre, M. D. Ashbaugh, and J. G. Oder, Department of Physics, University of Arizona, Tucson Arizona, 85721 USA.

P. H. Lissberger and J. M. Pearson, "The Performance and Structural Properties of Multilayer Optical Filters," Thin Solid Films 34, 349 (1976).

H. A. Macleod, *Thin-Film Optical Filters,* (Macmillan, New York, 1986).

L. I. Maissel and R. Glang, *Handbook of Thin Film Technology,* (McGraw-Hill, New York, 1970).

D. Marcuse, "Mode Conversion Caused by Surface Imperfections of a Dielectric Slab Waveguide," Bell Sys. Tech. J. 48, 3187 (1969).

D. Marcuse, "Power Distribution and Radiation Losses in Multimode Dielectric Slab Waveguides," Bell Sys. Tech. J. 51, 429 (1972).

D. Marcuse, *Theory of Dielectric Optical Waveguides,* (Academic Press, New York, 1974).

S. Miyanaga, M. Imai, and T. Asakura, " Radiation Pattern of Light Scattering from the Core Region of Dielectric-Slab-Optical Waveguides," IEEE J. Quantum Electron. QE-14, 30 (1978).

S. Miyanaga, T. Asakura, and M. Imai, "Scattering Characteristics of a Beam Mode in a Dielectric-Slab Optical Waveguide," Opt. and Quantum Electron. 11, 205 (1979).

S. Miyanaga, T. Asakura, and M. Imai, "Scattering Characteristics of a Beam Mode in a Dielectric-Slab Optical Waveguide. Part II,"Opt. and Quantum Electron. 12, 23 (1980).

R. A. Modavis and D. G. Hall, "In-Plane Scattering in Planar Optical Waveguides," Opt. Lett. 9, 96 (1984).

B. A. Movchan and A. V. Demchishin, Fiz. Met. Metalloved. 28, 653 (1969)

K. A. Nesmelov, L. D. Lazareva, and A. G. Gusev, "Dependence of the Properties of ZnS Films on the Rate of Deposition," Zhurn. Prikl. Spektrosk. 40, 136 (1984).

Y. Okamura, S. Yoshinaka, and S. Yamamoto, "Measuring Mode Propagation Losses of Integrated Optical Waveguides: a Simple Method," Appl. Opt. 22, 3892 (1983).

Y. Okamura, S. Sato, and S. Yamamoto, "Simple Method of Measuring Propagation Properties of Integrated Optical Waveguides: an Improvement," Appl. Opt. 24, 57 (1985).

E. D. Palik and A. Addamiano, "Zinc Sulfide," in *Handbook of Optical Constants of Solids*, ed. E. D. Palik (Academic Press, San Diego, 1985).

J. M. Pearson, "Electron Microscopy of Multilayer Thin Films," Thin Solid Films **6**, 349 (1970)

W. A. Pliskin, "Comparison of Properties of Dielectric Films Deposited by Various Methods," J. Vac. Sci. Technol. **14**, 1064 (1977).

H. K. Pulker and E. Jung, "Correlation Between Film Structure and Sorption Behavior of Vapour Deposited ZnS, Cryolite and MgF_2 Films," Thin Solid Films **9**, 57 (1971).

H. K. Pulker and J. Maser, "The Origin of Mechanical Stress in Vacuum-Deposited MgF_2 and ZnS Films," Thin Solid Films **59**, 65 (1979).

P. Roche, L. Bertrand, and E. Pelletier, "Influence of Temperature on the Optical Properties of Narrow-Band Interference Filters," Optica Acta, **23**, 433 (1976).

J. A. Ruffner, Optical Sciences Center, University of Arizona, Tucson, Arizona 85721 USA (1988).

S. G. Saxe, *Ion-Induced Processes in Optical Coatings*, (Ph. D. Dissertation, University of Arizona, 1985).

R. W. Sprague, *et al.*, "Effects of Design Parameters on ZnS Bistable Etalons," *Optical Thin Films II: New Developments*, Proc. SPIE **678**, 167 (1986).

G. I. Stegeman, Optical Sciences Center, University of Arizona, Tucson, Arizona 85721 USA (Personal communication, 1988).

H. Suche, *et al.*, "Parametric Fluorescence, Amplification and Oscillation in Ti:$LiNbO_3$ Optical Waveguides," *Integrated Optical Circuit Engineering II*, Proc. SPIE **578**, 156 (1985).

F. Suits, Optical Sciences Center, University of Arizona, Tucson, Arizona 85721 USA (Personal communication, 1988).

B. C. Svensson, *Nonlinear Distributed Couplers in ZnS Waveguides*, (Ph. D. Dissertation, University of Arizona, 1988).

Swanson and Fuyat, "ZnS," in *Inorganic Index to the Powder Diffraction File*, ed. J. V. Smith (American Society for Testing and Materials, Philadelphia, 1967).

T. Tamir and S. T. Peng, "Analysis and Design of Grating Couplers," Appl. Phys. **14**, 235 (1977).

J. A. Thornton, "Influence of Apparatus Geometry and Deposition Conditions on the Structure and Topograghy of Thick Sputtered Coatings," J. Vac. Sci. Technol. **11**, 666 (1974).

P. K. Tien, "Light Waves in Thin Films and Integrated Optics," Appl. Opt. **10**, 2395 (1971).

R. Ulrich, "Theory of the Prism-Film Coupler by Plane-Wave Analysis," J. Opt. Soc. Am. **60**, 1337 (1970).

D. W. Vahey, C. M. Verber, and V. E. Wood, "Sources of Scattering of Guided Light in Ti-Diffused $LiNbO_3$ Optical Waveguides," Ferroelectrics **27**, 81 (1980).

E. W. Van Stryland, *et al.*, "Two Photon Absorption, Nonlinear Refraction, and Optical Limiting in Semiconductors," Opt. Eng. **24**, 613 (1985).

D. J. Walter and J Houghton, "Attenuation in Thin Film Optical Waveguide Due to Roughness-Induced Mode Coupling," Thin Solid Films **52**, 461 (1978).

H. P. Weber, F. A. Dunn, and W. N. Leibolt, "Loss Measurements in Thin Film Optical Waveguides," Appl. Opt. **12**, 755 (1973).

R. P. Wenz and R. W. Hoffman, "Intrinsic Stress/Microstructure Investigations of ZnS Films," Proc. 7th Intern. Vac. Congr. and 3rd Intern. Conf. Solid Surfaces, 1643 (1977).

W. D. Westwood and J. S. Wei, "Guide Optics Techniques for Investigation of Films," Can. J. Phys. **57**, 1247 (1979).

M. T. Wlodarczyk, "Ray Optics of Scattering and Absorption in Planar Waveguides," J. Opt. Soc. Am. A. (Submitted January, 1987).

Y. H. Won, P. C. Jaussaud, and G. H. Chartier, "Three-prism Loss Measurements of Optical Waveguides," Appl. Phys. Lett. **37**, 269 (1980).

D. M. Wood and N. W. Ashcroft, Philosophical Magazine **35**, 269 (1977).